이학박사 학위논문

Change in the bottom water composition and lithological sediment provenance of the Bering Sea during the Pleistocene

: Insights from neodymium isotopes and NGR-based K, Th and U concentrations

네오디뮴 동위원소 및 NGR 기반 K, Th, U 농도를 이용한 플라이스토세 기간 베링해 중층수/심층수 조성 및 퇴적물 기원지 변화 추적 연구

2017년 8월

서울대학교 대학원
지구환경과학부 동위원소지구화학 전공
장 광 철

Abstract

The Bering Sea is an important location to understand global climate system because of its high sensitivity to advance/retreat of sea ice and continental ice sheet. Enhanced sea ice formation may induce the formation of the North Pacific Intermediate/Deep Water (NPIW/NPDW) in the Bering Sea, and the development of continental ice sheet in Alaska can potentially determine the provenance of the Bering Sea sediments. To examine the relationships between NPIW/NPDW formation, lithological sediment provenance and ice dynamics responding to glacial/interglacial cycles, here I present authigenic and detrital neodymium (Nd) isotopes and NGR-based K, Th and U concentration of marine sediments in the Bering Sea obtained during the Integrated Ocean Drilling Program (IODP) Expedition 323. Authigenic Nd isotopes is a quasi-conservative water mass tracer, and detrital Nd isotopes and NGR-based K, Th and U concentrations can be used as indicators of lithological sediment provenance. To acquire reliable authigenic Nd isotopes without contamination from labile volcanic components in sediments, Nd isotopes and elemental concentrations of six different authigenic fractions are compared each other.

Reconstructed authigenic Nd isotopes ($\varepsilon_{Nd,AUTH}$) at site U1345 on the Bering Slope over ~520 kyr showed average value of -3.3 ± 0.9 (1σ, n = 98) with large temporal fluctuations, which can be interpreted either as episodic occurrences of the NPIW formation or boundary exchange between seawater and sediments. Likewise, $\varepsilon_{Nd,AUTH}$ records at site U1343 over ~2.4 Myr showed average value of -

3.0 ± 1.1 (1σ, n = 155) with large temporal variation. Only one NPDW formation is attributed to this variation, and boundary exchange between seawater and sediments is the most likely reason for $\varepsilon_{Nd,AUTH}$ variation. The detrital Nd isotopes ($\varepsilon_{Nd,DET}$) at site U1343 showed average of -6.6 ± 1.5 (1σ, n = 70) with temporal variation, indicating change in lithological sediment provenance. Overall, Alaska is a dominant source over the Aleutian Arc at site U1343, and outstanding unradiogenic $\varepsilon_{Nd,DET}$ peaks can result from meltwater discharge from Alaska. Considering the repetitive occurrence of unradiogenic $\varepsilon_{Nd,DET}$ peaks after 2.4 Ma, extensive glaciation have probably developed in Alaska since at least 2.4 Myr ago. Spatial and temporal variation in terrigenous sediment provenance of the Bering Sea sediment are partly shown in NGR-based K/Th, K/U and Th/U ratios at sites U1341 and U1342 on the Bowers Ridge and sites U1343 and U1345 on the Bering Slope. The Bowers Ridge sediments showed distinct K/Th, K/U and Th/U ratios from the Bering Slope sediments. However, heavy mineral sorting and/or change in paleo-oceanic redox conditions can disturb primary signals from parent rocks, and therefore K/Th, K/U and Th/U ratios are only used as a preliminary result to trace lithological sediment provenance in the Bering Sea.

Keyword: Bering Sea, Neodymium Isotopes, North Pacific Intermediate Water formation, Boundary Exchange, NGR counts, IODP Expedition

Student Number: 2012-30895

Table of contents

Chapter 1. Introduction

Paleoclimate and paleoecanographic studies provide an insightful perspective on the complex nature of global climate system. Various geological samples such as rocks, sediments, ice and corals keep the past records, and characteristic climatic proxies such as sediment mineralogy, stable ($\delta^{13}C$ and $\delta^{18}O$) and radiogenic isotopes ($^{87}Sr/^{86}Sr$, $^{231}Pa/^{230}Th$ and $^{143}Nd/^{144}Nd$) and concentration of greenhouse gases (CO_2, CH_4 and N_2O) reveal what the past records mean (Barnola et al., 1987; Kaufman et al., 1993; Knudson and Ravelo, 2015; MacFarling Meure et al., 2006; Rutberg et al., 2000; Singer, 1984; Yu et al., 1996). Then, the meaning of the past records helps to understand the present climatic issues and to predict the future prospect. Therefore, it is an important to study the past climate history to understand the climate system dynamics.

The Bering Sea is a key location for paleoceanographic research owing to its high sensitivity to global climate change, as inferred from the intense warming of the high latitude regions in the Northern Hemisphere at present (Solomon, 2007). This climatic sensitivity in the Bering Sea is presumably related to sea ice and continental ice sheet because these ices can play an important role in climatic condition by controlling sea-ice albedo feedback (Curry et al., 1995) and interaction between ocean and atmosphere (Overland and Pease, 1982). Indeed, the sea ice extent in the Bering Sea has varied in response to glacial-interglacial variability since ~3.3 Ma, and, likewise, the appearance of continental ice sheet in adjacent continent Alaska has repetitively occurred since at least ~4.2 Ma (Horikawa et al., 2015). Accordingly, paleoclimate reconstruction in the Bering Sea is able to extend our knowledge about the behavior of ice-climate interactions.

Marine sediments can be as a great archive for paleoclimate reconstructions because they provide continuous high-resolution climatic records. During Integrated Ocean Drilling Program (IODP) Expedition 323, 5741 m of sediments were obtained at seven different sites on Umnak Plateau (site U1339), the Bowers Ridge (sites U1340, U1341 and U1342) and the Bering Slope (sites U1343, U1344 and U1345) in the Bering Sea (Fig. 1.1 and Table 1.1) (Expedition 323 Scientists, 2011). The oldest sediment of IODP cores reaches back to ~5 Ma, which records the various climate transitions, for example, warm Pliocene to cold Pleistocene (Filippelli and Flores, 2009) and global climate periodicity change from 41-kyr to 100-kyr during the mid-Pleistocene transition (MPT) (Clark et al., 2006). Temporal variation in climatic proxies of marine sediments reconstructs a detailed history of climate change in the Bering Sea from early Pliocene to the present. Since the MPT is defined based on the climatic proxies mostly from the Atlantic and equatorial Pacific (Elderfield et al., 2012), this paleoclimate reconstruction in the Bering Sea across the MPT can balance the biased data.

Three different areas including Umnak Plateau, the Bowers Ridge and the Bering Slope allow examining spatial and temporal variation in sediment distribution from Alaska and the Aleutian Arc (Horikawa et al., 2015; Jang et al., 2017). Umnak Plateau is proximal to entrance of modern Alaskan stream, while the Bowers Ridge is located near the entrance of glacial Alaskan stream. The Bering Slope sites are close to the mouth of Yukon River, which supplies >63% of the total terrigenous sediment in the Bering Sea (Eberl, 2004). The Bering Slope is also proximal to modern sea ice extent. Therefore, terrignous sediment distribution should be spatially and temporally variable in response to glacial-interglacial cycles. Indeed, regional variation in core-top detrital Nd isotopes indicates that the

Bering Slope sites are more influenced by the Alaskan-sourced materials than Umnak Plateau at present (Asahara et al., 2012). Furthermore, the temporal variation in detrital Nd isotopes at site U1341 showed that terrigenous sediments on the Bowers Ridge are mainly derived from the Aleutian Arc and the Alaska, and these binary mixing properties are governed by development of the Alaskan glacier (Horikawa et al., 2015). Since long-term variation in sediment components is only available in site from Bowers Ridge, it is necessary to reconstruct temporal change in sediment provenance at the Bering Slope sites to fully understand the relationship between sediment distribution and climatic change in the Bering Sea.

Different water depths of IODP sediment cores characterize vertical distribution of water mass (Table 1.1), from which the presence of the formation of North Pacific Intermediate Water (NPIW) and/or North Pacific Deep Water (NPDW) in the Bering Sea can be traced. The dense water formation is one of main issues for paleoceanography because it can sequester carbon dioxide from surface water into deep water and potentially drive global water circulation (Biastoch et al., 2008; Häkkinen and Rhines, 2004; Stouffer et al., 2006). Dense water formation is almost absent in the Bering Sea at present due to low salinity (Warner and Roden, 1995), but it is likely that dense water formed by brine rejection (e.g. Haley et al., 2007; Jang et al., 2013). As sea ice rejects amount of brine into seawater when it forms, brine rejection can be a driving force for dense water formation. Indeed, Knudson and Ravelo (2015) and Cook et al. (2016) suggested that the formation of the North Pacific Intermediate Water (NPIW) has episodically occurred in the Bering Sea, and the main cause for NPIW is brine rejection based on lighter benthic foraminifera $\delta^{18}O$ value. However, the main source for NPIW and the

periods for NPIW occurrence have not been identified, and the possibility for NPDW formation has not been evaluated.

The main aim of this Ph. D. thesis is to investigate the presence of NPIW and NPDW formation, to reconstruct spatial and temporal variation in terrigenous sediment provenance and to provide long-term variation in paleo-climatic proxies across the MPT. The IODP Exp. 323 sediment cores (U1341, U1342, U1343 and U1345) are used as samples, and Nd isotopes ($^{143}Nd/^{144}Nd$) and NGR-based K, Th and U contents are used as proxies. The highlights of this thesis includes the following.

- In Chapter 2, the principle and application of Nd isotopes are briefly demonstrated. Reliable method to acquire seawater-derived Nd isotopes is introduced.
- In Chapter 3, authigenic and detrital Nd isotopes are reconstructed at site U1345 over the last 520 kyrs. The presence of the NPIW formation is verified by authigenic Nd isotopes. The relationship between temporal change in sediment provenance and climate are examined. The main source for NPIW and the periods for NPIW occurrence are identified. The relationship between NPIW and NADW are evaluated.
- In Chapter 4, Nd isotopes of authigenic and detrital fractions are reconstructed at site U1343 over the last 2.4 Myr. Only one event for the NPDW formation is detected by authigenic Nd isotopes. Boundary exchange is highlighted as a main mechanism controlling deep-water Nd isotopes rather than lateral transport and/or vertical mixing. Long-term

variations in lithological sediment provenance suggest that the Alaskan glaciation has exited during the Pleistocene.

- In Chapter 5, K, Th and U contents are estimated from NGR spectra of sediments at sites U1341, U1342, U1343 and U1345 using a MATLAB algorithm provided by De Vleeschouwer et al. (2017). The potential utilities of K/Th and Th/U ratios as proxies of sediment provenance and paleo-oceanic redox conditions are evaluated.

References

Asahara, Y., Takeuchi, F., Nagashima, K., Harada, N., Yamamoto, K., Oguri, K., Tadai, O., 2012. Provenance of terrigenous detritus of the surface sediments in the Bering and Chukchi Seas as derived from Sr and Nd isotopes: Implications for recent climate change in the Arctic regions. Deep-Sea Res. II 61–64, 155-171.

Asahi, H., Kender, S., Ikehara, M., Sakamoto, T., Takahashi, K., Ravelo, A., Alvarez Zarikian, C., Khim, B., Leng, M., 2016. Orbital-scale benthic foraminiferal oxygen isotope stratigraphy at the northern Bering Sea Slope Site U1343 (IODP Expedition 323) and its Pleistocene paleoceanographic significance. Deep-Sea Res. II 125-126, 66-83.

Barnola, J.-M., Raynaud, D., Korotkevich, Y.S., Lorius, C., 1987. Vostok ice core provides 160,000-year record of atmospheric CO_2. Nature 329, 408-414.

Biastoch, A., Böning, C.W., Getzlaff, J., Molines, J.-M., Madec, G., 2008. Causes of interannual-decadal variability in the meridional overturning circulation of the midlatitude North Atlantic Ocean. J. Climate 21, 6599-6615.

Clark, P.U., Archer, D., Pollard, D., Blum, J.D., Rial, J.A., Brovkin, V., Mix, A.C., Pisias, N.G., Roy, M., 2006. The middle Pleistocene transition: characteristics, mechanisms, and implications for long-term changes in atmospheric pCO_2. Quat. Sci. Rev. 25, 3150-3184.

Cook, M.S., Ravelo, A.C., Mix, A., Nesbitt, I.M., Miller, N.V., 2016. Tracing subarctic Pacific water masses with benthic foraminiferal stable isotopes during the LGM and late Pleistocene. Deep-Sea Res. II 125, 84-95.

Curry, J.A., Schramm, J.L., Ebert, E.E., 1995. Sea ice-albedo climate feedback mechanism. J. Climate 8, 240-247.

De Vleeschouwer, D., Dunlea, A.G., Auer, G., Anderson, C.H., Brumsack, H., de Loach, A., Gurnis, M.C., Huh, Y., Ishiwa, T., Jang, K., 2017. Quantifying K, U, and Th contents of marine sediments using shipboard natural gamma radiation spectra measured on DV JOIDES Resolution. Geochem. Geophys. Geosyst., doi:10.1002/2016GC006715.

Eberl, D., 2004. Quantitative mineralogy of the Yukon River system: Changes with reach and season, and determining sediment provenance. Am. Mineral. 89, 1784-1794.

Elderfield, H., Ferretti, P., Greaves, M., Crowhurst, S., McCave, I.N., Hodell, D., Piotrowski, A.M., 2012. Evolution of ocean temperature and ice volume through the mid-Pleistocene climate transition. Science 337, 704-709.

Expedition 323 Scientists, 2011. Expedition 323 summary. In Takahashi, K., Ravelo, A.C., Alvarez Zarikian, C.A., and the Expedition 323 Scientists (Eds.), Proc. IODP, 323. Integrated Ocean Drilling Program Management International, Inc., Tokyo.

Filippelli, G.M., Flores, J.-A., 2009. From the warm Pliocene to the cold Pleistocene: A tale of two oceans. Geology 37, 959-960.

Häkkinen, S., Rhines, P.B., 2004. Decline of subpolar North Atlantic circulation during the 1990s. Science 304, 555-559.

Haley, B.A., Frank, M., Spielhagen, R.F., Eisenhauer, A., 2007. Influence of brine formation on Arctic Ocean circulation over the past 15 million years. Nat. Geosci. 1, 68-72.

Horikawa, K., Martin, E.E., Basak, C., Onodera, J., Seki, O., Sakamoto, T., Ikehara, M., Sakai, S., Kawamura, K., 2015. Pliocene cooling enhanced by flow of low-salinity Bering Sea water to the Arctic Ocean. Nat. Commun. 6,

7587.

Jang, K., Han, Y., Huh, Y., Nam, S.-I., Stein, R., Mackensen, A., Matthiessen, J., 2013. Glacial freshwater discharge events recorded by authigenic neodymium isotopes in sediments from the Mendeleev Ridge, western Arctic Ocean. Earth Planet. Sci. Lett. 369–370, 148-157.

Jang, K., Huh, Y., Han, Y., 2017. Authigenic Nd isotope record of North Pacific Intermediate Water formation and boundary exchange on the Bering Slope. Quat. Sci. Rev. 156, 150-163.

Kaufman, A.J., Jacobsen, S.B., Knoll, A.H., 1993. The Vendian record of Sr and C isotopic variations in seawater: implications for tectonics and paleoclimate. Earth Planet. Sci. Lett. 120, 409-430.

Knudson, K.P., Ravelo, A.C., 2015. North Pacific Intermediate Water circulation enhanced by the closure of the Bering Strait. Paleoceanography 30, 1287-1304.

MacFarling Meure, C., Etheridge, D., Trudinger, C., Steele, P., Langenfelds, R., Van Ommen, T., Smith, A., Elkins, J., 2006. Law Dome CO_2, CH_4 and N_2O ice core records extended to 2000 years BP. Geophys. Res. Lett. 33.

Overland, J.E., Pease, C.H., 1982. Cyclone climatology of the Bering Sea and its relation to sea ice extent. Mon. Weather Rev. 110, 5-13.

Rutberg, R.L., Hemming, S.R., Goldstein, S.L., 2000. Reduced North Atlantic Deep Water flux to the glacial Southern Ocean inferred from neodymium isotope ratios. Nature 405, 935-938.

Singer, A., 1984. The paleoclimatic interpretation of clay minerals in sediments—a review. Earth-Sci. Rev. 21, 251-293.

Solomon, S., 2007. Climate change 2007-the physical science basis: Working

group I contribution to the fourth assessment report of the IPCC. Cambridge Univ. Press.

Stouffer, R.J., Yin, J., Gregory, J., Dixon, K., Spelman, M., Hurlin, W., Weaver, A., Eby, M., Flato, G., Hasumi, H., 2006. Investigating the causes of the response of the thermohaline circulation to past and future climate changes. J. Climate 19, 1365-1387.

Warner, M.J., Roden, G.I., 1995. Chlorofluorocarbon evidence for recent ventilation of the deep Bering Sea. Nature 373, 409-412.

Yu, E.-F., Francois, R., Bacon, M.P., 1996. Similar rates of modern and last-glacial ocean thermohaline circulation inferred. Nature 379, 22.

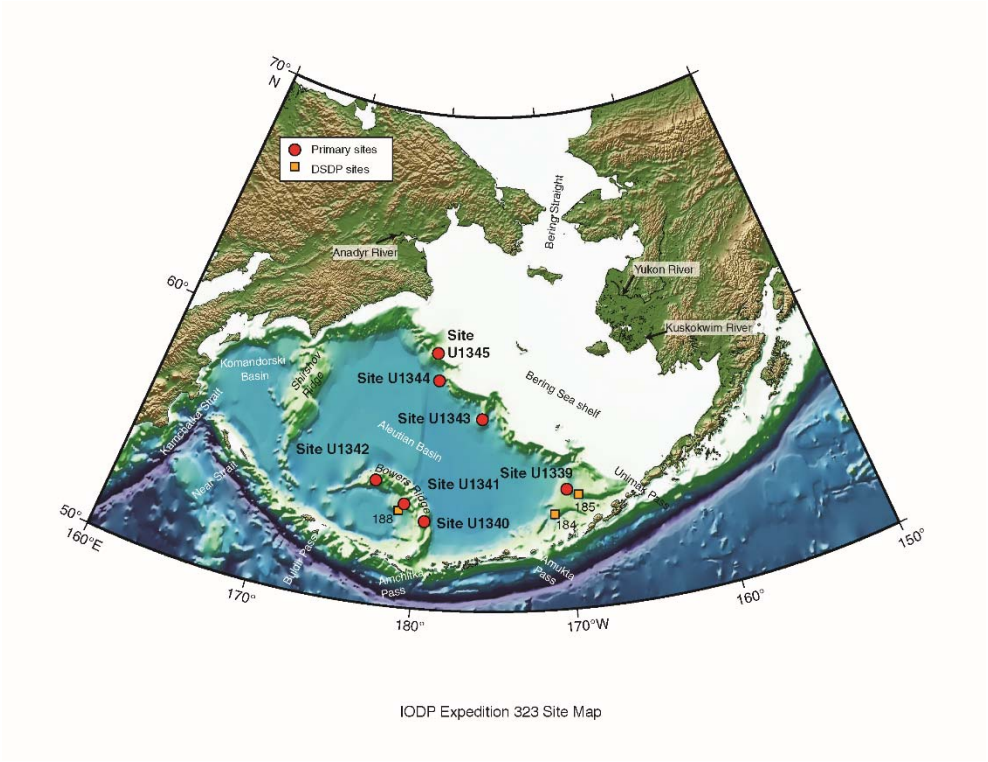

Figure 1.1. IODP Expedition 323 sites in the Bering Sea.

Table 1.1 Summary of IODP Exp. 323 sites in the Bering Sea. Modified from Expedition 323 Scientists (2011).

Location	Sampling site	Water depth (m)	Longest core length (m, DSF)	Age (Ma)
Umnak Plateau	U1339	1867.5	200	0.9*
Bowers Ridge	U1340	1294.6	600	5
	U1341	2139.5	600	4.3*
	U1342	818.6	45	1.7*
Bering Slope	U1343	1952.9	745	2.4*
	U1344	3173.1	745	1.9
	U1345	1007.8	150	0.5*

*Age models for sites U1339 and U1345 from Cook et al. (2016), site U1341 from Horikawa et al. (2015), site U1342 from Knudson and Ravelo (2015) and site U1343 from Asahi et al. (2016).

Chapter 2. The chemical treatment method for authigenic Nd isotopes to acquire reliable seawater signal

Kwangchul Jang, Youngsook Huh, and Yeongcheol Han

2.1. Introduction

The main objective of this chapter is to recover authentic seawater Nd isotopic signal from authigenic fraction of marine sediment. The strategy for the data reliability is to compare ε_{Nd} values and elemental concentrations of different authigenic fractions obtained using various traditional extraction method. The contents below are slightly modified from Jang et al. (2017) (chapter 3) and Jang et al. *in preparation* (chapter 4).

2.2. Neodymium isotopes

Neodymium (Nd) has seven naturally-occurring isotopes, ^{142}Nd (27.2%), ^{143}Nd (12.2%), ^{144}Nd (23.8%), ^{145}Nd (8.3%), ^{146}Nd (17.2%), ^{148}Nd (5.8%) and ^{150}Nd (5.6%) (Roederer et al., 2008). Among them, ^{143}Nd is a radiogenic isotope produced by alpha decay of ^{147}Sm with a decay constant $6.54 * 10^{-12}$ (yr^{-1}) (Lugmair, 1974). As there is a fractionation of Sm/Nd ratio during the differentiation of the silicate earth (Nd is more incompatible than Sm during melting process) (summarized in DePaolo and Wasserburg, 1976), Nd isotope ratios (^{143}Nd/^{144}Nd) vary depending on the rock's age and type. These deviations

are very small, so $^{143}Nd/^{144}Nd$ is typically expressed as ε_{Nd}, which is parts per 10^4 deviations from chondritic uniform reservoir (CHUR). For example,

$$\varepsilon_{Nd} = \left[\left\{\frac{(^{143}Nd/^{144}Nd)_{sample}}{(^{143}Nd/^{144}Nd)_{CHUR}}\right\} - 1\right] \times 10^4$$

where $(^{143}Nd/^{144}Nd)_{CHUR}$ is 0.512638 (Jacobsen and Wasserburg, 1980). As a result, old continental rocks have low ε_{Nd}, called "unradiogenic" while young mantle-derived rocks do high ε_{Nd}, called "radiogenic".

The interesting feature is that seawater ε_{Nd} reflects that of drained basin (Arsouze et al., 2007; Lacan and Jeandel, 2005; Lacan et al., 2012). Radiogenic ε_{Nd} value of the Pacific Ocean surrounded by volcanic rocks compared to the Atlantic Ocean surrounded by continental shield is one of examples (Goldstein and O'nions, 1981; Lacan et al., 2012; Piepgras and Wasserburg, 1980; Piepgras et al., 1979). It is primarily attributed to shorter residence time of Nd with 360 to 700 years (Rempfer et al., 2011; Siddall et al., 2008; Tachikawa et al., 2003) than oceanic mixing time with ~1,500 years (Broecker and Peng, 1982). This heterogeneity of seawater ε_{Nd} implies potential use of seawater ε_{Nd} as a water mass tracer. The good covariance of ε_{Nd} values with salinity and SiO_2 in deep seawater supports this speculation (reviews in Goldstein and Hemming, 2003).

Indeed, the neodymium isotope ratios ($^{143}Nd/^{144}Nd$) have been widely used as a quasi-conservative tracer of water mass in fields of paleoceanography and paleoclimate (e.g. Albarède et al., 1997; Jang et al., 2013; Jonkers et al., 2015; Piotrowski et al., 2004; Roberts et al., 2010; Rutberg et al., 2000). The South Atlantic Ocean has been ideal location to apply this proxy because two water

masses that flow into S. Atlantic have contrast ε_{Nd} signals (e.g. Jonkers et al., 2015; Piotrowski et al., 2004; Rutberg et al., 2000). Radiogenic ε_{Nd} excursions in the S. Atlantic during cold periods are interpreted as a result from reduction in the North Atlantic Deep Water formation. It is consistent with speculation from other water mass proxies such as Pa/Th ratio and benthic foraminifera $\delta^{13}C$, supporting the utility of Nd isotopes as a tracer of ocean circulation.

The nature is not too much optimistic. The deep-water ε_{Nd} are not only influenced by mixing of water mass but also by internal alterations such as the interaction between seawater and particles (Arsouze et al., 2007; Jeandel and Oelkers, 2015; Rempfer et al., 2011; Rickli et al., 2010; Wilson et al., 2012) and/or porewater diffusion (Abbott et al., 2015, 2016). In particular, the interaction between seawater and particles, called “boundary exchange” seems to be a key process under the stagnant bottom water condition, e.g. the Pacific Ocean (Jang et al., 2017; Siddall et al., 2008). Therefore, boundary exchange should be considered to interpret deep-water ε_{Nd} records. However, main questions including (1) what factors determine ε_{Nd} derived from boundary exchange and/or (2) what conditions intensify boundary exchange remain enigmatic.

The various archives have been used for seawater ε_{Nd}. The traditional archive is Fe-Mn crust (e.g. O'nions et al., 1978; Piepgras et al., 1979), which is useful to observe tectonic scale variation owing to its low growth rate. For the higher resolution, Fe-Mn oxyhydroxide extracted from bulk sediment (“authigenic fraction”) is a good alternative. As this archive is precipitate formed around bulk sediments during early-diagenesis, glacial-interglacial and millennial scale variations can be resolved depending on sedimentation rate (e.g. Gutjahr et al.,

2007; Jang et al., 2013; Piotrowski et al., 2009; Rutberg et al., 2000). The main problem for this archive is a potential contamination from labile terrigenous materials during chemical treatments (e.g. Jang et al., 2017; Kraft et al., 2013; Roberts et al., 2010; Wilson et al., 2013). The usage of biogenic archives such as fish teeth (e.g. Horikawa et al., 2011; Martin and Haley, 2000), deep-sea corals (e.g. Robinson et al., 2014; van de Flierdt et al., 2010) and Fe-Mn oxyhydroxide of foraminifera (e.g. Pena and Goldstein, 2014; Roberts et al., 2010) can be useful to minimize potential contamination.

Unfortunately, the sediments from the Bering Sea do not contain enough biological archives like foraminifera and fish teeth for Nd isotopes analysis (Expedition 323 Scientists, 2011a, b; Scientists, 2011c). The main biological product here is a diatom. There is a big possibility that Fe-Mn oxyhydroxide precipitated around opal can be useful archive for deep-water Nd isotope records like foraminifera. However, a difficulty to physically separate opal from terrigenous materials disturbs to use this new archive. Consequently, the authigenic fraction is only available in the Bering Sea, and hence site-specific extraction process should be developed to acquire authentic seawater signal.

2.3. Methods

2.3.1. *Separation of authigenic and detrital fractions*

2.3.1.1. Authigenic Fe-Mn oxyhydroxide fraction

The authigenic Fe-Mn oxyhydroxide fraction is the fraction that records past seawater composition and is therefore our main interest. During the extraction process, it is very important to avoid the dissolution of non-authigenic material.

The dissolution of terrigenous components mainly depends on lithology; therefore, the chemical protocol needs to be adjusted to the specific site (Wilson et al., 2013). To determine the most suitable extraction method for the Bering Slope sediments, we first carried out a test on four sediment samples from site U1345 representing opposing climate regimes (Holocene and marine isotope stage (MIS) 5.5 warm periods and LGM and MIS 4 cold periods) and four random samples from site U1343. Three different extraction methods are applied to four samples from site U1345 and one extraction method (1/10 *Wilson Authigenic*) is additionally used for four samples from site U1343.

The first method is modified from Rutberg et al. (2000) (hereafter, *Rutberg Authigenic*), and it subjects de-carbonated samples to 0.02 M hydroxylamine hydrochloride (HH) in 25% buffered acetic acid (Table 2.1). We applied different leaching time depending on sampling sites: 3 hours for site U1345 and 1 hour for site U1343. The reagent-to-sediment volume ratio is approximately 10. The second method is based on Wilson et al. (2013) (hereafter, *Wilson Authigenic*)(Table 2.1). There is no decarbonation step, the leaching time is shorter (1 hour), and the reagent-to-sediment volume ratio is lower (~1). The third method (hereafter, *Blaser Authigenic*) is similar to *Wilson Authigenic*, but the reducing reagent is different (0.005 M HH in 1.5% buffered acetic acid with 0.003 M Na-EDTA), and the reagent-to-sediment volume ratio is higher (> 30) (Blaser et al., 2016)(Table 2.1). The last method (hereafter 1/10 *Wilson Authigenic*) is the same as that of Wilson Authigenic, except that the chemical reagent became diluted 1/10 with deionized water (Table 2.1).

2.3.1.2. *Carbonate fraction and second authigenic fraction*

These two fractions are used to constrain the range of seawater ε_{Nd}. The best way to ensure the authenticity of the authigenic ε_{Nd} value is to compare it with the coating on biogenic material such as foraminifera (Roberts et al., 2010). However, the siliceous biogenic environment on the Bering Slope does not provide enough calcareous biogenic material for Nd isotope analysis. Thus, we resorted to the carbonate fraction and the second authigenic fraction (hereafter, *Second Authigenic*).

The carbonate fraction is extracted with 1 M buffered acetic acid (Table 2.1). The leaching times are 12 hours for U1345 sediments and 1 hour for U1343 sediments. The lack of detrital carbonate input into the Bering Sea assures us that the carbonate fraction is mainly composed of authigenic carbonate (Hein et al., 1979) and that it essentially reflects the sea water composition. Indeed, the carbonate fraction has been used as an archive for Nd isotopic composition of the bottom water in the Arctic Ocean (Haley and Polyak, 2013), although different leaching times (~30 min) were used for the extraction.

The *Second Authigenic* is obtained by submitting the remaining sediment after the *Rutberg Authigenic* extraction to a second round of Fe-Mn oxyhydroxide extraction, this time for 24 hours. The possibility of dissolution of labile terrigenous component increases with the leaching time; therefore, the *Second Authigenic* is a contaminable fraction. Consequently, the ε_{Nd} values of the carbonate fraction and the *Second Authigenic* can restrict the range in ε_{Nd} value of authigenic Fe-Mn oxyhydroxide.

2.3.1.3. *Detrital fraction*

After complete separation of the authigenic fraction, alkaline fusion is carried out on the residue (Bayon et al., 2009). We mix 0.1 g residue with 1.2 g Na_2O_2 (>95%, small beads, ACS grade, Sigma-Aldrich) and 0.6 g NaOH (>98.0%, pellet, ACS grade, Sigma-Aldrich) in a glassy carbon beaker (SIGRADUR, HTW). This mixture is fused at 650°C for 15 minutes and re-dissolved in deionized water after slight cooling at room temperature. The melt is transferred into a Teflon beaker and placed on the hotplate at 130°C for complete co-precipitation. After centrifugation, the precipitate is used for detrital Nd isotope analysis. The reference materials (JB-2 and BHVO-1) were also treated for accuracy test.

2.3.2. *Purification and instrumental analysis*

2.3.2.1. *Elemental concentrations of the different fractions*

We measured the concentrations of select elements (Al, Fe, Mn, Sr, and REEs) in the five non-detrital fractions of the LGM and MIS 5.5 sediment samples at site U1345. We used an inductively coupled plasma-sector field mass spectrometer (ICP-SFMS, Element 2, Thermo Scientific) at the National Center for Inter-University Research Facilities of Seoul National University. The oxide production rate was reduced using a desolvation nebulizer system (Aridus II, Cetac) ($^{135}Ba^{16}O/^{135}Ba$ ~0.01%). The external reproducibility was better than 5%. The average elemental concentrations for the river water reference material SLRS-4 agreed within literature values (Heimburger et al., 2013; Soyol-Erdene and Huh, 2013), except for Lu, which we do not use here.

2.3.2.2. *Column separation*

Two column separation steps were carried out using TRU resin (50-100 μm, Eichrom) and Ln resin (50-100 μm, Eichrom) with methods modified from Míková and Denková (2007) and Pin and Zalduegui (1997). The authigenic fractions were dissolved in 2 M HNO_3 and loaded onto the TRU resin. After eluting the fraction containing HREEs with 2 M HNO_3, LREEs were retrieved with 0.05 M HCl. The LREE fraction was loaded onto the Ln resin. With 0.15 M HCl, La, Ce, and Pr were eluted and Nd was retrieved.

2.3.2.3. *Nd isotope composition*

Nd isotope ratios were measured using the thermal ionization mass spectrometer (TIMS, Triton, Thermo Scientific) at the Korea Polar Research Institute and the multicollector inductively coupled plasma mass spectrometer (MC-ICP-MS, Neptune, Thermo Scientific) at the Korea Basic Science Institute. We used $^{147}Sm/^{146}Nd$ for interference correction and $^{146}Nd/^{144}Nd$ for mass fractionation correction by normalizing to 0.7219. The $^{143}Nd/^{144}Nd$ ratios of JB-2 and BHVO-1 were 0.513095 ± 0.000011 and 0.512983 ± 0.000010, respectively, which are consistent with literature values (Weis et al., 2005; Yang et al., 2009 and references therein).

2.3.3. *The ε_{Nd} comparison between Wilson Authigenic and Rutberg Authigenic*

We compared *Wilson Authigenic* from 102 sediment samples including four duplicates and *Rutberg Authigenic* from 113 sediment samples including 19 duplicates at site U1345. At site U1343, ε_{Nd} values of *Wilson Authigenic* from 21 sediments are compared with those of *Rutberg Authigenic* from 21 corresponding samples.

2.4. Results and discussion: the most suitable extraction method

2.4.1. *ε_{Nd} and elemental composition results at site U1345*

The Nd isotopic composition of the six different fractions of the four test samples is shown in Figs. 2.1A, B, K and L. When the extraction test was repeated, the ε_{Nd} of each fraction was reproduced within uncertainty (0.2 – 0.5 ε_{Nd}) (Fig. 2.1B). The detrital fraction had different ε_{Nd} in the duplicate extractions, probably due to sediment heterogeneity. Of the six different fractions, the detrital fraction has the lowest ε_{Nd} value. Among the non-detrital fractions, the carbonate fraction and *Wilson Authigenic* have lower ε_{Nd} values, and *Blaser Authigenic* and *Second Authigenic* have higher values. *Rutberg Authigenic* displays similar to slightly more radiogenic ε_{Nd} values than *Wilson Authigenic*.

The ε_{Nd} difference between fractions is prominent in samples #1 (MIS 5.5) and #4 (MIS 4): the carbonate fraction and *Wilson Authigenic* are distinctly less radiogenic than the other authigenic fractions. On the other hand, in samples #2 (LGM) and #3 (Holocene), the ε_{Nd} values of *Wilson Authigenic* and *Rutberg Authigenic* are similar. This sample-dependent ε_{Nd} variation among the different authigenic fractions can result from lithology. Volcanic material is most prone to inducing a radiogenic ε_{Nd} bias, and hence, a higher volcanic content is predicted for samples #1 and #4. The carbonate content is also important because its lability delays dissolution of the volcanic component. The decarbonation step for *Rutberg Authigenic* and *Second Authigenic* and the faster carbonate removal by EDTA for *Blaser Authigenic* may accelerate Nd isotope exchange with the volcanic component and introduce a radiogenic ε_{Nd} bias.

Unlike ε_{Nd}, elemental concentrations cannot independently distinguish whether terrigenous components are leached. We do not observe any significant correlation between ε_{Nd} and elemental concentrations. The Nd concentration is high in the *Blaser Authigenic* of both samples #1 and #2 (Figs. 2.1A and B), and judging from the radiogenic ε_{Nd} values, it indicates the dissolution of volcanic material. However, the other fractions display low Nd concentrations with varying ε_{Nd} values. Aluminum, an element abundant in clay minerals, exhibits a similar trend as Nd (Figs. 2.1C and 2.1D).

The Al/Nd ratio has been used as an indicator for dissolution of the detrital fraction (Gutjahr et al., 2007). For sample #1, there is a broad inverse relationship between Al/Nd and ε_{Nd}, with the lowest Al/Nd in *Second Authigenic* (Fig. 2.1C). For sample #2, there is no correlation between Al/Nd and ε_{Nd}, with relatively high Al/Nd in *Second Authigenic* (Fig. 2.1D). This irregular relationship between Al/Nd and ε_{Nd} requires further examination for the Al/Nd parameter (Martin et al., 2010; Wilson et al., 2013). Iron and manganese, main components of Fe-Mn oxyhydroxide, are also highest in *Blaser Authigenic* (Figs. 2.1E and F). We observe a roughly increasing trend of Fe concentration with increasing ε_{Nd} only in sample #2. The concentration of Sr is highest in *Blaser Authigenic*, which is consistent with the other elemental concentration (Figs. 2.1G and 2.1H). It is lowest in *Rutberg Authigenic* and *Second Authigenic*, which can be attributed to the removal of Sr in the decarbonation step.

We also examined the REE pattern to evaluate the seawater origin of leachate ε_{Nd} (Martin et al., 2010). The MREE/MREE* and HREE/LREE ratios quantify the extent of the MREE bulge and HREE enrichment, respectively. *Wilson Authigenic* displays the highest MREE/MREE* and HREE/LREE ratios and the

Second Authigenic the lowest (Figs. 2.1I and 2.1J). Most fractions show MREE bulge patterns (MREE/MREE* > 1) and moderate to enriched HREE (HREE/LREE > 1), which is consistent with typical hydrogenous Fe-Mn oxyhydroxides, fish teeth and Fe-Mn nodules (Axelsson et al., 2002; Bayon et al., 2002; Gutjahr et al., 2007; Jauhari and Pattan, 2000; Martin et al., 2010; Sherrell et al., 1999). *Second Authigenic* is the only exception, with an HREE/LREE ratio lower than 1. We do not detect a specific relationship between the REE pattern and ε_{Nd} in our restricted data set.

We compared the Nd isotopic compositions of *Wilson Authigenic* and *Rutberg Authigenic* (n = 113, including duplicates). They are mostly consistent with each other within uncertainty (n = 94), but 19 data points—18 *Rutberg Authigenic* and one *Wilson Authigenic*—are more radiogenic than the 1:1 line (Fig. 2.2). All duplicates of *Wilson Authigenic* have consistent ε_{Nd} values, but five of the 19 duplicates for *Rutberg Authigenic* display inconsistent ε_{Nd} values and are also more radiogenic than the corresponding *Wilson Authigenic*. Among the five ash layer samples, *Rutberg Authigenic* is more radiogenic than *Wilson Authigenic* in three samples, indicating the vulnerability of *Rutberg Authigenic* to contamination from volcanic material (Fig. 2.2, red symbols).

2.4.2. *ε_{Nd} results at site U1343*

The ε_{Nd} values of seven different fractions in four sediment samples at site U1343 show similar results with those at site U1345 (Fig. 2.3). In all sediments, ε_{Nd} values at 1/10 *Wilson Authigenic*, *Wilson Authigenic* and carbonate fractions are comparable to each other and lower than *Blaser Authigenic*, *Rutberg Authigenic* and *Second Authigenic*. The dilution of leaching reagent for 1/10 *Wilson Authigenic*

does not decrease in ε_{Nd} but rather increase its uncertainty (Fig. 2.3), and hence *Wilson Authigenic* is better as an archive of sea water composition. The ε_{Nd} of *Wilson Authigenic* is also comparable to that of the carbonate fraction, indicating that there is no significant ε_{Nd} difference between the Fe-oxide and the carbonate fraction including Mn-oxide. It implies the data reliability of *Wilson Authigenic*, and to some extent the lack of isotopic alteration by diagenetic carbonate overgrowth in the Bering Sea. The additional comparison between *Wilson Authigenic* and *Rutberg Authigenic* in U1343E samples (n = 25) shows a significant radiogenic excursion in all *Rutberg Authigenic* (Fig 2.4). The proximity of U1343 to the volcanic source region, Aleutian Arc, may be a probable reason for frequent radiogenic deviations of *Rutberg Authigenic* at site U1343.

2.4.3. *Leaching protocol for Bering Sea sediments*

We propose that the *Wilson* method is the most appropriate to extract an authentic seawater signal from the Bering Slope sediments. This is based on a comparable ε_{Nd} of *Wilson Authigenic* and carbonate fractions (Fig. 2.1 and 2.3), a lower ε_{Nd} of *Wilson Authigenic* compared to other authigenic fractions (Fig. 2.1 and 2.3), and the general consistency between the ε_{Nd} of *Wilson Authigenic* and *Rutberg Authigenic* at site U1345 (Fig. 2.2) and a more radiogenic *Rutberg Authigenic* where there are inconsistencies between the two (Fig. 2.2 and 2.4).

The comparable ε_{Nd} of *Wilson Authigenic* and carbonate fractions supports that *Wilson Authigenic* records a seawater-originated Nd isotopic signal. We consider the carbonate fraction to be free from contamination by terrigenous components, as this mildest leaching treatment reduces the risk of dissolution of labile terrigenous material. The carbonates at sites U1343 and U1345 are

dominantly authigenic and biogenic (Expedition 323 Scientists, 2011b; 2011c), which rules out the possibility of an ε_{Nd} shift by detrital carbonate. The influence of diagenetic carbonate overgrowth is probably minimal. The carbonate fraction displays an MREE bulge pattern (Figs 2.1I and J) that is distinct from the low MREE/MREE* and very high HREE/LREE of the neighboring pore waters (Soyol-Erdene and Huh, 2013). For these reasons, the carbonate fraction would essentially reflect a seawater Nd isotopic composition, as would *Wilson Authigenic*.

The lower ε_{Nd} of *Wilson Authigenic* compared to other authigenic fractions also indicates an authentic seawater signal. The stronger extraction of *Second Authigenic* than *Rutberg Authigenic* releases radiogenic volcanic material that is more reactive than the remaining detrital fraction (Fig. 2.1) (Wilson et al., 2013). Therefore, the lower ε_{Nd} values represent a reduced influence from terrigenous sources.

The general similarity of the ε_{Nd} between *Wilson Authigenic* and *Rutberg Authigenic* at site U1345 suggests data validity (Fig. 2.2). Radiogenic exceptions are mainly observed in *Rutberg Authigenic* (Figs. 2.2 and 2.4), suggesting that the stronger extraction of *Rutberg Authigenic* may release some terrigenous components. There was only one occasion of radiogenic bias for *Wilson Authigenic* at site U1345, and therefore, we consider the treatment method of *Wilson Authigenic* to be stable. We replaced the radiogenic outlier of *Wilson Authigenic* with the corresponding *Rutberg Authigenic* (Fig. 3.3B, blue symbol).

We cannot rely on elemental concentrations to detect unintended incorporation of terrigenous material into sediment leachate (Fig. 2.1). All elemental concentrations and the Al/Nd ratio are independent of ε_{Nd} variation. The Al/Nd ratio is highest in the carbonate and not the detrital fraction, suggesting that

re-adsorption of REEs during extraction may modify this ratio (Wilson et al., 2013). Therefore, careful use of elemental criteria is necessary.

We suggest that *Wilson Authigenic* is a reliable fraction for recording seawater-origin Nd isotopic compositions in the Bering Slope, although we cannot provide unambiguous proof due to the lack of ε_{Nd} data for foraminifera and the water column. *Wilson Authigenic* is appropriate especially for sediments whose detrital carbonate content is negligible. Because carbonate is more labile than volcanic material, the presence of carbonate delays the Nd isotopic exchange of leachate with volcanic material (Wilson et al., 2013). Low chemical reagent-to-sediment ratios provide sufficient available surface area for Nd re-adsorption, slowing down exchange with non-authigenic radiogenic components (Wilson et al., 2013). EDTA has a similar effect because it forms complexes with REEs and reduces re-adsorption (Gutjahr et al., 2007). Considering that *Rutberg Authigenic* and *Blaser Authigenic* were valid data sets for the Southern and Atlantic oceans, respectively, the extraction protocols for each location should be tested.

References

Abbott, A.N., Haley, B.A., McManus, J., 2015. Bottoms up: Sedimentary control of the deep North Pacific Ocean's ε_{Nd} signature. Geology 43, 1035-1035.

Abbott, A.N., Haley, B.A., McManus, J., 2016. The impact of sedimentary coatings on the diagenetic Nd flux. Earth Planet. Sci. Lett. 449, 217-227.

Albarède, F., Goldstein, S.L., Dautel, D., 1997. The neodymium isotopic composition of manganese nodules from the Southern and Indian oceans, the global oceanic neodymium budget, and their bearing on deep ocean circulation. Geochim. Cosmochim. Acta 61, 1277-1291.

Arsouze, T., Dutay, J.-C., Lacan, F., Jeandel, C., 2007. Modeling the neodymium isotopic composition with a global ocean circulation model. Chem. Geol. 239, 165-177.

Axelsson, M.D., Rodushkin, I., Ingri, J., Öhlander, B., 2002. Multielemental analysis of Mn–Fe nodules by ICP-MS: optimisation of analytical method. Analyst 127, 76-82.

Bayon, G., Barrat, J.A., Etoubleau, J., Benoit, M., Bollinger, C., Révillon, S., 2009. Determination of rare earth elements, Sc, Y, Zr, Ba, Hf and Th in geological samples by ICP-MS after Tm addition and alkaline fusion. Geostand. Geoanal. Res. 33, 51-62.

Bayon, G., German, C.R., Boella, R.M., Milton, J.A., Taylor, R.N., Nesbitt, R.W., 2002. An improved method for extracting marine sediment fractions and its application to Sr and Nd isotopic analysis. Chem. Geol. 187, 179-199.

Blaser, P., Lippold, J., Gutjahr, M., Frank, N., Link, J.M., Frank, M., 2016. Extracting foraminiferal seawater Nd isotope signatures from bulk deep sea sediment by chemical leaching. Chem. Geol. 439, 189-204.

Broecker, W.S., Peng, T.-H., 1982. Tracers in the Sea. Lamont-Doherty Geological Observatory, Columbia University, Palisades, 243 pp.

DePaolo, D.J., Wasserburg, G.J., 1976. Nd isotopic variations and petrogenetic models. Geophys. Res. Lett. 3, 249-252.

Expedition 323 Scientists, 2011a. Site U1341. In Takahashi, K., Ravelo, A.C., Alvarez Zarikian, C.A., and the Expedition 323 Scientists (Eds.), Proc. IODP, 323. Integrated Ocean Drilling Program Management International, Inc., Tokyo.

Expedition 323 Scientists, 2011b. Site U1343. In Takahashi, K., Ravelo, A.C., Alvarez Zarikian, C.A., and the Expedition 323 Scientists (Eds.), Proc. IODP, 323. Integrated Ocean Drilling Program Management International, Inc., Tokyo.

Expedition 323 Scientists, 2011c. Site U1345. In Takahashi, K., Ravelo, A.C., Alvarez Zarikian, C.A., and the Expedition 323 Scientists (Eds.), Proc. IODP, 323. Integrated Ocean Drilling Program Management International, Inc., Tokyo.

Goldstein, S., O'nions, R., 1981. Nd and Sr isotopic relationships in pelagic clays and ferromanganese deposits. Nature 292, 324-327.

Goldstein, S.L., Hemming, S.R., 2003. 6.17 - Long-lived Isotopic Tracers in Oceanography, Paleoceanography, and Ice-sheet Dynamics A2 - Holland, Heinrich D, in: Turekian, K.K. (Ed.), Treatise on Geochemistry. Pergamon, Oxford, pp. 453-489.

Gutjahr, M., Frank, M., Stirling, C.H., Klemm, V., van de Flierdt, T., Halliday, A.N., 2007. Reliable extraction of a deepwater trace metal isotope signal from Fe-Mn oxyhydroxide coatings of marine sediments. Chem. Geol. 242,

351-370.

Haley, B.A., Polyak, L., 2013. Pre-modern Arctic Ocean circulation from surface sediment neodymium isotopes. Geophys. Res. Lett. 40, 893-897.

Heimburger, A., Losno, R., Triquet, S., Nguyen, E.B., 2013. Atmospheric deposition fluxes of 26 elements over the Southern Indian Ocean: Time series on Kerguelen and Crozet Islands. Global Biogeochem. Cy. 27, 440-449.

Hein, J.R., O'NEIL, J.R., Jones, M.G., 1979. Origin of authigenic carbonates in sediment from the deep Bering Sea. Sedimentology 26, 681-705.

Horikawa, K., Martin, E.E., Asahara, Y., Sagawa, T., 2011. Limits on conservative behavior of Nd isotopes in seawater assessed from analysis of fish teeth from Pacific core tops. Earth Planet. Sci. Lett. 310, 119-130.

Jacobsen, S.B., Wasserburg, G.J., 1980. Sm-Nd isotopic evolution of chondrites. Earth Planet. Sci. Lett. 50, 139-155.

Jang, K., Han, Y., Huh, Y., Nam, S.-I., Stein, R., Mackensen, A., Matthiessen, J., 2013. Glacial freshwater discharge events recorded by authigenic neodymium isotopes in sediments from the Mendeleev Ridge, western Arctic Ocean. Earth Planet. Sci. Lett. 369–370, 148-157.

Jang, K., Huh, Y., Han, Y., 2017. Authigenic Nd isotope record of North Pacific Intermediate Water formation and boundary exchange on the Bering Slope. Quaternary Sci. Rev. 156, 150-163.

Jauhari, P., Pattan, J.N., 2000. Ferromanganese nodules from the central Indian Ocean basin. In: Cronan, D.S. (Ed.), Handbook of Marine Mineral Deposits. CRC Press, pp. 171-195.

Jeandel, C., Oelkers, E.H., 2015. The influence of terrigenous particulate material

dissolution on ocean chemistry and global element cycles. Chem. Geol. 395, 50-66.

Jonkers, L., Zahn, R., Thomas, A., Henderson, G., Abouchami, W., François, R., Masque, P., Hall, I.R., Bickert, T., 2015. Deep circulation changes in the central South Atlantic during the past 145 kyrs reflected in a combined $^{231}Pa/^{230}Th$, neodymium isotope and benthic $\delta^{13}C$ record. Earth Planet. Sci. Lett. 419, 14-21.

Kraft, S., Frank, M., Hathorne, E.C., Weldeab, S., 2013. Assessment of seawater Nd isotope signatures extracted from foraminiferal shells and authigenic phases of Gulf of Guinea sediments. Geochim. Cosmochim. Acta 121, 414-435.

Lacan, F., Jeandel, C., 2005. Neodymium isotopes as a new tool for quantifying exchange fluxes at the continent–ocean interface. Earth Planet. Sci. Lett. 232, 245-257.

Lacan, F., Tachikawa, K., Jeandel, C., 2012. Neodymium isotopic composition of the oceans: A compilation of seawater data. Chem. Geol. 300, 177-184.

Lugmair, G., 1974. Sm-Nd ages: a new dating method. Meteoritics 9, 369.

Míková, J., Denková, P., 2007. Modified chromatographic separation scheme for Sr and Nd isotope analysis in geological silicate samples. J. Geosci., 221-226.

Martin, E., Haley, B., 2000. Fossil fish teeth as proxies for seawater Sr and Nd isotopes. Geochim. Cosmochim. Acta 64, 835-847.

Martin, E.E., Blair, S.W., Kamenov, G.D., Scher, H.D., Bourbon, E., Basak, C., Newkirk, D.N., 2010. Extraction of Nd isotopes from bulk deep sea sediments for paleoceanographic studies on Cenozoic time scales. Chem. Geol. 269, 414-431.

O'nions, R., Carter, S., Cohen, R., Evensen, N., Hamilton, P., 1978. Pb, Nd and Sr isotopes in oceanic ferromanganese deposits and ocean floor basalts. Nature 273, 435-438.

Pena, L.D., Goldstein, S.L., 2014. Thermohaline circulation crisis and impacts during the mid-Pleistocene transition. Science 345, 318-322.

Piepgras, D.J., Wasserburg, G., 1980. Neodymium isotopic variations in seawater. Earth Planet. Sci. Lett. 50, 128-138.

Piepgras, D.J., Wasserburg, G., Dasch, E., 1979. The isotopic composition of Nd in different ocean masses. Earth Planet. Sci. Lett. 45, 223-236.

Pin, C., Zalduegui, J.S., 1997. Sequential separation of light rare-earth elements, thorium and uranium by miniaturized extraction chromatography: Application to isotopic analyses of silicate rocks. Anal. Chim. Acta 339, 79-89.

Piotrowski, A.M., Banakar, V.K., Scrivner, A.E., Elderfield, H., Galy, A., Dennis, A., 2009. Indian Ocean circulation and productivity during the last glacial cycle. Earth Planet. Sci. Lett. 285, 179-189.

Piotrowski, A.M., Goldstein, S.L., Hemming, S.R., Fairbanks, R.G., 2004. Intensification and variability of ocean thermohaline circulation through the last deglaciation. Earth Planet. Sci. Lett. 225, 205-220.

Rempfer, J., Stocker, T.F., Joos, F., Dutay, J.-C., Siddall, M., 2011. Modelling Nd-isotopes with a coarse resolution ocean circulation model: Sensitivities to model parameters and source/sink distributions. Geochim. Cosmochim. Acta 75, 5927-5950.

Rickli, J., Frank, M., Baker, A.R., Aciego, S., de Souza, G., Georg, R.B., Halliday, A.N., 2010. Hafnium and neodymium isotopes in surface waters of the

eastern Atlantic Ocean: Implications for sources and inputs of trace metals to the ocean. Geochim. Cosmochim. Acta 74, 540-557.

Roberts, N.L., Piotrowski, A.M., McManus, J.F., Keigwin, L.D., 2010. Synchronous deglacial overturning and water mass source changes. Science 327, 75-78.

Robinson, L.F., Adkins, J.F., Frank, N., Gagnon, A.C., Prouty, N.G., Roark, E.B., van de Flierdt, T., 2014. The geochemistry of deep-sea coral skeletons: a review of vital effects and applications for palaeoceanography. Deep-Sea Res. II 99, 184-198.

Roederer, I.U., Lawler, J.E., Sneden, C., Cowan, J.J., Sobeck, J.S., Pilachowski, C.A., 2008. Europium, samarium, and neodymium isotopic fractions in metal-poor stars. The Astrophysical Journal 675, 723.

Rutberg, R.L., Hemming, S.R., Goldstein, S.L., 2000. Reduced North Atlantic Deep Water flux to the glacial Southern Ocean inferred from neodymium isotope ratios. Nature 405, 935-938.

Sherrell, R.M., Field, M.P., Ravizza, G., 1999. Uptake and fractionation of rare earth elements on hydrothermal plume particles at 9°45′N, East Pacific Rise. Geochim. Cosmochim. Acta 63, 1709-1722.

Siddall, M., Khatiwala, S., van de Flierdt, T., Jones, K., Goldstein, S.L., Hemming, S., Anderson, R.F., 2008. Towards explaining the Nd paradox using reversible scavenging in an ocean general circulation model. Earth Planet. Sci. Lett. 274, 448-461.

Soyol-Erdene, T.-O., Huh, Y., 2013. Rare earth element cycling in the pore waters of the Bering Sea Slope (IODP Exp. 323). Chem. Geol. 358, 75-89.

Tachikawa, K., Athias, V., Jeandel, C., 2003. Neodymium budget in the modern

ocean and paleo-oceanographic implications. J. Geophys. Res-Oceans (1978 - 2012) 108, 3254, doi:3210.1029/1999JC000285.

van de Flierdt, T., Robinson, L.F., Adkins, J.F., 2010. Deep-sea coral aragonite as a recorder for the neodymium isotopic composition of seawater. Geochim. Cosmochim. Acta 74, 6014-6032.

Weis, D., Kieffer, B., Maerschalk, C., Pretorius, W., Barling, J., 2005. High-precision Pb-Sr-Nd-Hf isotopic characterization of USGS BHVO-1 and BHVO-2 reference materials. Geochem. Geophys. Geosyst. 6, Q02002, doi:02010.01029/02004GC000852.

Wilson, D.J., Piotrowski, A.M., Galy, A., Clegg, J.A., 2013. Reactivity of neodymium carriers in deep sea sediments: Implications for boundary exchange and paleoceanography. Geochim. Cosmochim. Acta 109, 197-221.

Wilson, D.J., Piotrowski, A.M., Galy, A., McCave, I.N., 2012. A boundary exchange influence on deglacial neodymium isotope records from the deep western Indian Ocean. Earth Planet. Sci. Lett. 341–344, 35-47.

Yang, Y., Wu, F., Xie, L., Zhang, Y., 2009. High-precision measurements of the $^{143}Nd/^{144}Nd$ isotope ratio in certified reference materials without Nd and Sm separation by multiple collector inductively coupled plasma mass spectrometry. Anal. Lett. 43, 142-150.

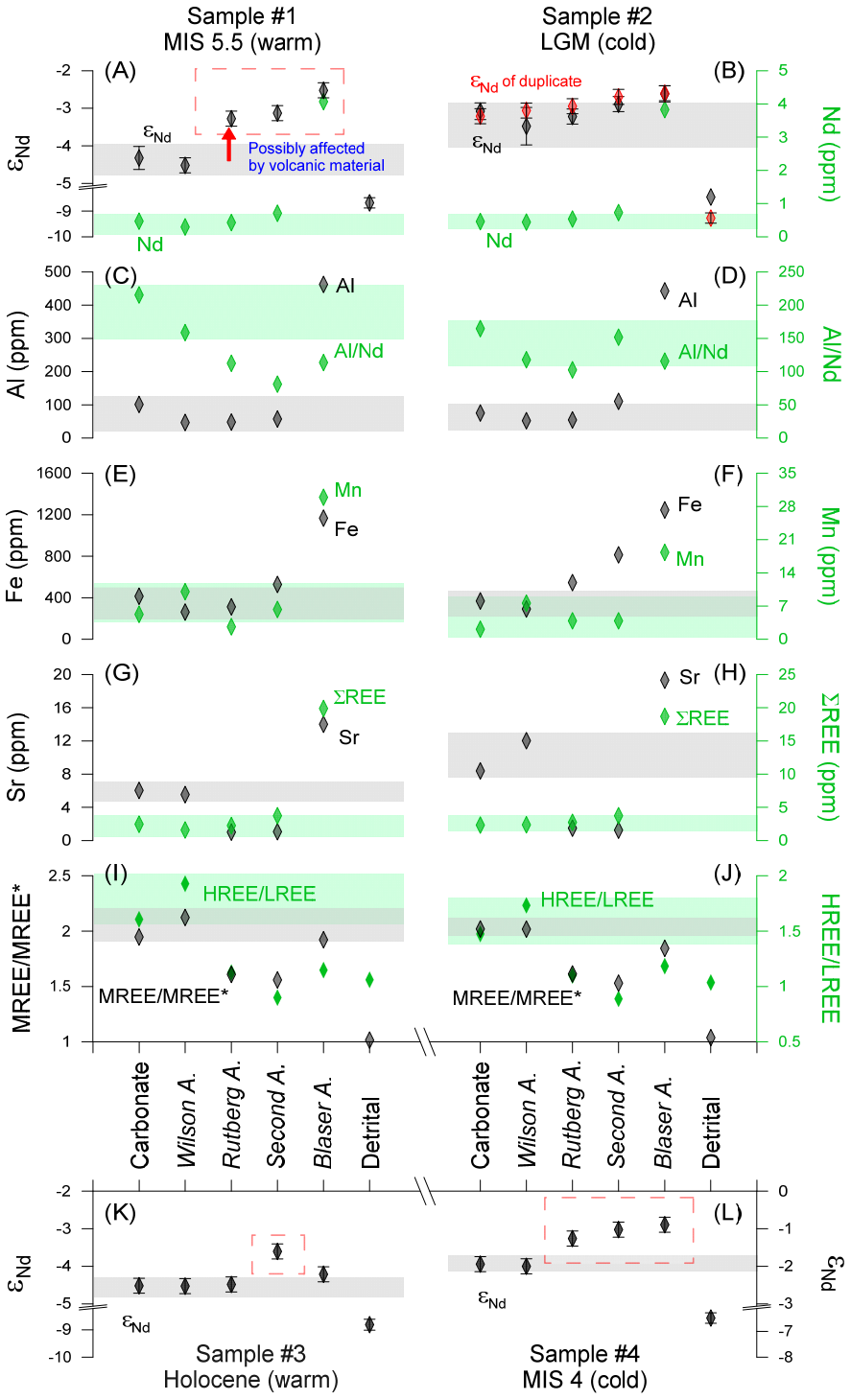

Figure 2.1. TIMS (ε_{Nd}) and ICP-SFMS (Nd, Al, Al/Nd, Fe, Mn, Sr, ΣREE, MREE/MREE* and HREE/LREE) results for six different fractions

(carbonate; authigenic Fe-Mn oxide of Wilson, Rutberg, and Blaser methods; *Second Authigenic*; and detrital) for the LGM and MIS 5.5 sediment samples at site U1345 (A to J). For the Holocene and MIS 4 (K and L) samples at site U1345, only ε_{Nd} was analyzed. MREE/MREE* = $(Gd_n+Tb_n+Dy_n)$ / $[\{(Tm_n+Yb_n\times2)+(La_n+Pr_n+Nd_n)\}/2]$, HREE/LREE = $(Tm_n+Yb_n\times2)$ / $(La_n+Pr_n+Nd_n)$ (subscript n denotes PAAS normalized concentration) (after Martin et al., 2010 with replacement of Lu_n by Yb_n). Dashed red boxes mark radiogenic ε_{Nd} results, possibly affected by labile terrigenous components. Gray and green shaded areas mark the data range of carbonate and *Wilson Authigenic* fractions, which we take to be the true authigenic fraction. Elemental concentrations are not powerful criteria to determine the data reliability of authigenic ε_{Nd}.

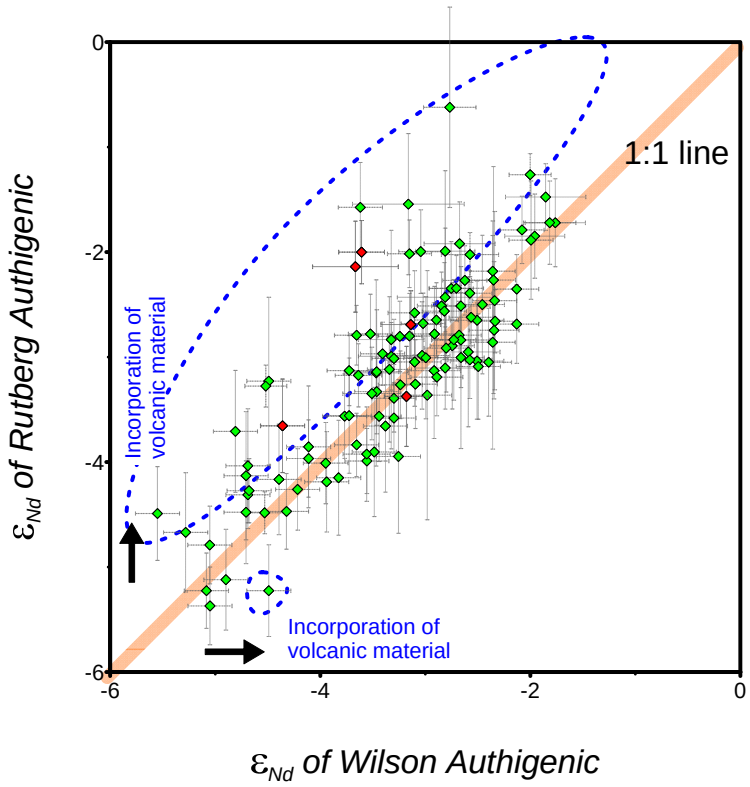

Figure 2.2. Comparison of Rutberg and Wilson methods (n = 113, including 19 duplicates) at site U1345. Dashed blue circles mark contaminated ε_{Nd} values, and the red symbols indicate the samples in ash layers.

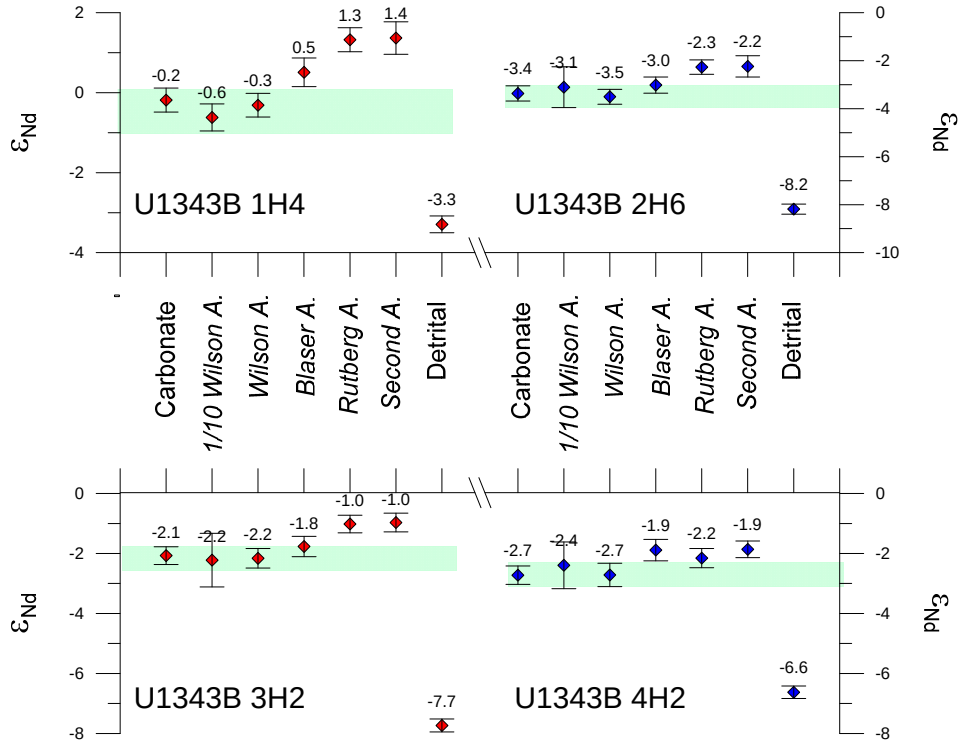

Figure 2.3. ε_{Nd} comparision of seven different fractions from 4 different sediments at site U1343. Fractions include 1/10 *Wilson Authigenic*, *Wilson Authigenic*, carbonate, *Blaser Authigenic*, *Rutberg Authigenic*, *Second Authigenic* and detrital fractions. At most sediments, *Blaser Authigenic*, *Rutberg Authigenic*, and *Second Authigenic* show radiogenic ε_{Nd} excursions, implying invasion of volcanogenic materials into those fractions during leaching.

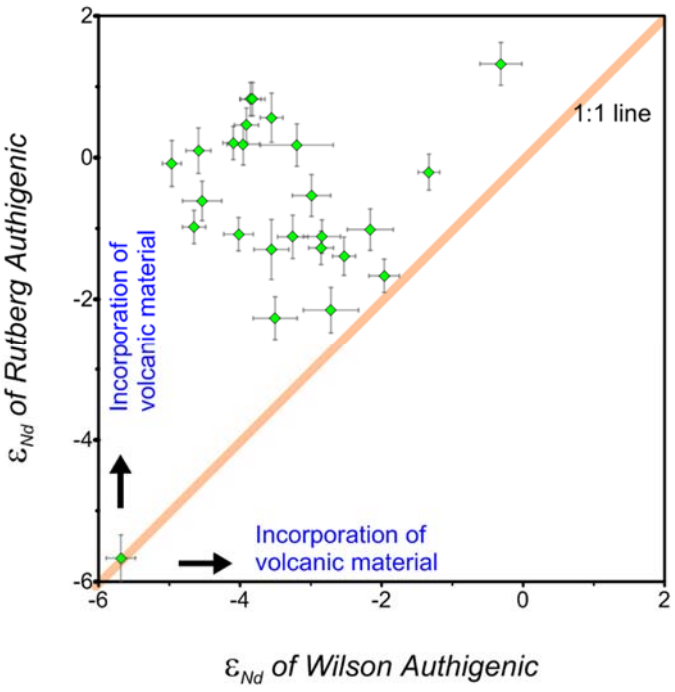

Figure 2.4. The ε_{Nd} comparison of *Wilson Authigenic* with *Rutberg Authigenic* (n = 25) at site U1343. Most of *Rutberg Authigenic* show more radiogenic ε_{Nd} than *Wilson Authigenic*.

Table 2.1. Three different extraction methods for authigenic Fe-Mn oxyhydroxide fraction

	Rutberg *et al.* (2000)		Wilson *et al.* (2013)		Blaser *et al.* (2014)	
Fraction	Reagent	Time (hr)	Reagent	Time (hr)	Reagent	Time (hr)
Carbonate	1 M Buffered acetic acid	1,12[b]	-	-	-	-
Fe-Mn oxide	0.02 M HH[a] in 25% buffered acetic acid	1,3[c]	0.02 M HH in 25% buffered acetic acid	1	0.005 M HH in 1.5% buffered acetic acid with 0.003 M Na-EDTA	1
Reagent/ Sample (v/v)	~10		~1		> 30	

[a]HH : hydroxylamine hydrochloride
[b]1 hour for U1343 samples, 12 hours for U1345 samples
[c]1 hour for U1343 samples, 3 hours for U1343 samples
*For 1/10 *Wilson Authigenic* fraction, 0.002 M HH in 2.5% buffered acetic acid was applied.

Chapter 3. Authigenic Nd isotope record of North Pacific Intermediate Water formation and boundary exchange on the Bering Slope

Kwangchul Jang, Youngsook Huh, and Yeongcheol Han

Published in *Quaternary Science Reviews*, 2017, v. 156, 150-163

Abstract

The Bering Sea is a potential location for the formation of the North Pacific Intermediate Water (NPIW), which drives the global ocean circulation as a counterpart to the North Atlantic Deep Water (NADW). To evaluate the NPIW-NADW seesaw hypothesis, we reconstructed the long-term variation of the bottom water Nd isotopic composition at site U1345 on the Bering Slope by extracting authigenic Fe-Mn oxyhydroxide from bulk sediments. The decarbonation step is omitted, and a low reagent-to-sediment ratio is adopted for extraction.

The reconstructed authigenic ε_{Nd} record for the last 520 kyr exhibits large temporal variations depending on whether the NPIW formation or the boundary exchange process is dominant. Periods of radiogenic ε_{Nd} can be attributed to NPIW formation triggered by brine rejection, as evidenced by the difference in $\delta^{18}O$ of benthic foraminifera between sites ($\Delta\delta^{18}O_{bf}$), high % sea-ice related diatoms, and low abundance of *Bulimina aff. Exilis* (low-oxygen deep fauna). Diminished supply of unradiogenic Nd from boundary exchange seems to intensify these radiogenic peaks. On the other hand, the unradiogenic ε_{Nd} intervals can be attributed to

stagnant bottom water conditions, as can be deduced from the $\Delta\delta^{18}O_{bf}$ values, low % sea-ice related diatoms, abundant *B. aff. Exilis*, and laminations. When there is no NPIW formation, the continental margin sediments are exposed to boundary exchange for a longer period of time, leading to release of unradiogenic Nd. The mid-MIS 6 and mid-MIS 5 are exceptions in that NPIW formation occurred yet the ε_{Nd} compositions are unradiogenic. NPIW formation and cold climate (closed Bering Strait) are not always correlated. Comparison to ε_{Nd} records of the South Atlantic suggests only an ambiguous NPIW-NADW seesaw for the last 200 kyr.

3.1. Introduction

The formation of intermediate and deep water plays an important role in the global climate system as a driving force of global ocean circulation and as a regulator of greenhouse gases such as carbon dioxide (CO_2) (Biastoch et al., 2008; Häkkinen and Rhines, 2004; Stouffer et al., 2006). The North Atlantic Deep Water (NADW) is one such example, and past variations in its strength are well documented, e.g., the reduction in NADW formation and related climate change during the Younger Dryas (YD) and the Heinrich events (HE) (Sarnthein et al., 1994; Seidov and Maslin, 1999). There is no deep-water formation in the North Pacific at present due to the low surface water salinity. Intermediate water forms in the Okhotsk Sea through brine rejection, but the magnitude is relatively small compared to the NADW (Shcherbina et al., 2003; Talley, 1991; Yasuda, 1997).

Recent research shows that the formation of the North Pacific Intermediate Water (NPIW) was stronger during glacial periods and that the Bering Sea was a probable location (Horikawa et al., 2010; Ohkushi et al., 2003; Rella et

al., 2012). For example, Ohkushi et al. (2003) propose that NPIW formed in the Bering Sea during the Last Glacial Maximum (LGM), based on the spatial distribution pattern of radiolarian species *Cycladophora davisiana*, which lives in a cold and well-oxygenated habitat such as the present NPIW environment. Supporting evidence comes from the $\delta^{18}O$ of benthic foraminifera ($\delta^{18}O_{bf}$) on the Bering Slope (MR06-04-23, 60°09.52'N, 179°27.82'W; 1,002 m water depth) (Rella et al., 2012) (Fig. 3.1). There is a positive $\delta^{18}O_{bf}$ excursion during the LGM that cannot be interpreted by an increase in global ice volume alone but requires the intrusion of colder and/or more saline water to the site (Rella et al., 2012). Rella et al. (2012) suggest that NPIW formed during other cold periods as well, such as HE 1 and 4 and YD, based on the positive $\delta^{18}O_{bf}$ gradient between the Bering Slope and the Okhotsk Sea. Horikawa et al. (2010) use a different proxy to arrive at similar conclusions. The neodymium (Nd) isotopic composition of the intermediate water on the Bowers Ridge in the Bering Sea (BOW-8A, 54˚47'N, 176˚55'E, 884 m water depth) over ~150 kyr shows radiogenic peaks during glacial periods, which they interpret as periods of NPIW formation (Horikawa et al., 2010) (Figs. 3.1 and 3.2).

Several model simulations suggest a seesaw relationship between NPIW/NPDW and NADW (Hu et al., 2012a; Okazaki et al., 2010; Saenko et al., 2004), but proxy studies are controversial. One proxy, the ^{14}C ventilation age, is determined by the difference in ^{14}C age between coexisting benthic and planktonic foraminifera. A low ^{14}C ventilation age indicates downwelling or upwelling. Okazaki et al. (2010) report an anti-phase relationship in ^{14}C ventilation ages between NPIW/NPDW (1,000 – 2,700 m water depth) and NADW during HE 1. Max et al. (2014) also show an anti-phase relationship between NPIW (700 – 1750

m water depth) and NADW during HE 1 and YD, but they argue against the seesaw with regard to NPDW (2100 – 2700 m water depth). An in-phase correlation between NPDW (2,300 m water depth) and NADW during HE 1 is documented by Sarnthein et al. (2013). Another proxy is the $\delta^{13}C_{bf}$ difference between two sites ($\Delta\delta^{13}C_{bf}$), which can be used as a proxy for NPIW or NADW formation (Knudson and Ravelo, 2015). A cross-spectral analysis of $\Delta\delta^{13}C_{bf}$ over 1.2 Myr does not exhibit an anti-correlation between NPIW (818 m) and NADW, and it challenges the orbital-scale "seesaw" behavior (Knudson and Ravelo, 2015). This disagreement among proxies may be due to several factors. First, the uncertainty in the carbon reservoir age leads the authors to propose incompatible NPDW behavior. For example, Okazaki et al. (2010) applied a smaller reservoir age (ΔR = 100 yr) than Max et al. (2014) (ΔR = 900 yr), which led them to propose NPDW formation during the cold HE 1 (Okazaki et al., 2010) and during the warm Bølling/Allerød (Max et al., 2014). Second, water mass-dependent variation in $\delta^{13}C_{bf}$ can be smoothed out by biological productivity, air-sea gas exchange and/or calcite preservation. Third, the seesaw behavior may be episodic, e.g., only when freshwater discharge interrupts NADW formation like during HE 1. Therefore, a sufficient data-set covering multiple glacial-interglacial cycles with different proxies is necessary.

The Nd isotope ratio is a quasi-conservative water mass tracer (Frank et al., 2002; Rutberg et al., 2000). ^{143}Nd is the daughter isotope of ^{147}Sm, and the $^{143}Nd/^{144}Nd$ ratio in rocks is primarily determined by their Sm/Nd ratio and age. The Nd isotopic composition is reported as ε_{Nd}, where $\varepsilon_{Nd} = [(^{143}Nd/^{144}Nd)_{sample}/(^{143}Nd/^{144}Nd)_{CHUR} - 1]\times10^4$ and $(^{143}Nd/^{144}Nd)_{CHUR}$ is 0.512638 (Jacobsen and Wasserburg, 1980). The ε_{Nd} values of local rocks influence those of adjacent sea

water, as indicated by the similarity of ε_{Nd} values between the ocean and the surrounding continents (e.g., Arsouze et al., 2007; Lacan and Jeandel, 2005). For example, the ε_{Nd} values of the Pacific Ocean (ε_{Nd} ~0 to +4) surrounded by young volcanic rocks are more radiogenic than the Atlantic Ocean (ε_{Nd} ~-13) surrounded by old continental rocks, and ε_{Nd} in the Circumpolar Deep Water (CDW) is intermediate, reflecting mixture of the two water masses (ε_{Nd} ~-9 to -6) (data from Albarède and Goldstein, 1992 and references therein; Albarède et al., 1997). This pattern attests to the residence time of Nd shorter than the ocean mixing time (Tachikawa et al., 1999) and to the utility of Nd isotopes as a quasi-conservative water mass tracer. The good correlation between ε_{Nd} and the salinity of seawater supports the effectiveness of this proxy (von Blanckenburg, 1999).

The bottom water ε_{Nd} is regulated by external and internal sources. External Nd sources are lateral advection (e.g. mixing between NADW and CDW; Rutberg et al., 2000) and vertical mixing (e.g. NADW formation) of water masses, and internal sources are boundary exchange (e.g., Arsouze et al., 2007) and pore water diffusion (e.g., Abbott et al., 2015). In the Atlantic, water circulation is relatively fast and vigorous due to NADW formation, and the effectiveness of internal sources is reduced. Thus, ε_{Nd} can be used as a water mass tracer (Siddall et al., 2008). In the Pacific, water circulation is more sluggish (Siddall et al., 2008), and internal sources need to be taken into account. Indeed, ε_{Nd} change in Pacific deep waters at present cannot be interpreted solely by water mass mixing (Abbott et al., 2016). Likewise, negligible NPIW formation in the Bering Sea at present (Warner and Roden, 1995) implies that seawater ε_{Nd} is mainly determined by internal sources. However, stronger NPIW formation in the Bering Sea in the past may switch the main Nd source from internal to the external, and provide the

perspective on the interplay between external and internal sources controlling bottom water ε_{Nd}.

We use the authigenic Fe-Mn oxyhydroxide coating of marine sediments as an archive of seawater Nd isotopic composition. Dissolved Nd is incorporated into the authigenic coating when it precipitates. Because this Fe-Mn oxyhydroxide coating is extracted from bulk sediments using chemical reagents, the dissolution of labile non-authigenic material (e.g., volcanic material) during the leaching process may bias the Nd isotope ratios (Roberts et al., 2010). The potential incorporation of non-authigenic components is tested by comparing the ε_{Nd} of bulk sediment leachate with that of biogenic material such as foraminifera or coral reef (Martin and Scher, 2004; Roberts et al., 2010; van de Flierdt et al., 2010). In these tests, elemental concentration criteria (e.g., Al/Nd and REE pattern) are used to verify the authenticity of the leachates (Blaser et al., 2016; Martin et al., 2010; Wilson et al., 2013).

Here, we provide orbital-scale variations in NPIW at 1,008 m using the isotope ratio of seawater-originated Nd on the Bering Slope, the most probable location of NPIW formation within the Bering Sea, as inferred from the distribution pattern of the *C. davisiana* during the LGM (Ohkushi et al., 2003). With the Nd isotope record, we can constrain whether NPIW formation or boundary exchange processes control the bottom water ε_{Nd} on the Bering Slope. Then, we examine the relationships between NPIW formation and cold climate and between NPIW and NADW.

3.2. Materials

3.2.1. Sampling location

Sediment core samples are from site U1345 (60°9'N, 179°28'W; 1,008 m water depth), drilled on the western part of the Bering Slope during the Integrated Ocean Drilling Program Expedition 323 (Fig. 3.1). Site U1345 is influenced by tidal mixing and the Bering Slope Current (BSC) that flows westward along the continental shelf. This water circulation contributes to the high nutrient concentration and high biological productivity at this site (Springer et al., 1996), and the high sedimentation rate (> 30 cm/kyr) is favorable for obtaining a high-resolution record. This site is near the present-day maximum sea ice extent (Katsuki and Takahashi, 2005) and is located in the modern oxygen minimum zone (OMZ) (Takahashi et al., 2011).

From a geological perspective, potential Nd sources to this site are the unradiogenic inflow from North America, e.g., the particulate matter carried by the Yukon River (ε_{Nd} ~-10.1 to -8.4)(data from VanLaningham et al., 2009), and the radiogenic inflows from the Aleutian Arc and the Kamchatka Arc, which are mainly composed of volcanic rocks (ε_{Nd} ~+6 to +10 and +6 to +9, respectively) (data from GEOROC, 2003) (Fig. 3.1). The Anadyr River in Siberia (ε_{Nd} ~-2 to +3) can be a possible source in case of low sea level (see section 3.4.3.1) (Fig. 3.1). The inflow from Kamchatka seems to be relatively small in terms of present-day water circulation.

3.2.2. *Core description*

Among the five cores (Holes A to E) at site U1345, we used Hole A

(60°9.19’N, 179°28.20’W; 1,007.3 m water depth; core depth 147.43 mbsf) as the main core to reconstruct Nd isotope ratios and Hole C (60°9.21’N, 179°28.22’W; 1,008.8 m water depth; core depth 148.53 mbsf) and D (60°9.22’N, 179°28.23’W; 1,008.3 m water depth; core depth 150.51 mbsf) as sub cores to complement its continuity. The stratigraphic correlation between them was based on the Whole-Round Multisensor Logger magnetic susceptibility (MS) data, gamma ray attenuation (GRA) bulk density, natural gamma radiation (NGR) count and color reflectance parameter b* data (Expedition 323 Scientists, 2011), and the revised depth scale is expressed in CCSF-A (m).

The sediments are mainly siliciclastic with a varying amount of diatoms and typically < 10% foraminifers and calcareous nannofossils. Laminations usually appear in diatom-rich layers with lower MS, GRA bulk density and NGR counts and higher b* values. Shipboard observations report a few ash layers in U1345A (0–4.39 CCSF-A (m)), U1345C (0.09–6.05 and 112.62–122.70 CCSF-A (m)), and U1345D (135.76–145.70 CCSF-A (m)), but ash layers are probably more widespread (Expedition 323 Scientists, 2011).

We applied the age model constructed by Cook et al. (2016). Eleven age control points were assigned based on the correlation of the oxygen isotope ratio of benthic foraminifera ($\delta^{18}O_{bf}$) with the global LR04 stack. The age of U1345 extends to ~520 ka, and the average sedimentation rate is ~31.3 cm kyr^{-1} without a significant difference between glacial (20.7–45.1 cm kyr^{-1}) and interglacial periods (19.7–46.4 cm kyr^{-1}).

3.3. Method

Ninety-seven *Wilson Authigenic* and one *Rutberg Authigenic* were used for reconstruction of the past oceanic neodymium isotopic composition (see chapter 2). Included were five samples from the four ash layers (see section 3.2.2). The average depth and age interval between samples are ~1.7 CCSF-A (m) and 5.3 kyr, respectively. Each sample covers 10 to 100 yr.

3.4. Results and Discussion

3.4.1. Temporal variation of ε_{Nd} over 520 kyr

3.4.1.1. Authigenic ε_{Nd} record

The uppermost sample (1.3 ka) at site U1345 has an authigenic ε_{Nd} value of -3.7±0.4 (2σ) (Fig. 3.3B and Table 3.1). It is significantly lower than the core top ε_{Nd} of Fe-Mn oxide from nearby site MR06-04-24 (-1.9±0.4, and -1.4±2.7) (60˚15.7'N, 179˚25.34'E, 851 m water depth; Asahara et al., 2012). This may be due to the age difference, different sample treatment method and/or recent invasion of volcanic material into the bottom water and *in situ* dissolution. The core top authigenic ε_{Nd} values increase southward. For instance, site U1345 in the mid-Holocene (4.3 ka) (-3.2±0.2) and early-MIS 6 (177 ka) (-3.3±0.2) is less radiogenic than at Bowers Ridge at 5.2 ka (-0.94±0.16) (BOW-8A; Horikawa et al., 2010) or the subarctic N. Pacific (-2.23±0.18, -2.41±0.22 at 180 ka) (13D-27A, 51˚27.8'N, 167˚38.2'E, 1800-1500 m water depth; van de Flierdt et al., 2004) (Fig. 3.1). The authigenic ε_{Nd} of U1345 is persistently lower than BOW-8A over the past 145 kyr (Fig. 3.2). The primary reason seems to be the diminishing influence from unradiogenic N. America with distance.

The average ε_{Nd} of the authigenic fraction over the last 520 kyr is -3.3±0.9 (1σ, n = 98), with large temporal variations (Fig. 3.3B). Radiogenic ε_{Nd} peaks beyond 1σ (-2.4 – -1.8) occur at the MIS 11/10 boundary, MIS 10, MIS 9, late MIS 8, late MIS 6, the MIS 5/4 boundary, and MIS 4 (dashed vertical lines in Fig. 3.3). Unradiogenic ε_{Nd} peaks beyond 1σ (-5.6 – -4.1) occur at the MIS 13/12 boundary, early-MIS 12, mid-MIS 12, MIS 7, mid-MIS 6, early-MIS 5, mid-MIS 5, and the MIS 2/1 boundary (dotted vertical lines in Fig. 3.3). The event at the MIS 2/1 boundary includes four different data points ~1,500 years apart. The higher ε_{Nd} signals are associated with cold stages, while the lower ε_{Nd} values occur during warm stages. However, there are exceptions, such as MIS 9 with higher ε_{Nd} and MIS 12 and mid-MIS 6 with lower ε_{Nd}. Horikawa et al. (2010) maintained that radiogenic ε_{Nd} peaks occurred during cold periods over 150 ka, and our ε_{Nd} result generally supports theirs for the past 150 kyr, but the correlation cannot be substantiated beyond that.

3.4.1.2. *Detrital ε_{Nd} record*

The average ε_{Nd} of the detrital fraction is -7.8 ± 0.9 (1σ, n = 48) (Fig. 3.3B). This value is closer to the less radiogenic N. America (ε_{Nd} ~-10.1 to -8.4) than to the radiogenic Aleutian Arc (ε_{Nd} ~+6 to +10), Kamchatka Arc (ε_{Nd} ~+6 to +9) and Siberia (ε_{Nd} ~-2 to +3). The lowest ε_{Nd} is -10.3, which is very similar to the Yukon River bedload (-10.1) (data from VanLaningham et al., 2009). The maximum ε_{Nd} is -5.7, indicating an increase in but still minor contribution of the radiogenic Aleutian Arc and Siberia. Unradiogenic ε_{Nd} values (< -8.7) occur in late MIS 10, MIS 7, mid-MIS 6, and at the MIS 2/1 boundary, while radiogenic values (> -6.9) are observed in MIS 11, early MIS 10, MIS 8, and at the MIS 4/3

boundary. The general feature is similar to the authigenic fraction, with a moderate positive correlation between the authigenic and detrital fractions ($r^2 = 0.45$, n = 40). The correlation is strong ($r^2 = 0.51$, n =22) where the ε_{Nd} values of the authigenic fraction are below average (-3.2) but are very weak when they are above average ($r^2 = 0.08$, n = 18).

3.4.2. *Mechanisms for authigenic ε_{Nd} variation on the Bering Slope*

At present, NPIW formation in the Bering Sea is weak (Warner and Roden, 1995). In the absence of NPIW formation, possible mechanisms for changing seawater ε_{Nd} at intermediate water depths are (1) lateral advection, (2) boundary exchange (e.g., Arsouze et al., 2007), and (3) pore water diffusion (e.g., Abbott et al., 2015). The Nd of bottom water at site U1345 is a sum of the laterally advected water mass plus the addition from internal sources (the terms in parentheses of equation 1 below) as the water mass travels to site U1345.

$$\varepsilon_{Nd,U1345} = \varepsilon_{Nd,adv} \cdot f_{Nd,adv} + \left(\varepsilon_{Nd,BE} \cdot f_{Nd,BE} + \varepsilon_{Nd,pw} \cdot f_{Nd,pw}\right) \quad (1)$$

$$f_{Nd,adv} + \left(f_{Nd,BE} + f_{Nd,pw}\right) = 1 \quad (2)$$

where f_{Nd} is the fraction of Nd flux from lateral advection (adv), boundary exchange (BE), and pore water diffusion (pw).

First, a comparison to the existing ε_{Nd} record at BOW-8A on the Bowers Ridge enables us to apply the two equations. The ε_{Nd} of BOW-8A ranges from -2 to +1 over 150 kyr and is always more radiogenic than site U1345 (Fig. 3.2). There are two possible interpretations for this ε_{Nd} gap between two sites. One is that there

are two distinct water masses with different ε_{Nd} values. Since the general circulation direction is counter clockwise in the Bering Sea (Fig. 3.1), the implication is that there is a hydrographic boundary between 884 and 1,008 m water depths in the Bering Sea and by extension also in the N. Pacific. However, the potential temperature gradient between the two depths in the N. Pacific (north of 47°N) is less than 0.5°C (Roemmich and McCallister, 1989 and references therein). The alternative interpretation is that ε_{Nd} is altered along the circulation path from BOW-8A to U1345 by internal sources. An ε_{Nd} gap between two sites is maintained at 2 to 3 ε_{Nd} over 150 kyrs, except for two time intervals when external sources are involved (see section 3.4.3.1 and 3.4.3.2; Fig. 3.2). The ε_{Nd} of internal source seems to be unradiogenic, since ε_{Nd} becomes more unradiogenic from site BOW-8A to U1345.

For the lateral advection term, $\varepsilon_{Nd,adv}$, we used the authigenic ε_{Nd} of BOW-8A (data from Horikawa et al., 2010). As discussed above, the difference between BOW-8A and U1345 are due to internal sources, and we consider BOW-8A to record the initial water mass value as it travels to site U1345 (Fig. 3.1).

The term boundary exchange "encompasses all chemical transfer reactions among particles and seawater, including adsorption/desorption, ion exchange, and dissolution/precipitation reactions" (Jeandel and Oelkers, 2015), and the importance of boundary exchange on the oceanic budget of Nd has been attested to by various field data and model simulations (Arsouze et al., 2007; Lacan and Jeandel, 2001; Lacan and Jeandel, 2005). Because site U1345 is on the continental margin, it is susceptible to boundary exchange. The dissolution of unradiogenic detrital fractions on the continental margins (Fig. 3.1) may supply unradiogenic Nd into the bottom water. The decrease in authigenic ε_{Nd} from BOW-

8A to U1345 is consistent with this (section 3.4.1.1 and Figs. 3.1 and 3.2).

Next, we will consider the pore water diffusion. Pore water diffusion results from Nd liberation during sediment diagenesis and subsequent upward diffusion to the bottom water (Abbott et al., 2015). Abbott et al. (2015) propose two mechanisms that determine the ε_{Nd} of pore water. One is isotopic exchange with reactive authigenic coating. This implies that the ε_{Nd} of pore water is determined by isotopic equilibrium with past seawater signal (i.e. authigenic coating). In order for the pore water diffusion to add radiogenic Nd, older authigenic coatings should be more unradiogenic. However, this is not what is observed in the authigenic record at U1345. The other mechanism is preferential dissolution of radiogenic minerals, but as was seen in comparison to BOW-8A record (Fig. 3.2), this is not significant at U1345. If there is preferential dissolution of radiogenic minerals (e.g. Aleutian origin volcanic material) during diagenesis, pore water should supply radiogenic Nd into the bottom water, which is inconsistent with unradiogenic ε_{Nd} shift from BOW-8A to U1345 (Fig. 3.2). For this reason, we propose that pore water diffusion is not a primary source for Nd in the Bering Sea.

A comparison of authigenic and detrital ε_{Nd} records at site U1345 (Fig. 3.3) offers supporting evidence that pore water diffusion is a minor internal source of Nd compared to boundary exchange on the Bering Slope. The similar pattern suggests that detrital ε_{Nd} affects the bottom water ε_{Nd} through boundary exchange. If pore water diffusion were an also important internal source to bottom water ε_{Nd} (Abbott et al., 2016), one would expect a time lag in the authigenic record, because pore water diffusion liberates past seawater signal captured in authigenic coatings of deposited sediments. The depth below the sediment-water interface where Nd is

liberated will vary with the productivity and redox conditions. At present the pore water profile of dissolved Nd (Nd_{pw}) at U1345 is relatively unvarying with depth compared to heavier REEs which display a large peak below the sulfate-methane transition zone (6.5 CCSF-A (m) from Soyol-Erdene and Huh, 2013) due to the reduction of Fe and Mn minerals associated with the anaerobic oxidation of methane. If we take the minor Nd_{pw} peak at 2.5 CCSF-A (m) attributed to the release during organoclastic reduction of Mn oxides, then the estimated time lag is approximately 10 kyrs. We do not observe such time lag in the authigenic record vs. the detrital. Accordingly, we are convinced that boundary exchange is the main mechanism changing seawater ε_{Nd} at this intermediate water depth on the Bering Slope.

We calculated the contribution from boundary exchange ($f_{Nd,BE}$) along the Bering Slope using equations (1) and (2) for two time periods, ~13 ka in the Last Glacial Termination and ~20 ka at the LGM. For simplification, we assumed that the Nd flux from pore water diffusion is insignificant ($f_{Nd,pw} \approx 0$). At ~13 ka, we assumed the laterally advected water mass to have $\varepsilon_{Nd,adv}$ = -2 (from authigenic ε_{Nd} at BOW-8A), boundary exchange on the continental margin to have $\varepsilon_{Nd,BE}$ = -9.5 (from detrital ε_{Nd} at U1345), and NPIW to have $\varepsilon_{Nd,U1345}$ = -5 (from authigenic ε_{Nd} at U1345). The result is that ~40% of the bottom water Nd at U1345 is derived from boundary exchange on the continental margin at ~13 ka, which is slightly higher than was estimated for the Madagascan margin (~30% from Wilson et al., 2012). The result for the LGM is slightly lower (~30%), probably due to low sea level conditions. Preferential release of radiogenic Nd by boundary exchange is not considered here (Noble et al., 2013; Wilson et al., 2012),

and detrital ε_{Nd} on the eastern part of the Bering shelf is more radiogenic than what we assumed for $\varepsilon_{Nd,BE}$ (Fig. 3.1), so the contribution from boundary exchange is a lower estimate. If we take the water transport time from BOW-8A to U1345 of 200 years (maximum estimate from modeling of ^{14}C data; Matsumoto, 2007), maximum water residence time for Nd is ~700 years, broadly consistent with currently accepted values (Tachikawa et al., 1999).

Consequently, we propose that boundary exchange is the main mechanism that influences the Nd isotopic composition in the Bering Sea, with a minor contribution from pore waters. It is important to note that boundary exchange processes supply unradiogenic Nd, and hence, NPIW formation is the only mechanism that can introduce radiogenic Nd to site U1345.

3.4.3. *NPIW formation*

It is likely that NPIW formed by brine rejection during sea ice formation (e.g., Haley et al., 2007; Jang et al., 2013). Being at the edge of the present-day maximum sea ice extent, there is potential for intensified brine formation at site U1345 (Rella et al., 2012). A useful proxy in this regard is $\Delta\delta^{18}O_{bf}$, the $\delta^{18}O_{bf}$ difference between sites at different water depths (sites U1339, U1342 and U1345) (Fig. 3.3F). Indeed, the $\Delta\delta^{18}O_{bf}$ values attest to periods of brine rejection within the Bering Sea (Cook et al., 2016; Knudson and Ravelo, 2015). For example, the glacial $\delta^{18}O_{bf}$ at site U1339 (54°40N, 169°59W; eastern Bering Slope) at a water depth of 1,867 m is 0.4 – 0.8 ‰ lighter than at site U1342 (54°50N, 176°55W; Bowers Ridge) at a water depth of 818 m (Cook et al., 2016). This is larger than the difference at present (~0.3 ‰), suggesting that brine rejection delivered the extremely low-$\delta^{18}O$ surface water to greater depths during the glacial (Brennan et

al., 2013; Hillaire-Marcel and de Vernal, 2008).

Neodymium isotopic composition records more "local" NPIW events. We observe a few time intervals where $\delta^{18}O_{bf}$ gradients between sites U1339 and U1345 are larger than at the present (Fig. 3.3F); however, not all of them have coincident ε_{Nd} excursions (e.g., MIS 2). One possible explanation is that NPIW did not originate in the Bering Sea. Let us suppose that NPIW forms by brine rejection in the Okhotsk Sea and flows into the Bering Sea. This water mass transfers light $\delta^{18}O$ to the Bering Sea, but the ε_{Nd} of the water mass is modified by boundary exchange during transit due to the short residence time of Nd (Tachikawa et al., 1999) (see section 4.3). Alternatively, if the ε_{Nd} of the sinking surface water is similar to that of the bottom water, the ε_{Nd} of the bottom water would not change even though NPIW forms. A third possibility is that the ε_{Nd} change by NPIW formation is muted when other Nd sources change the ε_{Nd} value in the opposite direction. Whichever the case may be, the Nd isotopic composition has an advantage in recording "local" NPIW formation events in the Bering Sea and pinpointing its source, although it may not record all events. This proxy can also provide ancillary information about boundary exchange.

Here, we focus on the ε_{Nd} variations to trace local NPIW formation on the Bering Slope and to constrain other Nd sources. We compare ε_{Nd} with biological proxies such as $\Delta\delta^{18}O_{bf}$ values, opal content, % sea-ice related diatoms, and the abundance of *B. aff. Exilis*. The $\delta^{18}O_{bf}$ values of sites U1339, U1342 and U1345 give perspective on the water mass properties at different depths (data for U1339 and U1345 from Cook et al., 2016; data for U1342 from Knudson and Ravelo, 2015). In particular, a large $\Delta\delta^{18}O_{bf}$ reflects the occurrence of brine rejection from shallower depths. The opal content is used as an indicator of biological productivity

here, with the high opal content typically associated with low GRA bulk density, low NGR count, and high color reflectance b* value (not shown). Sea-ice related diatoms include *T. antarctica* spores, *B. fragilis*, *D. confervacea*, *T. hyalina*, *P. glacialis* and *F. cylindrus* (data from Expedition 323 Scientists, 2011). They can trace sea ice expansion in the Bering Sea. Considering the trace amount of brine rejection at present (Warner and Roden, 1995), NPIW formation may have occurred when the percentage of sea-ice diatoms was higher than the modern value of 30%. *B. aff. Exilis* is one of the benthic foraminifera species (data from Expedition 323 Scientists, 2011) that has been used to indicate low oxygen conditions at depth (Bubenshchikova et al., 2008; Kaiho, 1994). At present, low ventilation and enhanced biological respiration accompanying high productivity cause *B. aff. Exilis* to flourish. On the other hand, low productivity and/or vigorous ventilation processes can reduce *B. aff. Exilis*.

3.4.3.1. Periods of radiogenic Nd input

We can attribute the radiogenic ε_{Nd} peaks to either NPIW formation from radiogenic surface water, a decrease in the extent of boundary exchange supplying unradiogenic Nd (section 4.3), or a combination of the two. Seawater that has circulated past the Anadyr River mouth and/or the Aleutian Arc can supply radiogenic Nd. At present, the Anadyr River water mainly flows through the Bering Strait into the Arctic Ocean, but model simulations suggest that it diverts into the Bering Sea if the Strait is closed (Hu et al., 2012b). All radiogenic events except for MIS 9 occur when the Bering Strait is nearly or completely closed, and in such cases, the Anadyr River is a possible additional radiogenic source (Fig. 3.3G, dashed vertical lines). We rule out the contribution from Kamchatka, because that

water mass mainly flows out along the western boundary to the N. Pacific regardless of sea level (Hu et al., 2012b). We will examine the seven radiogenic ε_{Nd} periods in four categories, starting with the proposed NPDW formation at the MIS 11/10 boundary, the NPIW formation at MIS 9, and the weak NPIW formation at MIS 10 and 6, the MIS 5/4 boundary, and MIS 4 (Fig. 3.3). Finally, there is no dense water formation at MIS 8.

The event at the MIS 11/10 boundary is possibly related to NPDW formation. The similar $\delta^{18}O_{bf}$ values at sites U1339, 1342, and 1345 indicate homogeneity of the water column between 818 and 1,867 m depths. The $\delta^{18}O_{bf}$ are ~0.2‰ lighter than the global LR04 stack, suggesting input of light surface water all the way down to 1,867 m (Fig. 3.3F). High % sea-ice diatoms and low *B. aff. Exilis* support dense water formation triggered by brine formation (Figs. 3.3D and E). Because the sea level was relatively low, the Anadyr River was an additional radiogenic source (Fig. 3.3G). Dynamic ocean circulation triggered by dense water formation probably decreased exposure time for boundary exchange and limited its effect (Siddall et al., 2008; Stewart et al., 2016). Hence, the radiogenic ε_{Nd} value at the MIS 11/10 boundary results from NPDW formation entraining radiogenic Nd and weakened unradiogenic Nd input.

The radiogenic signal during the peak interglacial at MIS 9 is an example of NPIW formation. The $\delta^{18}O_{bf}$ value of site U1345 is similar to that of site U1342 and is ~0.6‰ lower than that of site U1339 (Fig. 3.3F). This means that the water column between 818 and 1,008 m was homogenous and that the hydrographic boundary lay between 1,008 and 1,867 m, i.e., brine intruded to at least a ~1,008 m depth. Higher-than-modern % sea-ice diatoms are consistent with this interpretation (Fig. 3.3D). *B. aff. Exilis* decreases (Fig. 3.3E), and the opal content

increases during the same period (Fig. 3.3C). The unradiogenic input from boundary exchange was probably reduced due to the short exposure time.

The radiogenic events at MIS 10 and 6, the MIS 5/4 boundary, and MIS 4 result from weak NPIW formation. During these events, the $\delta^{18}O_{bf}$ values at site U1345 are between those at sites U1339 and 1342: they are 0.30 – 0.35‰ lighter than at site U1339 and 0.15 – 0.50‰ heavier than at site U1342 (Fig. 3.3F). This suggests that surface water only partially penetrated to ~1,008 m. High % sea-ice diatoms and low *B. aff. Exilis* support brine-induced NPIW formation—Late MIS 6 is an exception, as it may be an artifact of the low sample resolution (Figs. 3.3D and E). At these times, the sea level was low, and the nearly or completely closed Bering Strait implies inflow of the Anadyr River component in addition to the usual Aleutian Arc component (Fig. 3.3G). Model simulations predict a reduction in the Yukon River discharge by 78% during glacial periods. It can promote NPIW formation by increasing surface water salinity (Kim and Park, 2008). The diminished ε_{Nd} gap between sites U1345 and BOW-8A at MIS 4 supports the radiogenic NPIW formation on the Bering Slope as well as weakened unradiogenic flux due to low exposure time (Fig. 3.2, blue bar).

Whether NPIW formed at MIS 8 is highly uncertain. The $\delta^{18}O_{bf}$ value at site U1345 is indistinguishable from that at site U1339 but is significantly heavier than at site U1342 (~0.9‰) (Fig. 3.3F). This means that NPIW, if present, occupied a water depth shallower than ~1,008 m and that the water column between ~1,008 and 1,867 m was homogeneous. The low abundance of *B. aff. Exilis* can be attributed to the low oxygen consumption rather than to ventilation processes (Fig. 3.3E), which is consistent with the low opal content. Radiogenic ε_{Nd} of detrital fractions (Fig. 3.3A) implies that boundary exchange supplied radiogenic Nd.

In summary, we suggest that most radiogenic ε_{Nd} excursions record dense water formation such as NPIW and NPDW except for MIS 8 (Fig. 3.4A). The most probable sources for radiogenic Nd are the inflow from the Anadyr River and the Aleutian Arc, which penetrate to greater depths *via* brine formation. The radiogenic ε_{Nd} excursions during MIS 8 may be due to boundary exchange with radiogenic detrital material rather than formation of NPIW. The relationship between NPIW/NPDW formation and the closure of the Bering Strait as suggested by Knudson and Ravelo (2015) is circumstantial. Exceptionally, NPIW formation occurred at MIS 9, when the sea level was comparable to that of the present.

3.4.3.2. *Periods of unradiogenic Nd input*

The unradiogenic peaks result from an increase in NPIW formation from unradiogenic surface water, an increase in boundary exchange, or a combination of the two. The probable unradiogenic source to surface water is riverine or groundwater input from N. America, which is stronger during warm periods (Kim and Park, 2008). Under higher sea level conditions, the unradiogenic character is accentuated due to the lack of input from the Anadyr River. The six unradiogenic ε_{Nd} periods will be discussed in two categories, starting with NPIW formation in the mid-MIS 6 and mid-MIS 5 and no dense water formation at the MIS 13/12 boundary, early-MIS 12, mid-MIS 12, and MIS 7 (Fig. 3.3).

We consider the unradiogenic events in mid-MIS 6 and mid-MIS 5 to be partially influenced by NPIW formation. The situation is similar to the radiogenic event at MIS 10. A decreasing trend of $\delta^{18}O_{bf}$ from deep (U1339) to shallow (U1342) sites is observed, with site U1345 0.3 – 0.4‰ lighter than site U1339 and 0.2 – 0.3‰ heavier than U1342. This suggests that a portion of the surface water

sank to ~1,008 m. Brine formation is probable, based on the higher % sea-ice diatoms than present (Fig. 3.3D). *B. aff. Exilis* is abundant, although lower than at present. Intermediate to high opal productivity may cause low oxygen conditions even with partial ventilation, or this may be an artifact of the low sample resolution. The relatively low ε_{Nd} of the detrital fraction indicates that NPIW formation in mid-MIS 6 and mid-MIS 5 had unradiogenic Nd sources (Fig. 3.3A).

The unradiogenic events at the MIS 13/12 boundary, early-MIS 12, mid-MIS 12, and MIS 7 probably transpired through boundary exchange rather than NPIW formation (Fig. 3.4B). The $\delta^{18}O_{bf}$ values at site U1345 are similar to those of site U1339 at those times but are significantly heavier than at site U1342 (0.3 – 0.7‰) (Fig. 3.3F). The percent sea-ice diatoms are similar to those of the present. This implies the absence of NPIW formation at ~1,008 m. The oxygen-poor environment indicated by high *B. aff. Exilis* and/or lamination at those times is consistent with this implication (Fig. 3.3E). MIS 7 is an exception with low *B. aff. Exilis* and yet has lamination. The boundary exchange process may provide more unradiogenic Nd, considering the lower ε_{Nd} of the detrital fractions than average at those times (Fig. 3.3A) and stagnant bottom water waters in the absence of dense water formation (Siddall et al., 2008; Stewart et al., 2016).

We do not evaluate the unradiogenic events in early-MIS 5 and at the MIS 2/1 boundary. The $\delta^{18}O_{bf}$ value of site U1345 in early-MIS 5 is 0.3 and is ~1‰ heavier than U1339 and U1342, respectively. This inverse $\delta^{18}O_{bf}$ feature between sites U1345 and U1339 may be attributed to age uncertainty due to poor microfossil preservation in U1345 (Cook et al., 2016). The event at the MIS 2/1 boundary is more complicated. It includes four unradiogenic ε_{Nd} data points associated with different $\Delta\delta^{18}O_{bf}$ features: partial NPIW (similar to mid-MIS 5),

inverse $\Delta\delta^{18}O_{bf}$ (similar to early-MIS 5), no NPIW (similar to MIS 7), and inverse $\Delta\delta^{18}O_{bf}$ again, consecutively. This ambiguous $\Delta\delta^{18}O_{bf}$ series may reflect abrupt climate change during deglaciation or age uncertainty (several thousand years; Cook et al., 2016).

In summary, the Nd isotopic composition can trace "local" dense water formation on the Bering Slope when ε_{Nd} of surface water is distinct from that of deep water. We can detect NPIW/ NPDW formation at the MIS 11/10 boundary, in MIS 10 and 9, mid and late-MIS 6, mid-MIS 5, at the MIS 5/4 boundary, and in MIS 4. Considering $\Delta\delta^{18}O_{bf}$ between three sites (U1339, U1342, and U1345), we can estimate the intrusion depths (star symbols in Fig. 3.3). Whereas NPIW was observed regularly during extreme glacials (closed Bering Strait) at the relatively shallow U1342 (Knudson & Ravelo, 2015), NPIW episodes were short and did not regularly occur during all extreme glacials at the deeper U1345. This difference results from variation in the intrusion depth of NPIW, so the events detected by ε_{Nd} at site U1345 indicate more vigorous ventilation.

3.4.4. *Relationship between NPIW and NADW*

We examine the hypothesis concerning alternating strengths of NPIW and NADW (the seesaw hypothesis) by comparing the ε_{Nd} of the Bering Slope (site U1345) and the S. Atlantic (Fig. 3.5). The S. Atlantic records are from cores GeoB3808-6 (30.8°S, 14.7°W; 3,213 m water depth), core ODP 1088 (41.8°S, 13.3°E; 2,082 m water depth), and ODP 1087 (31.3°S, 15.2°E; 1,372 m water depth), which extend to 145 ka (Jonkers et al., 2015), 135 ka, and 200 ka, respectively (Hu et al., 2016). The deeper sites GeoB3808 and ODP 1088 are currently bathed by the lower and upper NADW and are well suited to monitor the

varying strength of NADW. ODP 1087 is shallower than the depths of NADW but displays very similar ε_{Nd} pattern to ODP 1088 during cold period such as MIS 4 and 2 (Hu et al., 2016). Thus, as GeoB3808 and ODP 1088 do not extend to MIS 6, we used ODP 1087 to gain a perspective on the ε_{Nd} variation beyond 145 ka. The low (high) ε_{Nd} of S. Atlantic cores result from northern (southern) component water and indicates strong (weak) NADW formation.

The premise of the seesaw hypothesis is that when NADW formation is diminished, NPIW formation regulates global climate system by driving global ocean circulation and by distributing heat from equator to pole (Okazaki et al., 2010). According to the seesaw hypothesis, periods of strong NPIW should correlate with those of weak NADW. The four NPIW periods over the last 200 kyrs in the Bering Sea coincided with periods of NADW reduction (Fig. 3.5). The NPIW formation with radiogenic excursions in late MIS 6 and MIS 4 on the Bering Slope coincides with the reduction in NADW, as do less certain events with unradiogenic ε_{Nd} in mid MIS 6 and mid-MIS 5. At those times, NPIW may have regulated the global climate system as a reservoir for carbon dioxide and as a heat distributor. However, the NADW reduction in mid-MIS 5 is only detected on ODP 1088 with 1.1 ε_{Nd} shift, and NADW variation recorded in GeoB3808 is relatively small. This site-dependent seesaw is probably due to the modest NADW change in mid-MIS 5 (Hu et al., 2016), different water mass source in the eastern and western basins of Atlantic Ocean (Oliver et al., 2010), or low sampling resolution in GeoB3808. We do not detect NPIW formation on the Bering Slope during the LGM when NADW formation is strongly reduced. Considering the low $\delta^{18}O_{bf}$ during the LGM (Cook et al., 2016), NPIW formation may have formed in other N. Pacific sites, or the ε_{Nd} records on NPIW formation in the Bering Sea may be

muted by boundary exchange (see section 4.4). In summary, the strength of NPIW is generally anti-correlated with that of NADW, supporting seesaw hypothesis (e.g. Hu et al., 2012a; Okazaki et al., 2010; Saenko et al., 2004). We could not resolve the NPIW-NADW seesaw across all climate transitions. An extended authigenic ε_{Nd} record in the Atlantic Ocean would be desirable for comparison to our record.

3.5. Conclusion

We reconstructed a 520-kyr record of the neodymium isotope ratio of the bottom water on the Bering Slope using the *Wilson* method that omitting the carbonate removal step and adopting a low reagent-to-sediment ratio. The reconstructed bottom water ε_{Nd} at site U1345 shows two features: radiogenic ε_{Nd} peaks and unradiogenic ε_{Nd} troughs. The authigenic ε_{Nd} variations represent an interplay between NPIW formation and boundary exchange. The radiogenic ε_{Nd} values seems to result from the dense water formation containing radiogenic Nd. Enhanced sea ice can trigger brine formation, and consequent North Pacific Intermediate Water (NPIW) can transport radiogenic Nd from the surface to depth. Such dynamic bottom water conditions can reduce the contact time between unradiogenic sediments and overlying water, resulting in diminished boundary exchange and enhanced radiogenic peaks. The magnitude of NPIW remains uncertain given available data. The unradiogenic ε_{Nd} events are primarily affected by boundary exchange processes. In the absence of NPIW formation, the contact time between sediments and overlying water should be longer, and hence unradiogenic Nd input from boundary exchange seems to be stronger. Exceptionally, the unradiogenic events in mid-MIS 6 and mid-MIS 5 may still be

related to NPIW formation.

The first bottom water ε_{Nd} reconstruction in the Bering Sea covering the last 520 kyr allows us to evaluate the NPIW-North Atlantic Deep Water (NADW) seesaw hypothesis suggested by many models (Hu et al., 2015; Okazaki et al., 2010). A tentative comparison with ε_{Nd} records from the S. Atlantic sites GeoB3808, ODP 1088 and ODP 1087 covering the last 200 kyr suggests that the NPIW formation in the Bering Sea played an important role in sequestering CO_2 into the bottom water and in regulating the global heat distribution when NADW was reduced during mid-MIS 6, late-MIS 6, mid-MIS 5 and MIS 4. Obtaining an extended authigenic ε_{Nd} record in the Atlantic Ocean will allow us to evaluate the seesaw hypothesis more fully.

Acknowledgements

This research was supported by the NRF Mid-Career Researcher Program (NRF-2011-0015174) and Basic Science Research Program (NRF-2014R1A1A3049836) funded by MSIP, Korea; the Gas Hydrate and Paleoceanographic Reconstruction in the Western Arctic Ocean (PE16062) and a KOPRI research grant (PE16010) funded by MOF, Korea; and the Integrated Ocean Drilling Program funded by the MLTMA, Korea. We thank M. Cook and K. Knudson for sharing oxygen isotope data, and H. Ashahi, K. Takahashi, B. Caissie for discussions on the age model and the sediment core, and JS. Ryu and C. Han for helping instrumental analysis. Comments from the editor and two anonymous reviewers helped improve the manuscript.

References

Abbott, A.N., Haley, B.A., McManus, J., 2015. Bottoms up: Sedimentary control of the deep North Pacific Ocean's ε_{Nd} signature. Geology 43, 1035-1035.

Abbott, A.N., Haley, B.A., McManus, J., 2016. The impact of sedimentary coatings on the diagenetic Nd flux. Earth Planet. Sci. Lett. 449, 217-227.

Akagi, T., Yasuda, S., Asahara, Y., Emoto, M., Takahashi, K., 2014. Diatoms spread a high ε_{Nd}-signature in the North Pacific Ocean. Geochem. J. 48, 121-131.

Albarède, F., Goldstein, S.L., 1992. World map of Nd isotopes in sea-floor ferromanganese deposits. Geology 20, 761-763.

Albarède, F., Goldstein, S.L., Dautel, D., 1997. The neodymium isotopic composition of manganese nodules from the Southern and Indian oceans, the global oceanic neodymium budget, and their bearing on deep ocean circulation. Geochim. Cosmochim. Acta 61, 1277-1291.

Arsouze, T., Dutay, J.-C., Lacan, F., Jeandel, C., 2007. Modeling the neodymium isotopic composition with a global ocean circulation model. Chem. Geol. 239, 165-177.

Asahara, Y., Takeuchi, F., Nagashima, K., Harada, N., Yamamoto, K., Oguri, K., Tadai, O., 2012. Provenance of terrigenous detritus of the surface sediments in the Bering and Chukchi Seas as derived from Sr and Nd isotopes: Implications for recent climate change in the Arctic regions. Deep-Sea Res. II 61–64, 155-171.

Axelsson, M.D., Rodushkin, I., Ingri, J., Öhlander, B., 2002. Multielemental analysis of Mn–Fe nodules by ICP-MS: optimisation of analytical method. Analyst 127, 76-82.

Bayon, G., Barrat, J.A., Etoubleau, J., Benoit, M., Bollinger, C., Révillon, S., 2009. Determination of rare earth elements, Sc, Y, Zr, Ba, Hf and Th in geological samples by ICP-MS after Tm addition and alkaline fusion. Geostand. Geoanal. Res. 33, 51-62.

Bayon, G., German, C.R., Boella, R.M., Milton, J.A., Taylor, R.N., Nesbitt, R.W., 2002. An improved method for extracting marine sediment fractions and its application to Sr and Nd isotopic analysis. Chem. Geol. 187, 179-199.

Biastoch, A., Böning, C.W., Getzlaff, J., Molines, J.-M., Madec, G., 2008. Causes of interannual-decadal variability in the meridional overturning circulation of the midlatitude North Atlantic Ocean. J. Climate 21, 6599-6615.

Blaser, P., Lippold, J., Gutjahr, M., Frank, N., Link, J.M., Frank, M., 2016. Extracting foraminiferal seawater Nd isotope signatures from bulk deep sea sediment by chemical leaching. Chem. Geol. 439, 189-204.

Brennan, C., Meissner, K., Eby, M., Hillaire-Marcel, C., Weaver, A., 2013. Impact of sea ice variability on the oxygen isotope content of seawater under glacial and interglacial conditions. Paleoceanography 28, 388-400.

Bubenshchikova, N., Nürnberg, D., Lembke-Jene, L., Pavlova, G., 2008. Living benthic foraminifera of the Okhotsk Sea: Faunal composition, standing stocks and microhabitats. Mar. Micropaleontol. 69, 314-333.

Cook, M.S., Ravelo, A.C., Mix, A., Nesbitt, I.M., Miller, N.V., 2016. Tracing subarctic Pacific water masses with benthic foraminiferal stable isotopes during the LGM and late Pleistocene. Deep-Sea Res. II 125, 84-95.

Expedition 323 Scientists, 2011. Site U1345. In Takahashi, K., Ravelo, A.C., Alvarez Zarikian, C.A., and the Expedition 323 Scientists (Eds.), Proc. IODP, 323. Integrated Ocean Drilling Program Management International,

Inc., Tokyo.

Frank, M., Whiteley, N., Kasten, S., Hein, J.R., O'Nions, K., 2002. North Atlantic Deep Water export to the Southern Ocean over the past 14 Myr: Evidence from Nd and Pb isotopes in ferromanganese crusts. Paleoceanography 17, 1022-1030.

GEOROC, 2003. Geochemistry of Rocks of the Oceans and Continents. Mainz, Germany, Max-Planck Institute fur Chemie. <http://georoc.mpch-mainz.gwdg.de/>.

Gutjahr, M., Frank, M., Stirling, C.H., Klemm, V., van de Flierdt, T., Halliday, A.N., 2007. Reliable extraction of a deepwater trace metal isotope signal from Fe-Mn oxyhydroxide coatings of marine sediments. Chem. Geol. 242, 351-370.

Häkkinen, S., Rhines, P.B., 2004. Decline of subpolar North Atlantic circulation during the 1990s. Science 304, 555-559.

Haley, B.A., Frank, M., Spielhagen, R.F., Eisenhauer, A., 2007. Influence of brine formation on Arctic Ocean circulation over the past 15 million years. Nat. Geosci. 1, 68-72.

Haley, B.A., Polyak, L., 2013. Pre-modern Arctic Ocean circulation from surface sediment neodymium isotopes. Geophys. Res. Lett. 40, 893-897.

Heimburger, A., Losno, R., Triquet, S., Nguyen, E.B., 2013. Atmospheric deposition fluxes of 26 elements over the Southern Indian Ocean: Time series on Kerguelen and Crozet Islands. Global Biogeochem. Cy. 27, 440-449.

Hein, J.R., O'NEIL, J.R., Jones, M.G., 1979. Origin of authigenic carbonates in sediment from the deep Bering Sea. Sedimentology 26, 681-705.

Hillaire-Marcel, C., de Vernal, A., 2008. Stable isotope clue to episodic sea ice formation in the glacial North Atlantic. Earth Planet. Sci. Lett. 268, 143-150.

Horikawa, K., Asahara, Y., Yamamoto, K., Okazaki, Y., 2010. Intermediate water formation in the Bering Sea during glacial periods: Evidence from neodymium isotope ratios. Geology 38, 435-438.

Hu, A., Meehl, G.A., Han, W., Abe-Ouchi, A., Morrill, C., Okazaki, Y., Chikamoto, M.O., 2012a. The Pacific-Atlantic seesaw and the Bering Strait. Geophys. Res. Lett. 39, L03702, doi:03710.01029/02011GL050567.

Hu, A., Meehl, G.A., Han, W., Otto-Bliestner, B., Abe-Ouchi, A., Rosenbloom, N., 2015. Effects of the Bering Strait closure on AMOC and global climate under different background climates. Prog. Oceanogr. 132, 174-196.

Hu, A., Meehl, G.A., Han, W., Timmermann, A., Otto-Bliesner, B., Liu, Z., Washington, W.M., Large, W., Abe-Ouchi, A., Kimoto, M., 2012b. Role of the Bering Strait on the hysteresis of the ocean conveyor belt circulation and glacial climate stability. Proc. Natl. Acad. Sci. 109, 6417-6422.

Hu, R., Noble, T.L., Piotrowski, A.M., McCave, I.N., Bostock, H.C., Neil, H.L., 2016. Neodymium isotopic evidence for linked changes in Southeast Atlantic and Southwest Pacific circulation over the last 200 kyr. Earth Planet. Sci. Lett. 455, 106-114.

Jacobsen, S.B., Wasserburg, G.J., 1980. Sm-Nd isotopic evolution of chondrites. Earth Planet. Sci. Lett. 50, 139-155.

Jang, K., Han, Y., Huh, Y., Nam, S.-I., Stein, R., Mackensen, A., Matthiessen, J., 2013. Glacial freshwater discharge events recorded by authigenic neodymium isotopes in sediments from the Mendeleev Ridge, western

Arctic Ocean. Earth Planet. Sci. Lett. 369–370, 148-157.

Jauhari, P., Pattan, J.N., 2000. Ferromanganese nodules from the central Indian Ocean basin. In: Cronan, D.S. (Ed.), Handbook of Marine Mineral Deposits. CRC Press, pp. 171-195.

Jonkers, L., Zahn, R., Thomas, A., Henderson, G., Abouchami, W., François, R., Masque, P., Hall, I.R., Bickert, T., 2015. Deep circulation changes in the central South Atlantic during the past 145 kyrs reflected in a combined $^{231}Pa/^{230}Th$, neodymium isotope and benthic $\delta^{13}C$ record. Earth Planet. Sci. Lett. 419, 14-21.

Kaiho, K., 1994. Benthic foraminiferal dissolved-oxygen index and dissolved-oxygen levels in the modern ocean. Geology 22, 719-722.

Kanematsu, Y., Takahashi, K., Kim, S., Asahi, H., Khim, B.-K., 2013. Changes in biogenic opal productivity with Milankovitch cycles during the last 1.3 Ma at IODP Expedition 323 Sites U1341, U1343, and U1345 in the Bering Sea. Quatern. Int. 310, 213-220.

Katsuki, K., Takahashi, K., 2005. Diatoms as paleoenvironmental proxies for seasonal productivity, sea-ice and surface circulation in the Bering Sea during the late Quaternary. Deep-Sea Res. II 52, 2110-2130.

Kim, S.J., Park, Y.G., 2008. Glacial ocean circulation and property changes in the North Pacific. Atmos. Ocean 46, 257-275.

Knudson, K.P., Ravelo, A.C., 2015. North Pacific Intermediate Water circulation enhanced by the closure of the Bering Strait. Paleoceanography 30, 1287-1304.

Lacan, F., Jeandel, C., 2001. Tracing Papua New Guinea imprint on the central Equatorial Pacific Ocean using neodymium isotopic compositions and rare

earth element patterns. Earth Planet. Sci. Lett. 186, 497-512.

Lacan, F., Jeandel, C., 2005. Neodymium isotopes as a new tool for quantifying exchange fluxes at the continent–ocean interface. Earth Planet. Sci. Lett. 232, 245-257.

Lisiecki, L.E., Raymo, M.E., 2005. A Plio-Pleistocene stack of 57 globally distributed benthic $\delta^{18}O$ records. Paleoceanography 20, PA1003, doi:1010.1029/2004PA001071.

Míková, J., Denková, P., 2007. Modified chromatographic separation scheme for Sr and Nd isotope analysis in geological silicate samples. J. Geosci., 221-226.

Martin, E., Scher, H., 2004. Preservation of seawater Sr and Nd isotopes in fossil fish teeth: bad news and good news. Earth Planet. Sci. Lett. 220, 25-39.

Martin, E.E., Blair, S.W., Kamenov, G.D., Scher, H.D., Bourbon, E., Basak, C., Newkirk, D.N., 2010. Extraction of Nd isotopes from bulk deep sea sediments for paleoceanographic studies on Cenozoic time scales. Chem. Geol. 269, 414-431.

Matsumoto, K., 2007. Radiocarbon-based circulation age of the world oceans. J. Geophys. Res. Oceans 112, C09004, doi:09010.01029/02007JC004095.

Max, L., Lembke-Jene, L., Riethdorf, J.-R., Tiedemann, R., Nürnberg, D., Kühn, H., Mackensen, A., 2014. Pulses of enhanced North Pacific Intermediate Water ventilation from the Okhotsk Sea and Bering Sea during the last deglaciation. Clim. Past 10, 591-605.

Noble, T.L., Piotrowski, A.M., McCave, I.N., 2013. Neodymium isotopic composition of intermediate and deep waters in the glacial southwest Pacific. Earth Planet. Sci. Lett. 384, 27-36.

Ohkushi, K.i., Itaki, T., Nemoto, N., 2003. Last Glacial–Holocene change in

intermediate-water ventilation in the Northwestern Pacific. Quaternary Sci. Rev. 22, 1477-1484.

Okazaki, Y., Timmermann, A., Menviel, L., Harada, N., Abe-Ouchi, A., Chikamoto, M.O., Mouchet, A., Asahi, H., 2010. Deepwater formation in the North Pacific during the Last Glacial Termination. Science 329, 200-204.

Oliver, K.I.C., Hoogakker, B.A.A., Crowhurst, S., Henderson, G.M., Rickaby, R.E.M., Edwards, N.R., Elderfield, H., 2010. A synthesis of marine sediment core $\delta^{13}C$ data over the last 150,000 years. Clim. Past 6, 645-673.

Pin, C., Zalduegui, J.S., 1997. Sequential separation of light rare-earth elements, thorium and uranium by miniaturized extraction chromatography: Application to isotopic analyses of silicate rocks. Anal. Chim. Acta 339, 79-89.

Rella, S.F., Tada, R., Nagashima, K., Ikehara, M., Itaki, T., Ohkushi, K.i., Sakamoto, T., Harada, N., Uchida, M., 2012. Abrupt changes of intermediate water properties on the northeastern slope of the Bering Sea during the last glacial and deglacial period. Paleoceanography 27, PA3203, doi:3210.1029/2011PA002205.

Roberts, N.L., Piotrowski, A.M., McManus, J.F., Keigwin, L.D., 2010. Synchronous deglacial overturning and water mass source changes. Science 327, 75-78.

Roemmich, D., McCallister, T., 1989. Large scale circulation of the North Pacific Ocean. Prog. Oceanogr. 22, 171-204.

Rohling, E.J., Braun, K., Grant, K., Kucera, M., Roberts, A.P., Siddall, M., Trommer, G., 2010. Comparison between Holocene and Marine Isotope Stage-11 sea-level histories. Earth Planet. Sci. Lett. 291, 97-105.

Rutberg, R.L., Hemming, S.R., Goldstein, S.L., 2000. Reduced North Atlantic Deep Water flux to the glacial Southern Ocean inferred from neodymium isotope ratios. Nature 405, 935-938.

Saenko, O.A., Schmittner, A., Weaver, A.J., 2004. The Atlantic-Pacific seesaw. J. Climate 17, 2033-2038.

Sarnthein, M., Schneider, B., Grootes, P.M., 2013. Peak glacial ^{14}C ventilation ages suggest major draw-down of carbon into the abyssal ocean. Clim. Past 9, 2595-2614.

Sarnthein, M., Winn, K., Jung, S.J., Duplessy, J.C., Labeyrie, L., Erlenkeuser, H., Ganssen, G., 1994. Changes in east Atlantic deepwater circulation over the last 30,000 years: Eight time slice reconstructions. Paleoceanography 9, 209-267.

Seidov, D., Maslin, M., 1999. North Atlantic deep water circulation collapse during Heinrich events. Geology 27, 23-26.

Shcherbina, A.Y., Talley, L.D., Rudnick, D.L., 2003. Direct observations of North Pacific ventilation: Brine rejection in the Okhotsk Sea. Science 302, 1952-1955.

Sherrell, R.M., Field, M.P., Ravizza, G., 1999. Uptake and fractionation of rare earth elements on hydrothermal plume particles at 9°45′N, East Pacific Rise. Geochim. Cosmochim. Acta 63, 1709-1722.

Siddall, M., Khatiwala, S., van de Flierdt, T., Jones, K., Goldstein, S.L., Hemming, S., Anderson, R.F., 2008. Towards explaining the Nd paradox using reversible scavenging in an ocean general circulation model. Earth Planet. Sci. Lett. 274, 448-461.

Soyol-Erdene, T.-O., Huh, Y., 2013. Rare earth element cycling in the pore waters

of the Bering Sea Slope (IODP Exp. 323). Chem. Geol. 358, 75-89.

Springer, A.M., McRoy, C.P., Flint, M.V., 1996. The Bering Sea Green Belt: shelf-edge processes and ecosystem production. Fish. Oceanogr. 5, 205-223.

Stabeno, P.J., Kachel, N.B., Moore, S.E., Napp, J.M., Sigler, M., Yamaguchi, A., Zerbini, A.N., 2012. Comparison of warm and cold years on the southeastern Bering Sea shelf and some implications for the ecosystem. Deep-Sea Res. II 65, 31-45.

Stewart, J.A., Gutjahr, M., James, R.H., Anand, P., Wilson, P.A., 2016. Influence of the Amazon River on the Nd isotope composition of deep water in the western equatorial Atlantic during the Oligocene–Miocene transition. Earth Planet. Sci. Lett. 454, 132-141.

Stouffer, R.J., Yin, J., Gregory, J., Dixon, K., Spelman, M., Hurlin, W., Weaver, A., Eby, M., Flato, G., Hasumi, H., 2006. Investigating the causes of the response of the thermohaline circulation to past and future climate changes. J. Climate 19, 1365-1387.

Tachikawa, K., Jeandel, C., Roy-Barman, M., 1999. A new approach to the Nd residence time in the ocean: the role of atmospheric inputs. Earth Planet. Sci. Lett. 170, 433-446.

Takahashi, K., Ravelo, A.C., Zarikian, C.A., 2011. IODP Expedition 323-Pliocene and Pleistocene Paleoceanographic Changes in the Bering Sea. Sci. Drill. 11, 4-13.

Talley, L.D., 1991. An Okhotsk Sea water anomaly: Implications for ventilation in the North Pacific. Deep-Sea Res. 38, S171-S190.

van de Flierdt, T., Frank, M., Lee, D.-C., Halliday, A.N., Reynolds, B.C., Hein, J.R., 2004. New constraints on the sources and behavior of neodymium and

hafnium in seawater from Pacific Ocean ferromanganese crusts. Geochim. Cosmochim. Acta 68, 3827-3843.

van de Flierdt, T., Robinson, L.F., Adkins, J.F., 2010. Deep-sea coral aragonite as a recorder for the neodymium isotopic composition of seawater. Geochim. Cosmochim. Acta 74, 6014-6032.

VanLaningham, S., Pisias, N.G., Duncan, R.A., Clift, P.D., 2009. Glacial–interglacial sediment transport to the Meiji Drift, northwest Pacific Ocean: Evidence for timing of Beringian outwashing. Earth Planet. Sci. Lett. 277, 64-72.

von Blanckenburg, F., 1999. Tracing past ocean circulation? Science 286, 1862-1863.

Warner, M.J., Roden, G.I., 1995. Chlorofluorocarbon evidence for recent ventilation of the deep Bering Sea. Nature 373, 409-412.

Weis, D., Kieffer, B., Maerschalk, C., Pretorius, W., Barling, J., 2005. High-precision Pb-Sr-Nd-Hf isotopic characterization of USGS BHVO-1 and BHVO-2 reference materials. Geochem. Geophys. Geosyst. 6, Q02002, doi:02010.01029/02004GC000852.

Wilson, D.J., Piotrowski, A.M., Galy, A., Clegg, J.A., 2013. Reactivity of neodymium carriers in deep sea sediments: Implications for boundary exchange and paleoceanography. Geochim. Cosmochim. Acta 109, 197-221.

Wilson, D.J., Piotrowski, A.M., Galy, A., McCave, I.N., 2012. A boundary exchange influence on deglacial neodymium isotope records from the deep western Indian Ocean. Earth Planet. Sci. Lett. 341–344, 35-47.

Yang, Y., Wu, F., Xie, L., Zhang, Y., 2009. High-precision measurements of the

$^{143}Nd/^{144}Nd$ isotope ratio in certified reference materials without Nd and Sm separation by multiple collector inductively coupled plasma mass spectrometry. Anal. Lett. 43, 142-150.

Yasuda, I., 1997. The origin of the North Pacific Intermediate water. J. Geophys. Res-Oceans (1978 - 2012) 102, 893-909.

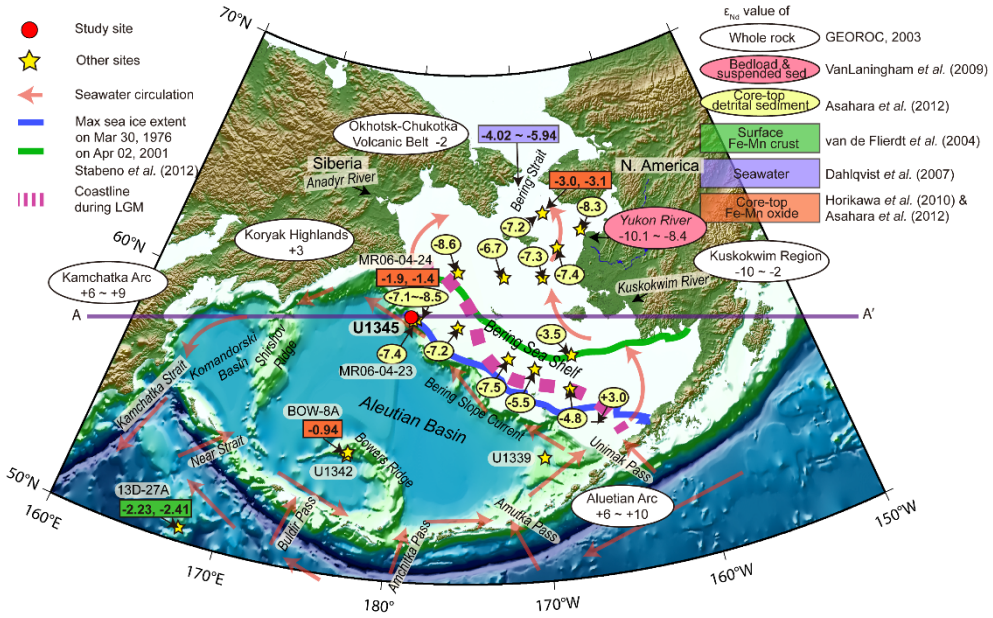

Figure 3.1. The Nd isotopic compositions (ε_{Nd}) near site U1345 (red circle) in the Bering Sea. The ε_{Nd} values are given in ellipses and rectangles. Red arrows indicate the direction of ocean circulation. Maximum sea ice extent in 1976 (cold winter) and in 2001 (warm winter) is shown with blue and green lines, respectively (Stabeno et al., 2012). Purple dashed line indicates the coastline at the LGM. The AA' cross section is schematically shown in Fig. 3.4.

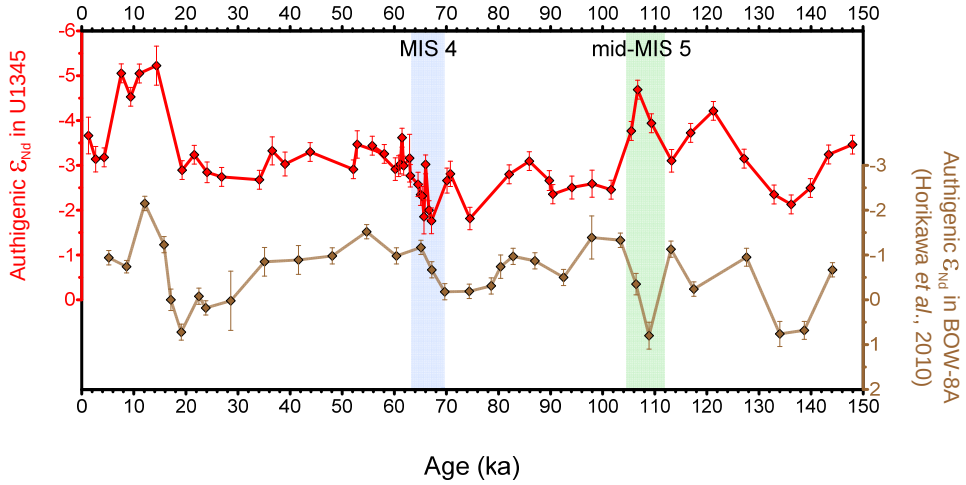

Figure 3.2. Comparison of ε_{Nd} values between sites U1345 (red) and BOW-8A (brown). The persistent offset (2 to 3 ε_{Nd}) between the two sites is likely due to unradiogenic input to site U1345 from boundary exchange processes. The gap decreases during MIS 4 (blue bar) and increases during mid-MIS 5 (green bar).

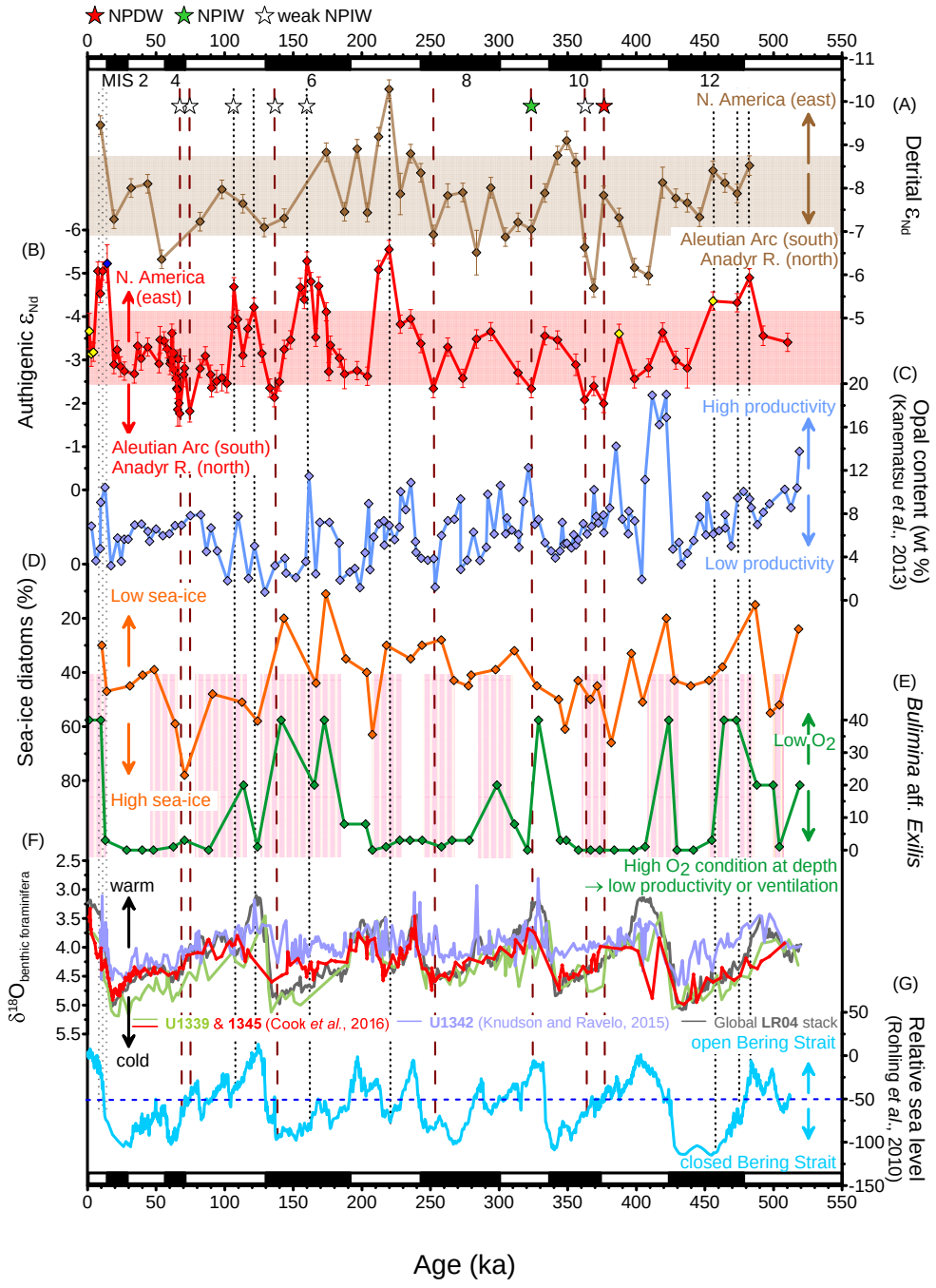

Figure 3.3. ε_{Nd} comparison of (A) detrital and (B) authigenic (red: *Wilson Authigenic*, yellow: *Wilson Authigenic* of ash layers, blue: *Rutberg Authigenic*) fractions with (C) opal content (data from Kanematsu et al., 2013); (D) % sea-ice

diatoms; (E) *B.* aff. *Exilis* abundance with laminated layer (pink stripe); (F) $\delta^{18}O_{bf}$ of U1339, U1345, U1342, and LR04 stack (gray; data from Lisiecki and Raymo, 2005); and (G) relative sea level (data from Rohling et al., 2010). The other proxy data (D, E) are from Expedition 323 Scientists (2011). Dense water formation events are marked with stars (red: NPDW penetration to > 1,867 m, green: NPIW penetration to > 1,008 m, white: partial NPIW penetration to 1,008 m). The brown (in A) and red (in B) shaded areas represent ±1σ variation from the average.

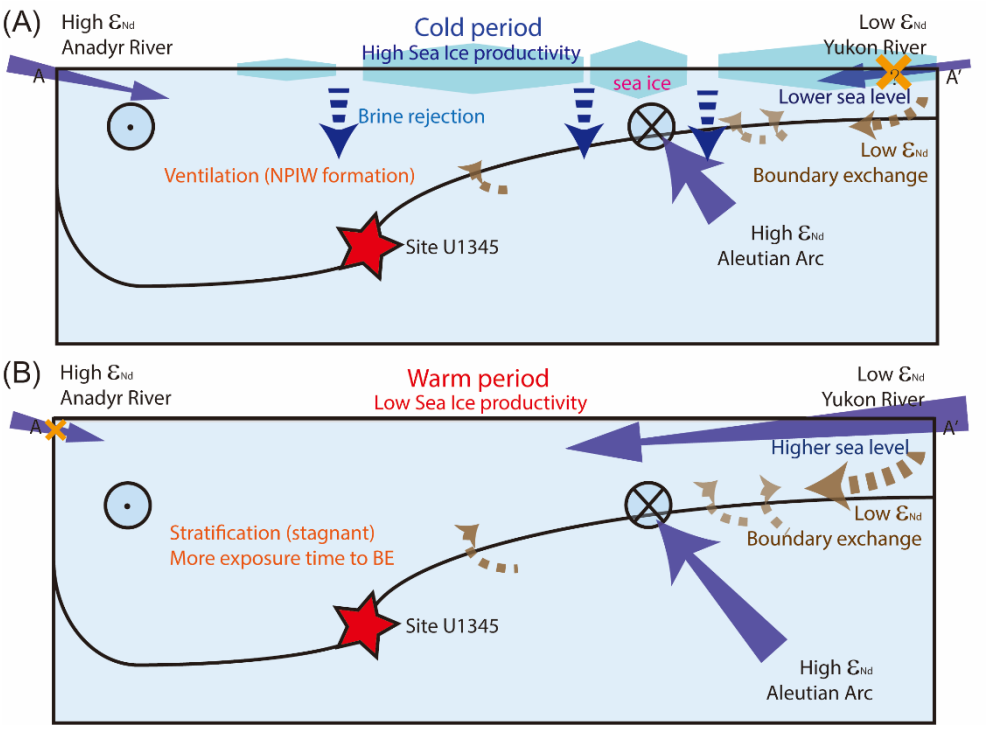

Figure 3.4. Schematic illustration of ocean circulation in the Bering Sea during typical low (A) and high (B) sea ice productivity conditions across the A-A' transect marked in Fig. 3.1. During cold periods, enhanced sea ice production can trigger NPIW formation through brine rejection, causing the sinking of water masses containing radiogenic Nd. Mid-MIS 6 and mid-MIS 5 are exceptions, when unradiogenic ε_{Nd} from N. America reached the Bering Sea and participated in NPIW formation. During warm periods, boundary exchange (BE) can supply unradiogenic Nd under stagnant bottom water conditions. In case of MIS 8, preferential release of reactive particulate matter is probable.

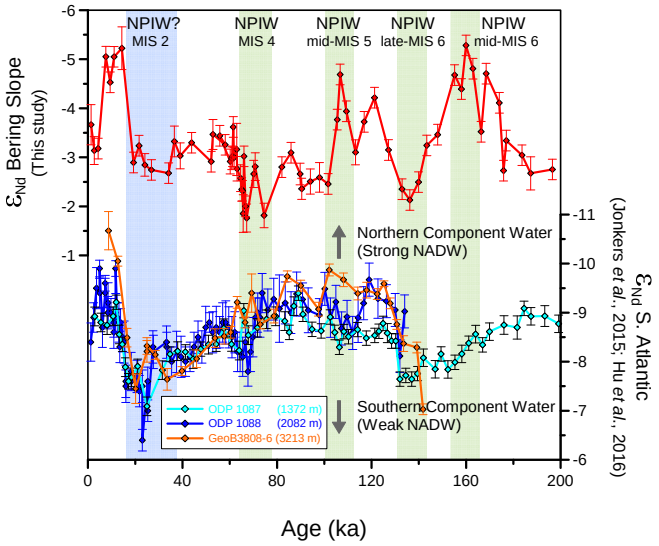

Figure 3.5. Comparison of the authigenic ε_{Nd} records for the Bering Slope and the South Atlantic to examine the NPIW-NADW Seesaw Hypothesis. NPIW events at site U1345 are compared with the strength of NADW recorded in GeoB (orange), ODP 1088 (blue) and 1087 (sky blue). The NPIW events discussed in section 4.4 are marked with green bars. At the LGM, ε_{Nd} does not record an NPIW event, but $\Delta\delta^{18}O_{bf}$ on the Bering Slope indicates a seesaw (blue bar).

Table 3.1. ε_{Nd} of bottom water composition at site U1345. The method is based on Wilson et al. (2013)

Sample	Depth (CCSF-A, m)	Age (ka)	ε_{Nd}	2σ	Sample	Depth (CCSF-A, m)	Age (ka)	ε_{Nd}	2σ
A 1H1 10	0.1	1.3	-3.7	0.4	A 4H3 4	27.4	90.4	-2.4	0.2
A 1H1 74	0.7	2.7	-3.1	0.3	A 4H3 76	28.1	94.1	-2.5	0.3
A 1H2 0	1.5	4.3	-3.2	0.2	A 4H4 2	28.9	98.0	-2.6	0.3
A 1H3 2	3.0	7.6	-5.1	0.2	A 4H4 74	29.6	101.6	-2.5	0.2
D 1H3 2	4.6	11.1	-5.1	0.2	A 4H5 0	30.4	105.5	-3.8	0.2
D 1H4 0*	6.1	14.4	-5.2	0.2	A 4H5 24	30.6	106.7	-4.7	0.2
D 1H5 2	7.6	19.3	-2.9	0.2	A 4H5 76	31.1	109.4	-3.9	0.2
D 1H5 74	8.4	21.6	-3.2	0.2	A 4H6 2	31.9	113.2	-3.1	0.3
D 1H6 0	9.1	24.1	-2.9	0.2	A 4H6 74	32.6	116.9	-3.7	0.2
C 2H3 0	10.0	26.9	-2.7	0.2	D 4H1 76	33.5	121.3	-4.2	0.2
C 2H4 74	12.2	34.1	-2.7	0.2	D 4H2 42	34.6	127.2	-3.2	0.2
C 2H5 0	13.0	36.6	-3.3	0.3	D 4H3 0	35.8	132.9	-2.4	0.2
C 2H5 76	13.7	39.0	-3.0	0.3	D 4H3 76	36.5	136.2	-2.1	0.2
C 2H6 75	15.2	43.9	-3.3	0.2	D 4H4 2	37.2	139.9	-2.5	0.2
D 2H5 0	17.8	52.2	-2.9	0.2	D 4H4 74	38.0	143.4	-3.2	0.2
A 3H3 110	18.0	52.9	-3.5	0.3	A 5H4 2	38.9	148.0	-3.5	0.2
A 3H4 120	19.6	58.1	-3.3	0.2	A 5H5 0	40.4	155.1	-4.7	0.2
D 2H5 112	18.9	55.8	-3.4	0.2	A 5H5 60	41.0	158.0	-4.4	0.2
A 3H5 35	20.3	60.2	-2.9	0.3	A 5H5 100	41.4	160.0	-5.3	0.2
A 3H5 55	20.5	60.8	-3.0	0.2	A 5H6 10	42.0	162.9	-4.8	0.2
A 3H5 65	20.6	61.2	-3.0	0.2	A 5H6 82	42.7	166.4	-3.5	0.2
A 3H5 75	20.7	61.5	-3.6	0.2	C 5H4 74	43.2	168.5	-4.7	0.2
A 3H5 85	20.8	61.8	-3.0	0.2	A 5HCC 30	44.3	174.1	-4.1	0.2
A 3H5 120	21.1	62.9	-3.2	0.5	C 5H5 76	44.7	175.9	-2.7	0.2
A 3H5 125	21.2	63.1	-2.8	0.3	C 5H5 100	44.9	177.0	-3.3	0.2
A 3H6 20	21.6	64.6	-2.6	0.3	A 6H1 76	46.3	183.6	-3.0	0.2
A 3H6 35	21.8	65.0	-2.4	0.2	A 6H2 2	47.0	187.3	-2.7	0.3
A 3H6 45	21.9	65.4	-2.3	0.2	A 6H4 2	50.0	196.5	-2.8	0.2
A 3H6 55	22.0	65.7	-1.9	0.4	A 6H6 2	53.0	204.0	-2.6	0.2
A 3H6 65	22.1	66.0	-3.0	0.2	C 6H6 76	56.3	212.2	-5.1	0.2
A 3H6 85	22.3	66.7	-2.0	0.3	D 6H4 74	59.4	219.8	-5.6	0.2
A 3H6 100	22.4	67.2	-1.8	0.3	C 7H3 76	62.7	228.0	-3.8	0.2
C 3H4 130	23.3	70.1	-2.7	0.3	C 7H5 76	65.7	235.5	-4.0	0.2
C 3H5 0	23.5	70.8	-2.8	0.3	D 7H4 74	68.7	242.9	-3.4	0.2
C 3H5 76	24.3	74.5	-1.8	0.3	D 7H6 74	71.6	252.1	-2.3	0.2
C 3H6 74	25.8	82.0	-2.8	0.2	C 8H4 76	75.0	262.5	-3.3	0.2
C 3H7 0	26.5	85.9	-3.1	0.2	C 8H6 131	78.5	273.5	-2.6	0.2

Sample	Depth (CCSF-A, m)	Age (ka)	ε_{Nd}	2σ	Sample	Depth (CCSF-A, m)	Age (ka)	ε_{Nd}	2σ
A 9H5 0	81.7	283.5	-3.5	0.2	C 13H3 0	126.2	408.8	-2.8	0.2
C 9H4 0	85.0	293.9	-3.7	0.2	C 13H5 0	129.2	419.2	-3.6	0.2
A 10H3 60	91.3	313.8	-2.7	0.3	D 13H6 2	132.2	428.8	-3.0	0.2
C 10H3 0	94.4	323.5	-2.3	0.2	A 14H4 75	135.0	437.2	-2.8	0.5
D 10H3 75	97.4	333.3	-3.6	0.2	D 14H4 80	141.3	455.9	-4.4	0.2
D 11H3 0	107.1	355.9	-2.9	0.3	A 15H5 75	147.2	473.5	-4.3	0.2
D 11H5 0	110.0	362.3	-2.1	0.2	A 15H7 75	150.2	482.5	-4.9	0.2
D 11H7 0	113.0	369.0	-2.4	0.2	D 15H5 75	153.5	492.4	-3.6	0.2
A 12H6 75	116.0	376.2	-2.0	0.2	C 16H4 0	159.5	510.3	-3.4	0.2
C 12H6 0	119.6	387.4	-3.6	0.2	D 16H4 75	162.4	518.8	-3.5	0.3
A 13H3 75	123.3	398.7	-2.6	0.2					

*****Data obtained using the method based on *Jang et al. (2013)*

Chapter 4. Early-Pleistocene glaciation of Alaska and its influence on deep-water Nd isotopic composition in the Bering Sea across the mid-Pleistocene transition

Kwangchul Jang, Youngsook Huh, and Yeongcheol Han

Abstract

The mid-Pleistocene transition (MPT, ~1.2 to ~0.8 Ma) from 41-kyr periodicity to 100-kyr periodicity of the glacial-interglacial variability are based on the benthic foraminifera $\delta^{18}O$ ($\delta^{18}O_{bf}$) records mostly in Atlantic Ocean and eastern equatorial Pacific, and the only available long-term $\delta^{18}O_{bf}$ records in the Bering Sea does not show 41-kyr periodicity before the MPT. Lack of 41-kyr periodicity in $\delta^{18}O_{bf}$ has been attributed to low sampling resolution, but it may rather reflect an exceptional ice-history in the Bering Sea. To resolve this uncertainty, we here reconstructed the variation in deep-water composition and sediment provenance at site U1343 (1,950 m) in the Bering Sea over the last 2.4 Myr using the authigenic ($\varepsilon_{Nd,AUTH}$) and detrital ε_{Nd} ($\varepsilon_{Nd,DET}$). The deep-water ε_{Nd} has the average value of -3.0 ± 1.1 (1σ, n = 154) with large fluctuations. Considering the uniform ε_{Nd} inflow from N. Pacific recorded in Fe-Mn crust and general absence of North Pacific Deep Water formation inferred from heavy $\delta^{18}O_{bf}$ and high *Actinocyclus spp.*, the change of deep seawater ε_{Nd} in the Bering Sea is primarily caused by boundary exchange. Given the broad correlation between $\varepsilon_{Nd,AUTH}$ and $\varepsilon_{Nd,DET}$ (r = 0.49), ε_{Nd} input from boundary exchange ($\varepsilon_{Nd,BE}$) relies partly on sediment lithology although $\varepsilon_{Nd,BE}$ can

be altered by the preferential release of radiogenic Nd during boundary exchange.

The reconstructed $\varepsilon_{Nd,DET}$ represents average value of -6.6 ± 1.5 (1σ, n = 70) with repetitive occurrences of unradiogenic $\varepsilon_{Nd,DET}$ peaks down to -8 ~ -9. Unradiogenic $\varepsilon_{Nd,DET}$ peaks are primarily attributed to high flux of meltwater from Alaska, and hence their repetitive occurrences imply that the Alaskan glaciation has existed during the Pleistocene. Lack of numerical difference in unradiogenic $\varepsilon_{Nd,DET}$ peaks over 2.4 Myr may be interpreted as that the Alaskan glaciation reached to maximum volume during early-Pleistocene, but general obliquity-like variation in $\varepsilon_{Nd,AUTH}$ (80-kyr periodicity) over the last 2.4 Myr suggest that this scenario is unlikely as seawater ε_{Nd} in the Bering Sea is primarily governed by $\varepsilon_{Nd,DET}$ as determined from the Alaskan glaciation. The absence of 100-kyr periodicity since the MPT and discontinuity of 41-kyr periodicity over 2.4 Myr presumably result from an increase in uncertainty of spectral analysis caused by preferential release of radiogenic Nd during boundary exchange and by poor time resolution of $\varepsilon_{Nd,AUTH}$ rather than from an exceptional ice-history in the Bering Sea. Overall, our ε_{Nd} dataset both highlights the strong influence of sediment-water interaction on deep-water ε_{Nd} and the presence of the Alaskan glaciation during the Pleistocene.

4.1. Introduction

The mid-Pleistocene transition (MPT) indicates the dominant periodicity of glacial-interglacial cycle changed from 41-kyr obliquity to 100-kyr eccentricity in the absence of any significant change in external astronomical forcing (Imbrie et al., 1992; Laskar et al., 2004; Ravelo et al., 2004; Shackleton and Opdyke, 1976). The MPT began ~1.25 Ma and ended by ~0.7 Ma with low frequency and high amplitude glacial-interglacial variability (Clark et al., 2006). The possible origin of

the MPT that allows for the development of larger ice sheets invokes the long-term cooling associated with pCO_2 decrease (e.g. Berger et al., 1999; Mudelsee and Schulz, 1997; Raymo et al., 1997), the reorganization of global ocean circulation (e.g. Pena and Goldstein, 2014; Schmieder et al., 2000), and/or change in ice dynamics relating to exposure of high-friction regolith (e.g. Clark et al., 2006). However, the main mechanism that causes the MPT is still under debate.

Our understanding of the MPT largely depends on benthic foraminifera $\delta^{18}O$ ($\delta^{18}O_{bf}$) records mostly from the Atlantic Ocean and the eastern equatorial Pacific Ocean, which may generate bias (Elderfield et al., 2012). To complement this caveat, climatic records from the Bering Sea, including $\delta^{18}O_{bf}$ (Asahi et al., 2016), biogenic opal content (Kim et al., 2014) and biological assemblage (Teraishi et al., 2016) have been reported since the Integrated Ocean Drilling Program (IODP) Expedition 323. The changes in periodicity of opal contents from 41-kyr to 100-kyr and biological assemblage variation in the Bering Sea across the MPT agree with glacial-interglacial variability across the MPT (Kim et al., 2014; Teraishi et al., 2016). In case of $\delta^{18}O_{bf}$, however, 41-kyr periodicity is absent prior to 1.5 Ma and overall values are relatively heavier than the LR04 stack before the MPT (Asahi et al., 2016). These characteristic $\delta^{18}O_{bf}$ records in the Bering Sea can result from low sampling resolution of $\delta^{18}O_{bf}$ before the MPT (Asahi et al., 2016) and the local hydrographic signal (Elderfield et al., 2012) but also from an exceptional ice-history across the MPT. Therefore, a sufficient number of climatic records in the Bering Sea is necessary to understand the paleoceanography in the Bering Sea across the MPT.

We reconstructed neodymium isotope ratios ($^{143}Nd/^{144}Nd$) of the authigenic and detrital fractions from the marine sediments in the Bering Sea over

2.4 Myr. The ε_{Nd} values ($\varepsilon_{Nd} = [(^{143}Nd/^{144}Nd)_{sample}/(^{143}Nd/^{144}Nd)_{CHUR} - 1]\times10^4$ and $(^{143}Nd/^{144}Nd)_{CHUR}$ is 0.512638 after Jacobsen and Wasserburg (1980)) of authigenic and detrital fractions have been used as a quasi-conservative water mass tracer (Frank et al., 2002; Jang et al., 2013; Piotrowski et al., 2004; Rutberg et al., 2000) and sediment provenance tracer (Vroon et al., 1995; Winter et al., 1997), respectively. This utility of ε_{Nd} comes from the short residence time of dissolved Nd (Tachikawa et al., 1999) and insignificant isotopic alteration during weathering and diagenesis (Goldstein and Hemming, 2003; Goldstein et al., 1984). Authigenic ε_{Nd} in the Atlantic Ocean is primarily determined by vertical and lateral mixing of water mass that retains distinct ε_{Nd} of surrounding rocks (e.g., Arsouze et al., 2007; Lacan and Jeandel, 2005), and hence it has been used as a water mass tracer. Unlike the Atlantic Ocean, authigenic ε_{Nd} in the Bering Sea is largely influenced by internal alteration like boundary exchange as well as water mixing because of stagnant bottom water condition (Jang et al., 2017). Thus, boundary exchange needs to be considered to interpret the change in authigenic ε_{Nd} of the Bering Sea. The measurement of concurrent detrital ε_{Nd} can be used to evaluate the effect of boundary exchange (Du et al., 2016). Detrital ε_{Nd} is further used to trace the development of the Alaskan glaciation since meltwater from Alaskan glaciation can result in ε_{Nd} decrease of the Bering Sea sediments (e.g. Horikawa et al., 2015). Therefore, the reconstruction of authigenic and detrital ε_{Nd} in the Bering Sea across the MPT can provide unique insight on ocean circulation, boundary exchange and the development of the Alaskan glaciation.

Here we present the first 2.4 Myr ε_{Nd} records of deep-water at 1,950 m and detrital sediments from the Bering Sea. First, we test the role of boundary exchange and North Pacific Deep Water (NPDW) formation in the deep-water Nd

budget of the Bering Sea. Then, we reconstruct the development of the Alaskan glaciation across the MPT using the variation in detrital ε_{Nd} and the periodicity of deep-water ε_{Nd}.

4.2. Materials

4.2.1. *Site information*

Sediment core samples were retrieved from site U1343 (57°3'N, 175°5'W; 1,950 m water depth) located on the continental margin of the Bering Sea during the IODP Expedition 323 (Fig. 4.1). Five holes were cored at site U1343, and the total length of recovered cores was 1,178.43 m with 96.5% recovery (Expedition 323 Scientists, 2011). The longest hole was U1343E with 700.27 m recovered, and its age extended to ~2.4 Myr based on the age model constructed by Asahi et al. (2016). It covers almost the entire Pleistocene. Site U1343 is obviously separated from the shelf area on the Bering Sea, which allows site U1343 to be less affected by reworked sediment from shelf area during interglacials and by eolian dust from exposed area during glacials (Expedition 323 Scientists, 2011).

The potential Nd sources are the Aleutian Arc and Alaska in the geological perspective since the direction of water circulation in the Bering Sea is anti-clockwise (Jang et al., 2017)(Fig. 4.1). The Aleutian Arc is a potential source for radiogenic Nd, as inferred from the measurement results of Nd isotopes from various rock samples there (ε_{Nd} ~ +6 to +10) (data from GEOROC, 2003), while Alaska is likely to be a source for unradiogenic Nd, as is evident from unradiogenic ε_{Nd} of bedload and suspended load in the Yukon River (ε_{Nd} ~ -10.1 to -8.4) (data

from VanLaningham et al., 2009). The Anadyr River from Siberia (ε_{Nd} ~ -2 to +3) (data from GEOROC, 2003) is also probable when the Bering Strait is closed during the glacial sea level lowstands (Hu et al., 2012; Jang et al., 2017).

4.2.2. Core description

We mainly used Hole U1343E to reconstruct dissolved Nd isotopic composition in the Bering Sea. The sediments here alternate between siliciclastic sediments (< 40% biogenic components) and mixed siliciclastic-biogenic sediments (Expedition 323 Scientists, 2011). Siliciclastic sediments are mainly composed of diatom-rich clayey silt/silt/silty clay, and mixed siliciclastic-biogenic sediments further include diatom ooze and a minor amount of foraminifera, calcareous nannofossils, and sponge spicules (<5%). The carbonate content and TOC content are typically less than 4% and 1%, respectively.

The age model at site U1343 was based on the Asahi et al. (2016). This model was constructed by correlation of the $\delta^{18}O_{bf}$ values between site U1343 and global LR04 stack. Ninety-two boundaries of marine isotope stages (MIS) and 344 tie points were assigned. The average sedimentation rate was ~32.8 cm kyr^{-1} with temporal fluctuations (11.6–72.0 cm kyr^{-1}), and this fluctuations were randomly variable regardless of the G-IG cycles.

4.3. Method

4.3.1. *Authigenic and detrital Nd isotopes*

We analyzed Nd isotope ratios of authigenic fraction from 154 sediment samples and those of detrital fraction from 70 sediment samples. The samples were

essentially chosen to reflect extreme glacial-interglacial (G-IG) cycle based on $\delta^{18}O$ values of LR04 stack (Lisiecki and Raymo, 2005). Data cover entire Pleistocene, and the average sampling intervals for authigenic and detrital ε_{Nd} are one sample every ~15.4 kyr and ~33.9 kyr, respectively.

4.3.2. *Spectral analysis on authigenic ε_{Nd}*

The periodicity of authigenic ε_{Nd} was quantified using continuous wavelet transform (Torrence and Compo, 1998) and REDFIT cross spectral analyses (Schulz and Mudelsee, 2002). We used re-sampled ε_{Nd} data by linear interpolation at every 15.4 kyr, which is the average value of sampling intervals ranging from 0.6 to 48 kyr. For continuous wavelet transform, Morlet wavelet is used as the shape of the mother wavelet. The significance level corresponding to $p = 0.05$ is determined by chi-squared test based on red-noise AR(1) process with lag-1 of 0.63. For REDFIT spectral analysis, Blackman-Harris window was applied, and significance level was calculated based on 95% Monte-Carlo simulation. Two different spectral analyses with independent methods provide data robustness. All analyses were performed using the software, PAST provided by Hammer et al. (2001).

4.4. Results and discussion

4.4.1. *The seawater-derived Nd isotopes*

One hundred and fifty-four isotope analyses of authigenic ε_{Nd} ($\varepsilon_{Nd,AUTH}$) at site U1343 show average value of -3.0 ± 1.1 (1σ) (Fig. 4.2A). There were large fluctuations, but we did not observe any significant G-IG cycle on $\varepsilon_{Nd,AUTH}$ (Fig.

4.2A). Radiogenic $\varepsilon_{Nd,AUTH}$ values are detected not only during glacial periods (blue symbols in Fig. 4.2A) but also during interglacial periods (red symbols in Fig. 4.2A). It is contrast to the climatic response of seawater-origin ε_{Nd} in other sites such as the S. Atlantic and SW Pacific. Glacial ε_{Nd} values in the S. Atlantic and SW Pacific are typically more radiogenic than interglacial values, which is interpreted as the decrease in the flux of the North Atlantic Component Water (Hu et al., 2016; Rutberg et al., 2000). Considering the oceanic pathway from the Southern Ocean to the N. Pacific, the climatic variation in ε_{Nd} of the SW Pacific can be propagated into the N. Pacific and further into the Bering Sea. Therefore, lack of $\varepsilon_{Nd,AUTH}$ pattern in response to climate variation in the Bering Sea implies that seawater ε_{Nd} in the Bering Sea is not only affected by the northward propagation of water mass but also by secondary factors such as episodic NPDW formation (e.g. Okazaki et al., 2010), boundary exchange process (e.g. Jang et al., 2017; Stewart et al., 2016) and/or pore water diffusion (e.g. Abbott et al., 2016; Du et al., 2016).

The $\varepsilon_{Nd,AUTH}$ value of youngest sample at 21.8 ka is -3.4 ± 0.2, which is comparable with direct measurement of deep-water from a nearby site TPS47 39-1 in the N. Pacific (47˚00'N, 161˚08' E, 1,795 water depth) (ε_{Nd} = -3.2 ± 0.5 from Piepgras and Jacobsen, 1988). It is also similar to contemporary $\varepsilon_{Nd,AUTH}$ value at site U1345 (60°9’N, 179°3’W; 1,008 m water depth) located on western side of the Bering Slope (ε_{Nd} ~ -3.2 from Jang et al., 2017) (Fig. 4.2B), indicating homogeneous water mass from 1,008 to 1,950 m water depth during the LGM. On the other hand, $\varepsilon_{Nd,AUTH}$ at site U1343 is distinctly less radiogenic than site BOW-8A on the Bowers Ridge (54˚47'N, 176˚55'E, 884 m water depth) during the LGM (ε_{Nd} ~-0.1 at 22.5 ka from Horikawa et al., 2010)(Fig. 4.2B). There are two hypotheses to interpret this unradiogenic bias between sites BOW-8A and U1343

(Fig. 4.3A). One possibility is that there was a distinct hydrographic boundary at between 884 m and 1,008 m water depths in the Bering Sea at that time. Although modern equilibrium calcite $\delta^{18}O$ calculated from hydrocast temperature and salinity in the Bering Sea does not show any sharp hydrographic boundary at the water depth below the ~300 m (Cook et al., 2016) (Fig. 4.3B), an increase in $\Delta\delta^{18}O_{bf}$ between site U1342 (54˚50'N, 176˚55'E; 818 m water depth) and U1345 (1008 m) during the LGM (Fig. 4.3B) indicates that water condition was different at that time. We cannot rule out this speculation. Another explanation is that $\varepsilon_{Nd,AUTH}$ at U1343 is locally altered in transit from sites BOW-8A to U1343 by episodic NPDW formation and/or internal Nd sources such as boundary exchange and/or pore water diffusion during the LGM (e.g. Jang et al., 2017), supporting the speculation from non-climatic pattern of $\varepsilon_{Nd,AUTH}$. Regardless of which hypothesis is correct, our ε_{Nd} data underline the important role of the secondary factors in deep-water Nd budget of the Bering Sea. In the next two sections, we evaluate the role of NPDW formation, boundary exchange and pore water diffusion.

4.4.2. *The possibility of NPDW formation*

The possibility of NPDW formation in the Bering Sea is tested. The Bering Sea is a potential location for the brine-induced dense water formation during the LGM, as inferred from abundant *Cycladophora davisiana*, which is an indicator of cold and well-oxygenated water (Ohkushi et al., 2003). Indeed, temporal variation of proxy records such as $\delta^{13}C_{bf}$ and $\delta^{18}O_{bf}$ suggested the episodic North Pacific Intermediate Water (NPIW) formation within the Bering Sea over the last 1.2 Myr (Knudson and Ravelo, 2015; Rella et al., 2012). Likewise, ε_{Nd} variation at the intermediate depths in the Bering Sea can be interpreted as NPIW

formation (Horikawa et al., 2010; Jang et al., 2017). However, the occurrence of NPDW formation in the Bering Sea has not been evaluated thoroughly, and its role in ε_{Nd} variation is enigmatic.

We traced the NPDW formation in the Bering Sea over 2.4 Myr based on the $\delta^{18}O_{bf}$ difference between sites U1342 (data from Knudson and Ravelo, 2015), U1343 (data from Asahi et al., 2016) and the LR04 stack (data from Lisiecki and Raymo, 2005) (Fig. 4.4B). For the direct comparisons between U1342 and U1343, composite $\delta^{18}O_{bf}$ at site U1343 was corrected to *Uvigerina bifurcate* based on Asahi et al. (2016). The $\delta^{18}O_{bf}$ difference between sites can trace the position of hydrographic boundary because brine rejection delivers light $\delta^{18}O$ from surface water to the bottom without significant isotopic fractionation (Brennan et al., 2013; Hillaire-Marcel and de Vernal, 2008). Let us suppose that $\Delta\delta^{18}O_{bf}$ between sites U1342 (818 m) and U1343 (1,950 m) gets larger compared to the present when dense water formation is absent (Warner and Roden, 1995). It can be interpreted by the migration of hydrographic boundary, probably due to brine-induced NPIW formation that delivers light $\delta^{18}O$ into the depth between 818 m and 1,950 m (e.g. Cook et al., 2016; Knudson and Ravelo, 2015). If the NPDW formation occurs, $\Delta\delta^{18}O_{bf}$ between two sites should be smaller, and overall $\delta^{18}O_{bf}$ values of two sites are likely to be lighter than the LR04 stack.

The difference of $\delta^{18}O_{bf}$ between sites U1342 and U1343 is highly variable, ranging from 0 to 0.8 ‰ over 1.2 Myr (Fig. 4.4B). During cold periods, $\Delta\delta^{18}O_{bf}$ values are generally higher than the estimated equilibrium $\delta^{18}O$ of calcite at the present ($\Delta\delta^{18}O_{bf}$ ~0.3 ‰ from Cook et al., 2016). The lighter $\delta^{18}O_{bf}$ values at site U1342 give rise to these large gradients. Light $\delta^{18}O_{bf}$ at site U1342 is not interpreted solely by temperature and salinity changes and rather requires local

water source such as brine-induced NPIW formation (Knudson and Ravelo, 2015). This new water mass bathed to water depth at least 818 m but not to 1,950 m, and therefore $\varepsilon_{Nd,AUTH}$ values associated with large $\Delta\delta^{18}O_{bf}$ seem to be independent of the NPDW formation.

We observed almost zero gradient of $\delta^{18}O_{bf}$ between sites U1342 and U1343 (Fig. 4.4B) at ~0.25, ~0.4, ~0.6, ~0.66, ~0.8 Ma and so on, but only one of them is probably result from the NPDW formation. Lack of $\delta^{18}O_{bf}$ gradient indicates that the water column between 818 m and 1,950 m was homogenous. In most cases for the zero gradients, $\Delta\delta^{18}O_{bf}$ between site U1343 and the LR04 stack is comparable to usual. It means that the hydrographic boundary was above the 818 m, and that ventilation process was not vigorous in the Bering Sea. Only one exception occurred at ~660 ka. At that time, $\delta^{18}O_{bf}$ at site U1343 is lighter than LR04 stack and $\varepsilon_{Nd,AUTH}$ is radiogenic (Figs. 4.4A and B). Brine-induced NPDW formation probably resulted in radiogenic $\varepsilon_{Nd,AUTH}$ excursion. Slightly higher % sea-ice diatom supports this interpretation (Fig. 4.4C).

The NPDW formation was not likely to occur before the MPT, as inferred from higher $\Delta\delta^{18}O_{bf}$ between site U1343 and LR04 stack (Fig. 4.4B). Heavy $\delta^{18}O_{bf}$ values at site U1343 before the MPT indicate that brine-induced NPDW formation that delivers light $\delta^{18}O_{bf}$ is unlikely. Considering that the NPDW formation is absent in the Bering Sea at the present owing to fresh surface water, salinity-induced NPDW formation like the modern NADW formation is also implausible because the sea surface salinity in the Bering Sea before the MPT was similar to or lower than that after the MPT as previously suggested by temporal variation in $C_{37:4}$ alkenone (Horikawa et al., 2015). Furthermore, the colder and/or saltier deep-water in the Bering Sea before the MPT, as indicated by higher $\delta^{18}O_{bf}$, implies an

increase in the density differences between surface and deep waters, restricting the possibility of salinity-induced NPDW formation.

We therefore suggest that $\varepsilon_{Nd,AUTH}$ variation within the Bering Sea over 2.4 Myr is not induced by NPDW formation except for one event at ~660 ka. General abundance of *Actinocyclus spp.*, which lives in stratified surface water related to meltwater (Onodera et al., 2016; Sancetta and Silvestri, 1986), supports poorly ventilated environment over 2.4 Ma (Fig. 4.4D). The NPDW formation (1,867 m) at MIS 11/10 boundary as previously suggested by Jang et al. (2017), is not detected based on $\Delta\delta^{18}O_{bf}$. The shallower hydrographic boundary than 1,950 m or age uncertainty between sites U1343 and U1345 is probable reason.

4.4.3. *Sediment-water interaction controlling ε_{Nd} in the Bering Sea*

Lack of NPDW formation indicates that the large fluctuation in $\varepsilon_{Nd,AUTH}$ (~8 ε_{Nd} unit) of the Bering Sea is governed by lateral advection from N. Pacific and/or internal sources such as boundary exchange and pore water diffusion. The lateral advection scenario can be excluded based on the uniform ε_{Nd} values of Fe-Mn crust from site 13D-27A in the N. Pacific over 2.3 Myr (51˚28'N, 167˚38'E, 1800-1500 m water depth) (van de Flierdt et al., 2004) (Fig. 4.2A). The uniform ε_{Nd} values in the N. Pacific may result from the averaging effect by the extremely low growth rate of Fe-Mn crust at site 13D-27A, but general low-$\varepsilon_{Nd,AUTH}$ at site U1343 compared to N. Pacific (Fig. 4.2A) indicates the presence of unradiogenic internal source in the Bering Sea, supporting the internal source scenario (Fig. 4.2A).

The best candidate for internal source is sediment-water interaction such as boundary exchange and pore water diffusion. Boundary exchange process represents overall chemical interaction between dissolved Nd (seawater) and

particulate Nd (sediments), including dissolution/precipitation, adsorption/desorption and isotopic exchange (Jeandel and Oelkers, 2015). This process occurs at land-ocean contact, for example, river mouths (weathering of river particulate matter), continental margins (submarine weathering) and subterranean estuaries (submarine groundwater discharge) (Jeandel, 2016). Since detrital sediments on the continental margin in the Bering Sea have typically unradiogenic ε_{Nd} (Fig. 4.1), boundary exchange could potentially supply unradiogenic Nd into the bottom water. The moderate correlation between $\varepsilon_{Nd,AUTH}$ and $\varepsilon_{Nd,DET}$ ($r = 0.49$) supports this speculation (Fig. 4.2B).

Pore water diffusion is also probable source of unradiogenic Nd in the Bering Sea. This process is the result of the interplay between dissolved Nd (pore water) and particulate Nd (sediments) during early diagenesis (Abbott et al., 2015, 2016; Du et al., 2016). That is, the mechanism controlling the ε_{Nd} flux from pore water is conceptually similar to boundary exchange, but participating sediments are older. How old are they? Preliminary pore water study at site U1343 on the Bering Slope shows that the sulfate-methane transition zone is located at ~8 m CCSF-A, which corresponds to ~34 kyr (Expedition 323 Scientists, 2011). Therefore, ε_{Nd} flux from pore water at site U1343 is primarily affected by the interaction of pore water with the sediments ranging in age from 0 to 34-kyr. Since this age interval for participating sediments is comparable to average sampling interval of $\varepsilon_{Nd,DET}$, the correlation coefficient between $\varepsilon_{Nd,AUTH}$ (t) and $\varepsilon_{Nd,DET}$ (t+1) can examine the relative influence of Nd flux from the older sediments relative to that from the younger ones. The lag-1 correlation is relatively weak ($r = 0.12$), implying that pore water diffusion from the older sediments is relatively limited. Consequently, boundary exchange and/or pore water diffusion from the younger sediments can be

more dominant sources at site U1343. Here we included pore water diffusion to a large extent of boundary exchange because diagenetic Nd flux from the younger sediments cannot be distinguished from boundary exchange within our sampling resolution.

Then, next question would be: "Does ε_{Nd} input from boundary exchange ($\varepsilon_{Nd,BE}$) follow ε_{Nd} of sediments contacting with water?". As shown in sequential chemical extraction (e.g. Bourlès et al., 1989; Tessier et al., 1979), each component in the sediment has different chemical reactivity (e.g. Bayon et al., 2016; Bayon et al., 2006). Volcanic materials are relatively more reactive as shown in many leaching experiments (Wilson et al., 2013; Wilson et al., 2012), and hence high % volcanic sediment can generate preferential release of radiogenic Nd during boundary exchange (Abbott et al., 2016; Noble et al., 2013; Wilson et al., 2012). Accordingly, $\varepsilon_{Nd,BE}$ does not always follow $\varepsilon_{Nd,DET}$, and this decoupling between $\varepsilon_{Nd,BE}$ and $\varepsilon_{Nd,DET}$ should be more intense when the sediments contain reactive volcanic materials.

We tentatively constrained the range of $\varepsilon_{Nd,BE}$ to evaluate the effect of the preferential release of radiogenic Nd during boundary exchange based on the following equation modified from Jang et al. (2017):

$$\varepsilon_{Nd,U1343} = \varepsilon_{Nd,adv} \cdot f_{Nd,adv} + \varepsilon_{Nd,BE} \cdot f_{Nd,BE} \quad (1)$$

$$f_{Nd,adv} + f_{Nd,BE} = 1 \quad (2)$$

where ε_{Nd} is the Nd isotopic flux from lateral advection (adv) and boundary exchange (BE), while f_{Nd} is the fraction of Nd flux from each source.

Two assumptions were considered here. First, we assumed $\varepsilon_{Nd,adv}$ to

have -2.2, which is ε_{Nd} value of the N. Pacific deep-water recorded in Fe-Mn crust at site 13D-27A over 2.3 Myr (van de Flierdt et al., 2004)(Fig. 4.2A). Secondly, the fraction of Nd flux from boundary exchange ($f_{Nd,BE}$) along the water circulation path from the N. Pacific (site 13D-27A) to the Bering Sea (site U1343) was assumed to be > 0.3, which is the minimum estimate from the Bering Sea (Jang et al., 2017) and the Madagascan margin (Wilson et al., 2012). Note that previous estimate ($f_{Nd,BE}$ = 0.3) is calculated without consideration of the preferential release of radiogenic Nd, so it is a minimum estimate. We do not consider NPDW formation here (section 4.4.2).

The results are shown in Figure 4.5. The estimated $\varepsilon_{Nd,BE}$ values are broadly correlated with $\varepsilon_{Nd,DET}$ (r = 0.49), suggesting that Nd isotopic composition of sediments is an important factor to determine $\varepsilon_{Nd,BE}$ to some extent. However, irregular $\varepsilon_{Nd,BE}$ deviations from $\varepsilon_{Nd,DET}$ imply that there are uncertain factors to determine $\varepsilon_{Nd,BE}$. For example, the estimated $\varepsilon_{Nd,BE}$ are mostly higher than $\varepsilon_{Nd,DET}$ (y-axis > 0) where $\varepsilon_{Nd,AUTH}$ are above -4.5 (Fig. 4.5). These radiogenic $\varepsilon_{Nd,BE}$ deviations can be attributed to *in situ* preferential release of radiogenic Nd during boundary exchange and/or the interaction with radiogenic sediments on the eastern side of continental margin (Fig. 4.1). Extremely high estimated $\varepsilon_{Nd,BE}$ values up to +4.3 support the preferential release hypothesis. We cannot constrain the appropriate f_{BE} values where $\varepsilon_{Nd,BE}$ values are higher than $\varepsilon_{Nd,DET}$ in a given dataset. On the other hand, some estimated $\varepsilon_{Nd,BE}$ values are lower than $\varepsilon_{Nd,DET}$ (y-axis < 0) under low f_{BE} condition where the $\varepsilon_{Nd,AUTH}$ are below -5 (Fig. 4.5). Since the preferential release of unradiogenic Nd during boundary exchange seems to be unrealistic, f_{BE} values would be greater than 0.5 for these periods (Fig. 4.5). Higher f_{BE} can be satisfied with the stagnant bottom water condition that provides higher

exposure time for the interaction between particle and seawater and (Jang et al., 2017; Siddall et al., 2008; Stewart et al., 2016) and/or with the condition of corrosive seawater that stimulates the reaction between seawater and particles. Future proxies and modelling studies are necessary to fully understand the boundary exchange system.

4.4.4. *Sediment binary mixing system between Alaska and the Aleutian Arc*

Seventy isotope analyses of detrital Nd isotopes at site U1343 represent average $\varepsilon_{Nd,\ DET}$ value of -6.6 ± 1.5 (1σ) with large fluctuations (Fig. 4.4A). The maximum $\varepsilon_{Nd,\ DET}$ value is up to -2.3, while the minimum is down to -9.0. Considering the contrast ε_{Nd} values of two main provenance areas: radiogenic Aleutian Arc and unradiogenic Alaska, this $\varepsilon_{Nd,\ DET}$ fluctuation can be interpreted by sediment binary mixing between the Aleutian Arc and Alaska (Horikawa et al., 2015; Jang et al., 2017). That is, relative contribution from each source determines $\varepsilon_{Nd,\ DET}$. For example, Aleutian Arc-sourced detrital materials (ε_{Nd} ~ +8, [Nd] ~ 12 ppm after Horikawa et al., 2015) and Alaskan-sourced detrital materials (ε_{Nd} ~ -9, [Nd] ~ 18.3 ppm after Horikawa et al., 2015) accounted for 35% and 65% of detrital sediment at site U1343 during the LGM ($\varepsilon_{Nd,\ DET}$ ~ -3.1), respectively (Fig. 4.4A). Overall, Alaska is dominant source for detrital sediment at site U1343, and its contribution occasionally reached to ~100% (e.g. 960 ka).

Higher proportion of the Alaskan-sourced materials results from the retreat of the Alaskan glaciation. At present, the sediment input from Alaska is mainly accomplished by the Yukon River, which provides more than half of the total sediment into the Bering Sea (Eberl, 2004), and sediment export from the Yukon River primarily occurs when snow (spring) and glaciers melt (summer-

autumn) (Dornblaser and Striegl, 2009). It means that meltwater can be a key process for supplying Alaskan-sourced sediments. Indeed, the decrease in diatom $\delta^{18}O$ at RC14-121 (54°5'N, 170°4'W; 2,530 m water depth) on Unmak Plateau (Sancetta et al., 1984) and associated unradiogenic $\varepsilon_{Nd,\ DET}$ at site U1341 (54˚2'N, 179˚0'E, 2,150 m water depth) on the Bowers Ridge (Horikawa et al., 2015) during the last deglaciation indicates that a large flux of meltwater from Alaska have transported Alaskan-sourced detrital sediments. Furthermore, the decreases in $\varepsilon_{Nd,DET}$ at site U1341 are generally accompanied by increases in meltwater indicators such as *Actinocyclus spp.* and $C_{37:4}$ alkenone, supporting this hypothesis (Horikawa et al., 2015). Since the flux of snowmelt is relatively limited, unradiogenic $\varepsilon_{Nd,\ DET}$ peaks can be attributed to the large flux of meltwater from Alaska.

We can therefore predict time of onset of glaciation in Alaska using $\varepsilon_{Nd,DET}$ at site U1343. One of the prominent features of $\varepsilon_{Nd,DET}$ records at site U1343 is the repetitive occurrences of unradiogenic peaks down to -8 ~ -9, indicating dominant Alaskan-sourced sediments (e.g. Jang et al., 2017). The first unradiogenic $\varepsilon_{Nd,DET}$ peak occurred as early as data were available, and these peaks occurred continuously over the last ~2.4 Myr without considerable numerical difference in $\varepsilon_{Nd,DET}$ (Fig. 4.4A). Since unradiogenic $\varepsilon_{Nd,\ DET}$ peaks can result from massive meltwater discharge from Alaska as mentioned above, these observations probably indicate that extensive glaciation in Alaska, for example, the Cordilleran Ice Sheet has existed since at least ~2.4 Myr (Froese et al., 2000; Hidy et al., 2013), and that its retreat has supplied substantial sediments from Alaska to the Bering Sea.

Is it possible for numerical difference in $\varepsilon_{Nd,DET}$ to estimate the scale of the Alaskan glaciation? Lack of numerical difference between unradiogenic $\varepsilon_{Nd,DET}$

peaks over the last ~2.4 Myr may be interpreted that there is no significant difference in magnitude of meltwater flux and perhaps the scale of glaciation in Alaska across the MPT, which can be supported by general absence of 41-kyr periodicity of $\delta^{18}O_{bf}$ at site U1343 and heavier $\delta^{18}O_{bf}$ of site U1343 than LR04 stack before the MPT. However, this speculation could be wrong because duration of each peak cannot be considered due to low sampling resolution, and both observations in $\delta^{18}O_{bf}$ can also be interpreted as low sampling resolution of $\delta^{18}O_{bf}$ (Asahi et al., 2016) and local hydrographic condition (e.g. Elderfield et al., 2012), respectively. Furthermore, elevated glacigenic sediment deposition in the Gulf of Alaska since the MPT suggest that increased volume of ice and/or duration of glaciation in Alaska (Gulick et al., 2015). Consequently, the scale of the Alaskan glaciation is not likely to be similar across the MPT, and this conclusion can be further evaluated using the periodicity of appropriate proxies such as $\varepsilon_{Nd,DET}$ and $\varepsilon_{Nd,AUTH}$.

4.4.5. *Cross spectrum analysis across the MPT*

The estimation of periodicity of $\varepsilon_{Nd,DET}$ in the Bering Sea possibly provides the perspective on the scale of the Alaskan glaciation across the MPT instead of $\delta^{18}O_{bf}$. However, low sampling resolution of $\varepsilon_{Nd,DET}$ at site U1343 (~33.9 kyr resampling) restricts to resolve obliquity (41-kyr) and eccentricity (100-kyr) variations. Indeed, 200-kyr and 150-kyr periodicity were partially recognized in $\varepsilon_{Nd,DET}$ at 95% confidence level of the continuous wavelet transform, and no dominant periodicity was detected at 95% confidence level of REDFIT analysis (not shown). Since $\varepsilon_{Nd,AUTH}$ is primarily affected by boundary exchange, and ε_{Nd} flux from boundary exchange is broadly determined by $\varepsilon_{Nd,DET}$ at site U1343

(section 4.4.3), $\varepsilon_{Nd,AUTH}$ may be an alternative of $\varepsilon_{Nd,DET}$.

We therefore tentatively traced the scale of the Alaskan glaciation over 2.4 Myr using the periodicity of $\varepsilon_{Nd,AUTH}$. Re-sampled $\varepsilon_{Nd,AUTH}$ data at every 15.4 kyr are broadly consistent with measured ones, but fluctuations in $\varepsilon_{Nd,AUTH}$ before the MPT (e.g. 2.0 to 1.8 Ma) and during the MPT (e.g. 1.1 to 0.9 Ma) are not well reproduced due to higher sampling resolution at those time (Fig. 4.6A). Both statistical results (Fig. 4.6B and D) do not precisely correspond to the global trend that represents the shift from 41-kyr to 100-kyr periodicity across the MPT (Figs. 4.6C and E). Continuous wavelet transform analysis displays 80-kyr periodicity only at 0.2 to 0.4 Ma and 1.0 to 1.5 Ma in addition to ~160-kyr periodicity at 1.4 to 2.0 Ma (Fig. 4.6B), while REDFIT spectral analysis shows 84-kyr periodicity over 2.4 Myr at the 95% confidence level (Fig. 4.6D).

Dominant 80-kyr and 84-kyr periodicities of $\varepsilon_{Nd,AUTH}$ are nearly twice the period of obliquity (e.g. Sen et al., 2009), implying that obliquity forcing drives deep-water Nd isotopic composition. This obliquity-like periodicity partially corresponds to global $\delta^{18}O_{bf}$ trend showing 41-periodicity during Pleistocene (Ford et al., 2016; Pisias and Moore, 1981; Raymo and Nisancioglu, 2003; Shackleton and Opdyke, 1976) (Figs. 4.6C, E and F). A possible scenario is that the Alaskan glaciation controls the sediment binary mixing in the Bering Sea (Horikawa et al., 2015), and consequent sediment provenance determines ε_{Nd} inflow from boundary exchange and further seawater ε_{Nd}. Discontinuity of 80-kyr periodicity over 2.4 Myr and lack of 100-kyr periodicity since the MPT can be caused by the involvement of preferential release of radiogenic Nd during boundary exchange as inferred from irregular deviation of $\varepsilon_{Nd,AUTH}$ from $\varepsilon_{Nd,DET}$ (section 4.4.3), which may increase uncertainty for spectral analyses. Poor time resolution of $\varepsilon_{Nd,AUTH}$ is also

likely reason. Incomplete reconstruction in the scale of the Alaskan glaciation using $\varepsilon_{Nd,AUTH}$ and $\delta^{18}O_{bf}$ at site U1343 can be complemented by future analyses of $\delta^{18}O_{bf}$ in the Gulf of Alaska.

4.5. Conclusion

We present ε_{Nd} records in authigenic (*Wilson Authigenic*) and detrital fractions of marine sediments at site U1343 (1,950 m) on the Bering Slope over 2.4 Myr. The reconstructed ε_{Nd} of deep-water in the Bering Sea shows average value of -3.0 ± 1.1 (1σ) with large fluctuations. Considering uniform ε_{Nd} values of contemporaneous deep-water in the N. Pacific as recorded in Fe-Mn crust, temporal variation in deep-water ε_{Nd} in the Bering Sea can be interpreted by boundary exchange and NPDW formation rather than large-scale ocean mixing and circulation. The heavier $\delta^{18}O_{bf}$ of site U1343 than LR04 stack and shallower site U1342, and general abundance of *Actinocyclus spp.* implies the absence of NPDW formation over 2.4 Myr except for one event at ~660 ka, suggesting boundary exchange as the main mechanism controlling deep-water ε_{Nd} in the Bering Sea. The ε_{Nd} values derived from boundary exchange are difficult to constrain due to preferential release of radiogenic Nd, but it is likely to rely on sediment provenance as inferred from moderate correlation of ε_{Nd} between authigenic and detrital fractions.

The variation in detrital ε_{Nd} shows binary mixing system between Aleutian Arc and Alaska in the Bering Sea over 2.4 Myr, and the first occurrence of minimum detrital ε_{Nd} and its continuous emergence implies that the Alaskan glaciation has existed since at least ~2.4 Ma. The scale of the Alaskan glaciation

across the MPT was tentatively traced using the periodicity of $\varepsilon_{Nd,AUTH}$, and general 80-kyr periodicity of $\varepsilon_{Nd,AUTH}$ implies that obliquity-like variation drives Nd isotopic composition of deep-water. We speculate that the development of the Alaskan Glaciation controls sediment binary mixing system in the Bering Sea, causing change in ε_{Nd} derived from boundary exchange and further seawater ε_{Nd} in the Bering Sea. Lack of 100-kyr periodicity since the MPT and discontinuous obliquity-like periodicity over 2.4 Myr can result from preferential release of radiogenic Nd during boundary exchange and poor time resolution of $\varepsilon_{Nd,AUTH}$.

References

Abbott, A.N., Haley, B.A., McManus, J., 2015. Bottoms up: Sedimentary control of the deep North Pacific Ocean's ε_{Nd} signature. Geology 43, 1035-1035.

Abbott, A.N., Haley, B.A., McManus, J., 2016. The impact of sedimentary coatings on the diagenetic Nd flux. Earth Planet. Sci. Lett. 449, 217-227.

Arsouze, T., Dutay, J.-C., Lacan, F., Jeandel, C., 2007. Modeling the neodymium isotopic composition with a global ocean circulation model. Chem. Geol. 239, 165-177.

Asahi, H., Kender, S., Ikehara, M., Sakamoto, T., Takahashi, K., Ravelo, A., Alvarez Zarikian, C., Khim, B., Leng, M., 2016. Orbital-scale benthic foraminiferal oxygen isotope stratigraphy at the northern Bering Sea Slope Site U1343 (IODP Expedition 323) and its Pleistocene paleoceanographic significance. Deep-Sea Res. II 125-126, 66-83.

Bayon, G., Skonieczny, C., Delvigne, C., Toucanne, S., Bermell, S., Ponzevera, E., André, L., 2016. Environmental Hf–Nd isotopic decoupling in world river clays. Earth Planet. Sci. Lett. 438, 25-36.

Bayon, G., Vigier, N., Burton, K., Jean Carignan, A., Etoubleau, J., Chu, N., 2006. The control of weathering processes on riverine and seawater hafnium isotope ratios. Geology 34, 433.

Berger, A., Li, X., Loutre, M., 1999. Modelling Northern Hemisphere ice volume over the last 3Ma. Quat. Sci. Rev. 18, 1-11.

Bourlès, D., Raisbeck, G.M., Yiou, F., 1989. ^{10}Be and ^{9}Be in marine sediments and their potential for dating. Geochim. Cosmochim. Acta 53, 443-452.

Brennan, C., Meissner, K., Eby, M., Hillaire-Marcel, C., Weaver, A., 2013. Impact

of sea ice variability on the oxygen isotope content of seawater under glacial and interglacial conditions. Paleoceanography 28, 388-400.

Clark, P.U., Archer, D., Pollard, D., Blum, J.D., Rial, J.A., Brovkin, V., Mix, A.C., Pisias, N.G., Roy, M., 2006. The middle Pleistocene transition: characteristics, mechanisms, and implications for long-term changes in atmospheric pCO_2. Quat. Sci. Rev. 25, 3150-3184.

Cook, M.S., Ravelo, A.C., Mix, A., Nesbitt, I.M., Miller, N.V., 2016. Tracing subarctic Pacific water masses with benthic foraminiferal stable isotopes during the LGM and late Pleistocene. Deep-Sea Res. II 125, 84-95.

Dornblaser, M.M., Striegl, R.G., 2009. Suspended sediment and carbonate transport in the Yukon River Basin, Alaska: Fluxes and potential future responses to climate change. Water Resour. Res. 45, W06411, doi:06410.01029/02008WR007546.

Du, J., Haley, B.A., Mix, A.C., 2016. Neodymium isotopes in authigenic phases, bottom waters and detrital sediments in the Gulf of Alaska and their implications for paleo-circulation reconstruction. Geochim. Cosmochim. Acta 193, 14-35.

Eberl, D., 2004. Quantitative mineralogy of the Yukon River system: Changes with reach and season, and determining sediment provenance. Am. Mineral. 89, 1784-1794.

Elderfield, H., Ferretti, P., Greaves, M., Crowhurst, S., McCave, I.N., Hodell, D., Piotrowski, A.M., 2012. Evolution of ocean temperature and ice volume through the mid-Pleistocene climate transition. Science 337, 704-709.

Expedition 323 Scientists, 2011. Site U1343. In Takahashi, K., Ravelo, A.C., Alvarez Zarikian, C.A., and the Expedition 323 Scientists (Eds.), Proc.

IODP, 323. Integrated Ocean Drilling Program Management International, Inc., Tokyo.

Ford, H.L., Sosdian, S.M., Rosenthal, Y., Raymo, M.E., 2016. Gradual and abrupt changes during the Mid-Pleistocene Transition. Quat. Sci. Rev. 148, 222-233.

Frank, M., Whiteley, N., Kasten, S., Hein, J.R., O'Nions, K., 2002. North Atlantic Deep Water export to the Southern Ocean over the past 14 Myr: Evidence from Nd and Pb isotopes in ferromanganese crusts. Paleoceanography 17, 1022-1030.

Froese, D., Barendregt, R., Enkin, R., Baker, J., 2000. Paleomagnetic evidence for multiple late Pliocene-early Pleistocene glaciations in the Klondike area, Yukon Territory. Can. J. Earth Sci. 37, 863-877.

GEOROC, 2003. Geochemistry of Rocks of the Oceans and Continents. Mainz, Germany, Max-Planck Institute fur Chemie. <http://georoc.mpch-mainz.gwdg.de/>.

Goldstein, S.L., Hemming, S.R., 2003. 6.17 - Long-lived isotopic tracers in oceanography, paleoceanography, and ice-sheet dynamics A2 - Holland, Heinrich D, In: Turekian, K.K. (Ed.), Treatise on Geochemistry. Pergamon, Oxford, pp. 453-489.

Goldstein, S.L., O'Nions, R.K., Hamilton, P.J., 1984. A Sm-Nd isotopic study of atmospheric dusts and particulates from major river systems. Earth Planet. Sci. Lett. 70, 221-236.

Gulick, S.P., Jaeger, J.M., Mix, A.C., Asahi, H., Bahlburg, H., Belanger, C.L., Berbel, G.B., Childress, L., Cowan, E., Drab, L., 2015. Mid-Pleistocene climate transition drives net mass loss from rapidly uplifting St. Elias

Mountains, Alaska. Proc. Natl. Acad. Sci. 112, 15042-15047.

Hammer, Ø., Harper, D.A.T., Ryan, P.D., 2001. PAST: Paleontological Statistics Software Package for Education and Data Analysis. Paleontol. Electron. 4, 1-9.

Hidy, A.J., Gosse, J.C., Froese, D.G., Bond, J.D., Rood, D.H., 2013. A latest Pliocene age for the earliest and most extensive Cordilleran Ice Sheet in northwestern Canada. Quat. Sci. Rev. 61, 77-84.

Hillaire-Marcel, C., de Vernal, A., 2008. Stable isotope clue to episodic sea ice formation in the glacial North Atlantic. Earth Planet. Sci. Lett. 268, 143-150.

Horikawa, K., Asahara, Y., Yamamoto, K., Okazaki, Y., 2010. Intermediate water formation in the Bering Sea during glacial periods: Evidence from neodymium isotope ratios. Geology 38, 435-438.

Horikawa, K., Martin, E.E., Basak, C., Onodera, J., Seki, O., Sakamoto, T., Ikehara, M., Sakai, S., Kawamura, K., 2015. Pliocene cooling enhanced by flow of low-salinity Bering Sea water to the Arctic Ocean. Nat. Commun. 6, 7587.

Hu, A., Meehl, G.A., Han, W., Timmermann, A., Otto-Bliesner, B., Liu, Z., Washington, W.M., Large, W., Abe-Ouchi, A., Kimoto, M., 2012. Role of the Bering Strait on the hysteresis of the ocean conveyor belt circulation and glacial climate stability. Proc. Natl. Acad. Sci. 109, 6417-6422.

Hu, R., Noble, T.L., Piotrowski, A.M., McCave, I.N., Bostock, H.C., Neil, H.L., 2016. Neodymium isotopic evidence for linked changes in Southeast Atlantic and Southwest Pacific circulation over the last 200 kyr. Earth Planet. Sci. Lett. 455, 106-114.

Imbrie, J., Boyle, E., Clemens, S., Duffy, A., Howard, W., Kukla, G., Kutzbach, J., Martinson, D., McIntyre, A., Mix, A., 1992. On the structure and origin of major glaciation cycles 1. Linear responses to Milankovitch forcing. Paleoceanography 7, 701-738.

Jacobsen, S.B., Wasserburg, G.J., 1980. Sm-Nd isotopic evolution of chondrites. Earth Planet. Sci. Lett. 50, 139-155.

Jang, K., Han, Y., Huh, Y., Nam, S.-I., Stein, R., Mackensen, A., Matthiessen, J., 2013. Glacial freshwater discharge events recorded by authigenic neodymium isotopes in sediments from the Mendeleev Ridge, western Arctic Ocean. Earth Planet. Sci. Lett. 369–370, 148-157.

Jang, K., Huh, Y., Han, Y., 2017. Authigenic Nd isotope record of North Pacific Intermediate Water formation and boundary exchange on the Bering Slope. Quat. Sci. Rev. 156, 150-163.

Jeandel, C., 2016. Overview of the mechanisms that could explain the 'Boundary Exchange' at the land–ocean contact. Phil. Trans. R. Soc. A 374, 20150287.

Jeandel, C., Oelkers, E.H., 2015. The influence of terrigenous particulate material dissolution on ocean chemistry and global element cycles. Chem. Geol. 395, 50-66.

Katsuki, K., Takahashi, K., 2005. Diatoms as paleoenvironmental proxies for seasonal productivity, sea-ice and surface circulation in the Bering Sea during the late Quaternary. Deep-Sea Res. II 52, 2110-2130.

Kim, S., Takahashi, K., Khim, B.-K., Kanematsu, Y., Asahi, H., Ravelo, A.C., 2014. Biogenic opal production changes during the mid-Pleistocene transition in the Bering Sea (IODP Expedition 323 Site U1343). Quat. Res. 81, 151-157.

Knudson, K.P., Ravelo, A.C., 2015. North Pacific Intermediate Water circulation enhanced by the closure of the Bering Strait. Paleoceanography 30, 1287-1304.

Lacan, F., Jeandel, C., 2005. Neodymium isotopes as a new tool for quantifying exchange fluxes at the continent–ocean interface. Earth Planet. Sci. Lett. 232, 245-257.

Laskar, J., Robutel, P., Joutel, F., Gastineau, M., Correia, A., Levrard, B., 2004. A long-term numerical solution for the insolation quantities of the Earth. Astron. Astrophys. 428, 261-285.

Lisiecki, L.E., Raymo, M.E., 2005. A Plio-Pleistocene stack of 57 globally distributed benthic $\delta^{18}O$ records. Paleoceanography 20, PA1003, doi:1010.1029/2004PA001071.

Mudelsee, M., Schulz, M., 1997. The mid-Pleistocene climate transition: onset of 100 ka cycle lags ice volume build-up by 280 ka. Earth Planet. Sci. Lett. 151, 117-123.

Noble, T.L., Piotrowski, A.M., McCave, I.N., 2013. Neodymium isotopic composition of intermediate and deep waters in the glacial southwest Pacific. Earth Planet. Sci. Lett. 384, 27-36.

Ohkushi, K.i., Itaki, T., Nemoto, N., 2003. Last Glacial–Holocene change in intermediate-water ventilation in the Northwestern Pacific. Quat. Sci. Rev. 22, 1477-1484.

Okazaki, Y., Timmermann, A., Menviel, L., Harada, N., Abe-Ouchi, A., Chikamoto, M.O., Mouchet, A., Asahi, H., 2010. Deepwater formation in the North Pacific during the last glacial termination. Science 329, 200-204.

Onodera, J., Takahashi, K., Nagatomo, R., 2016. Diatoms, silicoflagellates, and

ebridians at Site U1341 on the western slope of Bowers Ridge, IODP Expedition 323. Deep-Sea Res. II 125, 8-17.

Pena, L.D., Goldstein, S.L., 2014. Thermohaline circulation crisis and impacts during the mid-Pleistocene transition. Science 345, 318-322.

Piepgras, D.J., Jacobsen, S.B., 1988. The isotopic composition of neodymium in the North Pacific. Geochim. Cosmochim. Acta 52, 1373-1381.

Piotrowski, A.M., Goldstein, S.L., Hemming, S.R., Fairbanks, R.G., 2004. Intensification and variability of ocean thermohaline circulation through the last deglaciation. Earth Planet. Sci. Lett. 225, 205-220.

Pisias, N.G., Moore, T.C., 1981. The evolution of Pleistocene climate: A time series approach. Earth Planet. Sci. Lett. 52, 450-458.

Ravelo, A.C., Andreasen, D.H., Lyle, M., Lyle, A.O., Wara, M.W., 2004. Regional climate shifts caused by gradual global cooling in the Pliocene epoch. Nature 429, 263-267.

Raymo, M., Oppo, D., Curry, W., 1997. The mid-Pleistocene climate transition: A deep sea carbon isotopic perspective. Paleoceanography 12, 546-559.

Raymo, M.E., Nisancioglu, K.H., 2003. The 41 kyr world: Milankovitch's other unsolved mystery. Paleoceanography 18, 1011, doi:1010.1029/2002PA000791.

Rella, S.F., Tada, R., Nagashima, K., Ikehara, M., Itaki, T., Ohkushi, K.i., Sakamoto, T., Harada, N., Uchida, M., 2012. Abrupt changes of intermediate water properties on the northeastern slope of the Bering Sea during the last glacial and deglacial period. Paleoceanography 27, PA3203, doi:3210.1029/2011PA002205.

Rutberg, R.L., Hemming, S.R., Goldstein, S.L., 2000. Reduced North Atlantic

Deep Water flux to the glacial Southern Ocean inferred from neodymium isotope ratios. Nature 405, 935-938.

Sancetta, C., Heusser, L., Labeyrie, L., Naidu, A.S., Robinson, S.W., 1984. Wisconsin-Holocene paleoenvironment of the Bering Sea: Evidence from diatoms, pollen, oxygen isotopes and clay minerals. Mar. Geol. 62, 55-68.

Sancetta, C., Silvestri, S., 1986. Pliocene-Pleistocene evolution of the North Pacific Ocean-Atmosphere system, interpreted from fossil diatoms. Paleoceanography 1, 163-180.

Schmieder, F., von Dobeneck, T., Bleil, U., 2000. The mid-Pleistocene climate transition as documented in the deep South Atlantic Ocean: initiation, interim state and terminal event. Earth Planet. Sci. Lett. 179, 539-549.

Schulz, M., Mudelsee, M., 2002. REDFIT: estimating red-noise spectra directly from unevenly spaced paleoclimatic time series. Comput. Geosci. 28, 421-426.

Sen, A.K., Filippelli, G.M., Flores, J.-A., 2009. An application of wavelet analysis to paleoproductivity records from the Southern Ocean. Comput. Geosci. 35, 1445-1450.

Shackleton, N., Opdyke, N., 1976. Oxygen-isotope and paleomagnetic stratigraphy of Pacific core V28-239 late Pliocene to latest Pleistocene. Geol. Soc. Am, Mem. 145, 449-464.

Siddall, M., Khatiwala, S., van de Flierdt, T., Jones, K., Goldstein, S.L., Hemming, S., Anderson, R.F., 2008. Towards explaining the Nd paradox using reversible scavenging in an ocean general circulation model. Earth Planet. Sci. Lett. 274, 448-461.

Springer, A.M., McRoy, C.P., Flint, M.V., 1996. The Bering Sea Green Belt: shelf-

edge processes and ecosystem production. Fish. Oceanogr. 5, 205-223.

Stabeno, P.J., Kachel, N.B., Moore, S.E., Napp, J.M., Sigler, M., Yamaguchi, A., Zerbini, A.N., 2012. Comparison of warm and cold years on the southeastern Bering Sea shelf and some implications for the ecosystem. Deep-Sea Res. II 65, 31-45.

Stewart, J.A., Gutjahr, M., James, R.H., Anand, P., Wilson, P.A., 2016. Influence of the Amazon River on the Nd isotope composition of deep water in the western equatorial Atlantic during the Oligocene–Miocene transition. Earth Planet. Sci. Lett. 454, 132-141.

Tachikawa, K., Jeandel, C., Roy-Barman, M., 1999. A new approach to the Nd residence time in the ocean: the role of atmospheric inputs. Earth Planet. Sci. Lett. 170, 433-446.

Teraishi, A., Suto, I., Onodera, J., Takahashi, K., 2016. Diatom, silicoflagellate and ebridian biostratigraphy and paleoceanography in IODP 323 Hole U1343E at the Bering slope site. Deep-Sea Res. II 125-126, 18-28.

Tessier, A., Campbell, P.G.C., Bisson, M., 1979. Sequential extraction procedure for the speciation of particulate trace metals. Anal. Chem. 51, 844-851.

Torrence, C., Compo, G.P., 1998. A practical guide to wavelet analysis. B. Am. Meteorol. Soc. 79, 61-78.

van de Flierdt, T., Frank, M., Lee, D.-C., Halliday, A.N., Reynolds, B.C., Hein, J.R., 2004. New constraints on the sources and behavior of neodymium and hafnium in seawater from Pacific Ocean ferromanganese crusts. Geochim. Cosmochim. Acta 68, 3827-3843.

VanLaningham, S., Pisias, N.G., Duncan, R.A., Clift, P.D., 2009. Glacial–interglacial sediment transport to the Meiji Drift, northwest Pacific Ocean:

Evidence for timing of Beringian outwashing. Earth Planet. Sci. Lett. 277, 64-72.

Vroon, P., Van Bergen, M., Klaver, G., White, W., 1995. Strontium, neodymium, and lead isotopic and trace-element signatures of the East Indonesian sediments: provenance and implications for Banda Arc magma genesis. Geochim. Cosmochim. Acta 59, 2573-2598.

Warner, M.J., Roden, G.I., 1995. Chlorofluorocarbon evidence for recent ventilation of the deep Bering Sea. Nature 373, 409-412.

Wilson, D.J., Piotrowski, A.M., Galy, A., Clegg, J.A., 2013. Reactivity of neodymium carriers in deep sea sediments: Implications for boundary exchange and paleoceanography. Geochim. Cosmochim. Acta 109, 197-221.

Wilson, D.J., Piotrowski, A.M., Galy, A., McCave, I.N., 2012. A boundary exchange influence on deglacial neodymium isotope records from the deep western Indian Ocean. Earth Planet. Sci. Lett. 341–344, 35-47.

Winter, B.L., Johnson, C.M., Clark, D.L., 1997. Strontium, neodymium, and lead isotope variations of authigenic and silicate sediment components from the Late Cenozoic Arctic Ocean: Implications for sediment provenance and the source of trace metals in seawater. Geochim. Cosmochim. Acta 61, 4181-4200.

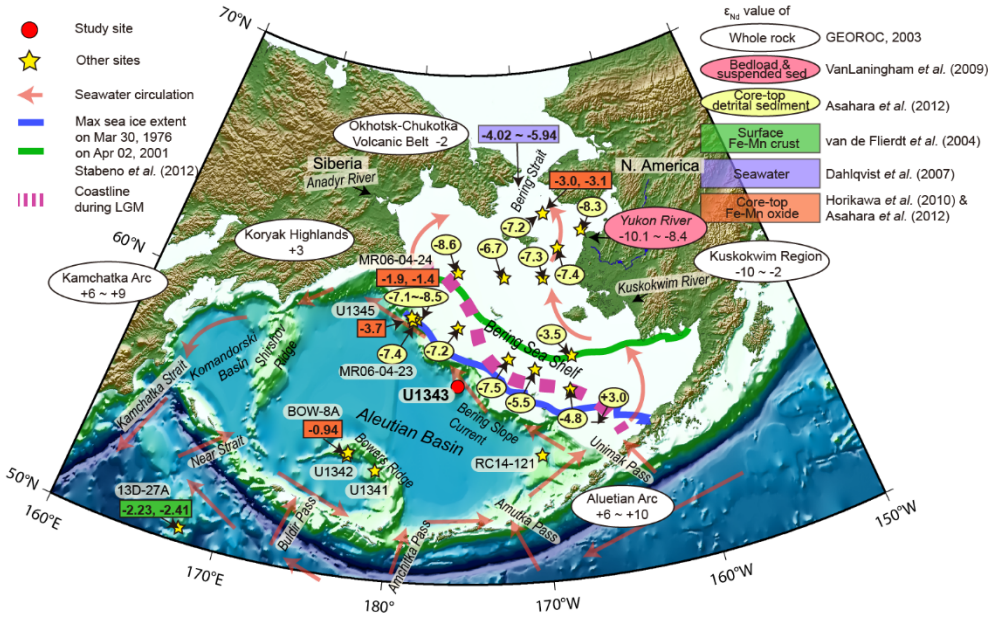

Figure 4.1. The Nd isotopic composition (ε_{Nd}) of U1343 (red circle) and neighboring sites in the Bering Sea. The ε_{Nd} values represent in ellipses and rectangles with different colors. The water mass from the N. Pacific flows into the Bering Sea through the pathways in the Aleutian Arc, and which either circulates anticlockwise along the shelf break, or flows northward (red arrows). The modern maximum and minimum extent of seasonal sea ice are remarked in blue and green lines (Stabeno et al., 2012). Gray dashed line indicates the coastline during the LGM sea level lowstand. The figure is modified from Jang et al. (2017).

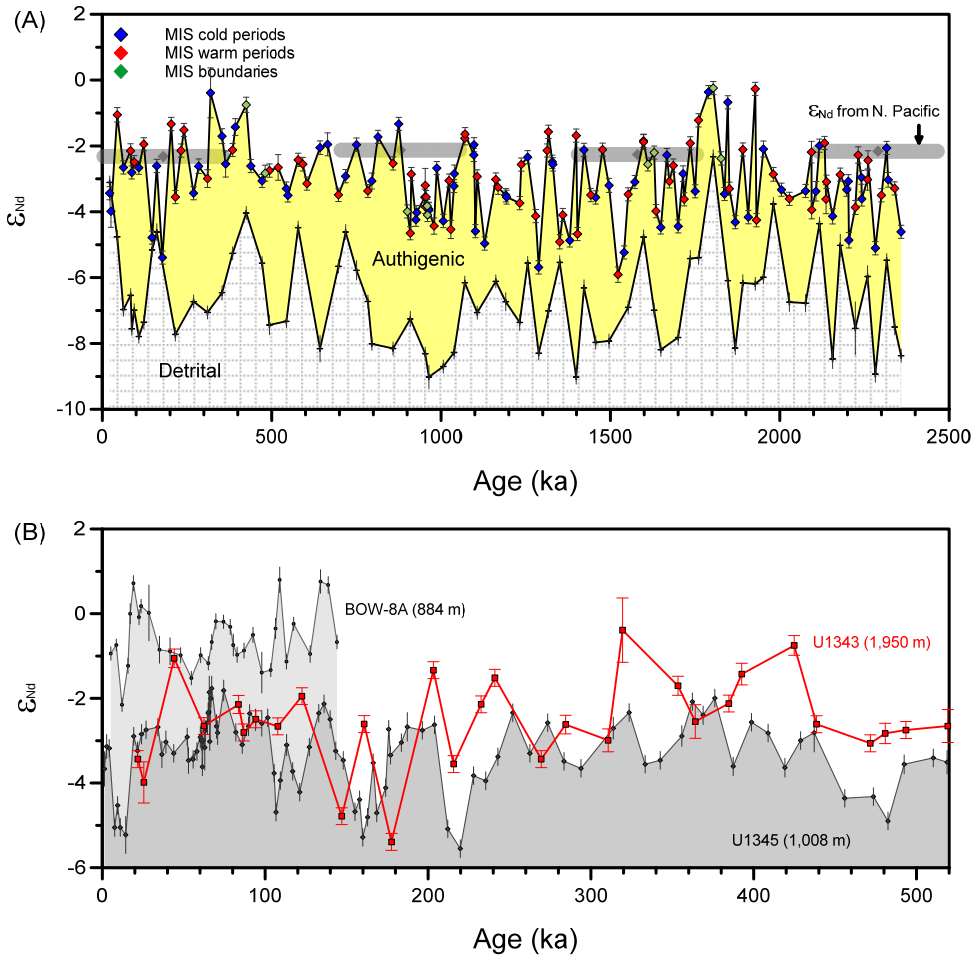

Figure 4.2. The comparison results of authigenic ε_{Nd} at site U1343 with (A) detrital ε_{Nd} at the same site over 2.4 Myr and (B) authigenic ε_{Nd} at sites BOW-8A (data from Horikawa et al., 2010) and U1345 (data from Jang et al., 2017). Blue, red and green symbols of authigenic ε_{Nd} in (A) mark different climate periods like MIS cold and warm periods and MIS boundaries, respectively. Gray thick lines in (A) indicate ε_{Nd} of N. Pacific deep water recorded in Fe-Mn crust (data from van de Flierdt et al., 2004), and their lengths are estimated coverage ages.

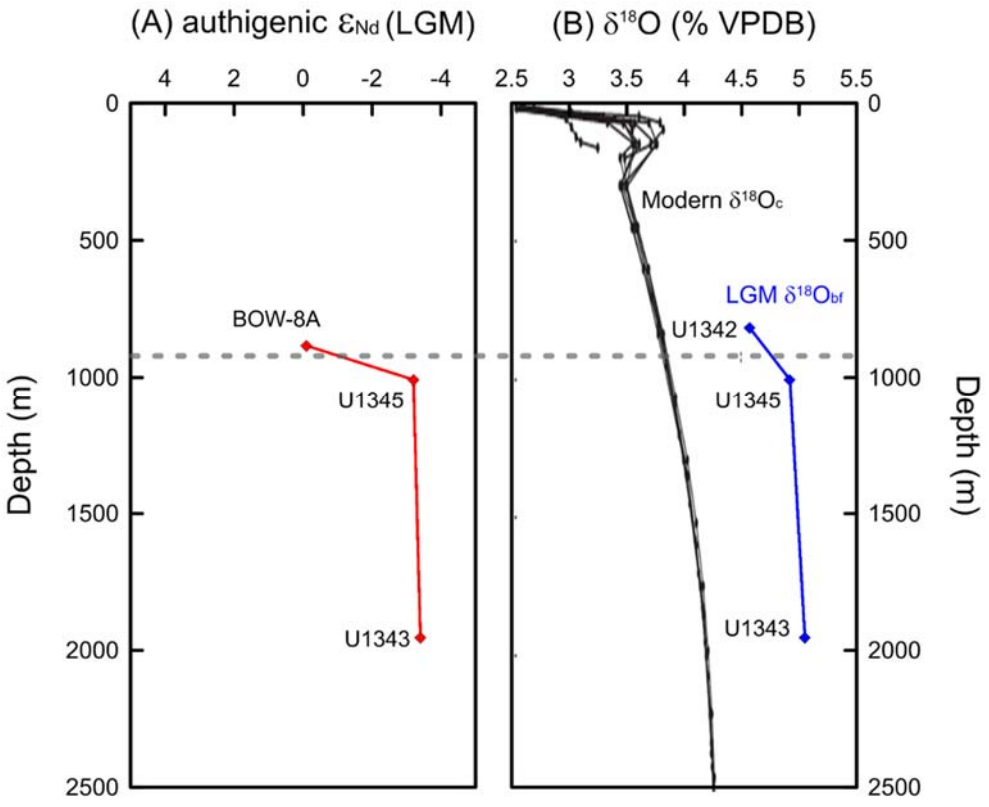

Figure 4.3. (A) Authigenic ε_{Nd} at different depths in the Bering Sea during the LGM and (B) $\delta^{18}O$ profiles at present (black) and during the LGM (blue). Modern equilibrium calcite $\delta^{18}O$ ($\delta^{18}O_c$) in the Bering Sea was calculated from hydrocast temperature and salinity by Cook et al. (2016). Authigenic ε_{Nd} data are from Horikawa et al. (2010) and Jang et al. (2017), and $\delta^{18}O_{bf}$ data during the LGM are from Cook et al. (2016), Knudson and Ravelo (2015) and Asahi et al. (2016). Gray dashed line indicates possible hydrographic boundary during the LGM.

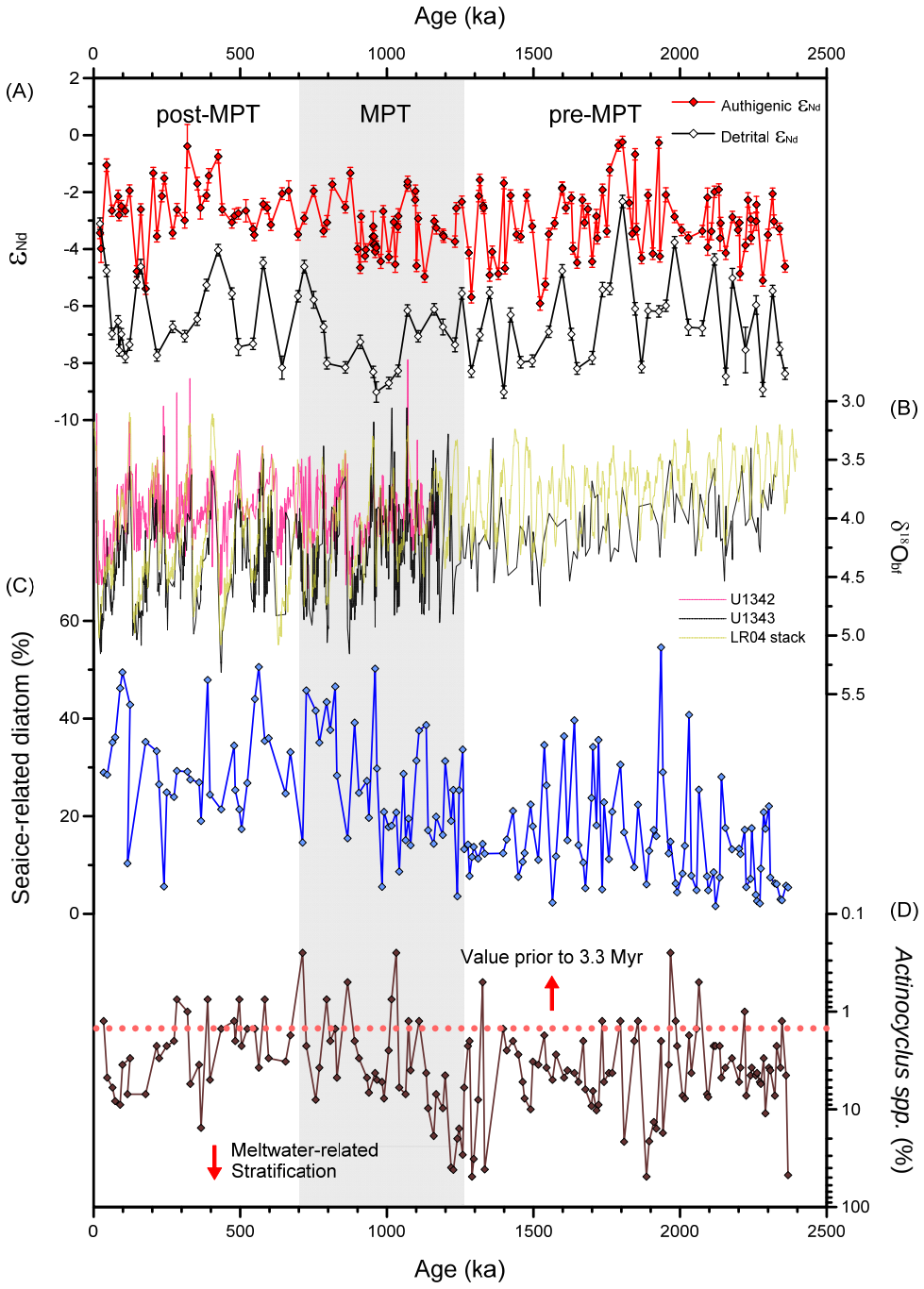

Figure 4.4. Reconstructed (A) ε_{Nd} values of authigenic (red diamonds) and detrital fractions (open diamonds) with (B) $\delta^{18}O_{bf}$ of global LR04 stack (yellow; Lisiecki and Raymo, 2005), sites U1343 (black; Asahi et al., 2016) and site U1342 (magenta; Knudson and Ravelo, 2015), (C) % of sea ice-related diatom

and (D) % of *Actinocyclus spp.* (blue and dark brown; Teraishi et al., 2016). Gray bar indicates approximate range of MPT period (Elderfield et al., 2012), and red dotted line in (D) represents % of *Actinocyclus spp.* prior to 3.3 Myr when the meltwater from Alaskan glacier is absent (Horikawa et al., 2015).

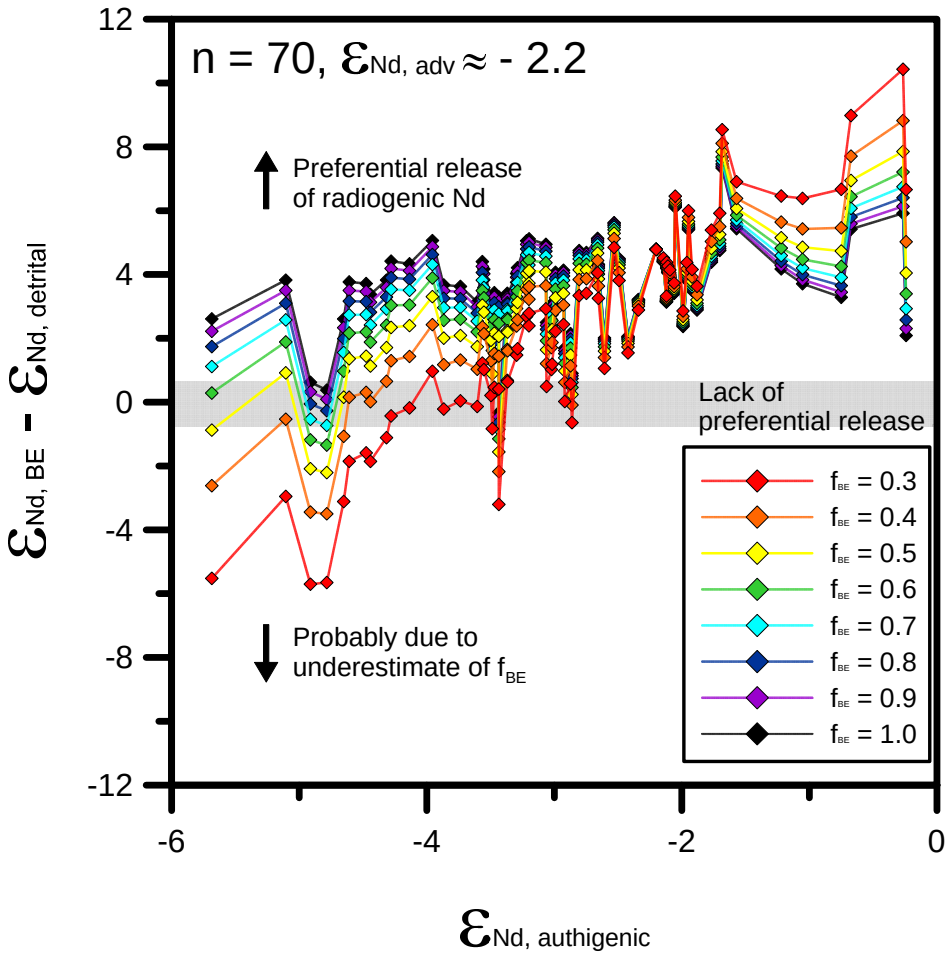

Figure 4.5. The differences between estimated ε_{Nd} input from boundary exchange and detrital ε_{Nd}. The differences are variable in response to the contribution of boundary exchange to Nd budget in the Bering Sea (f_{BE}). The positive values of y-axis indicate preferential release of radiogenic Nd, while negative values do incorrect estimation possibly due to underestimated f_{BE}.

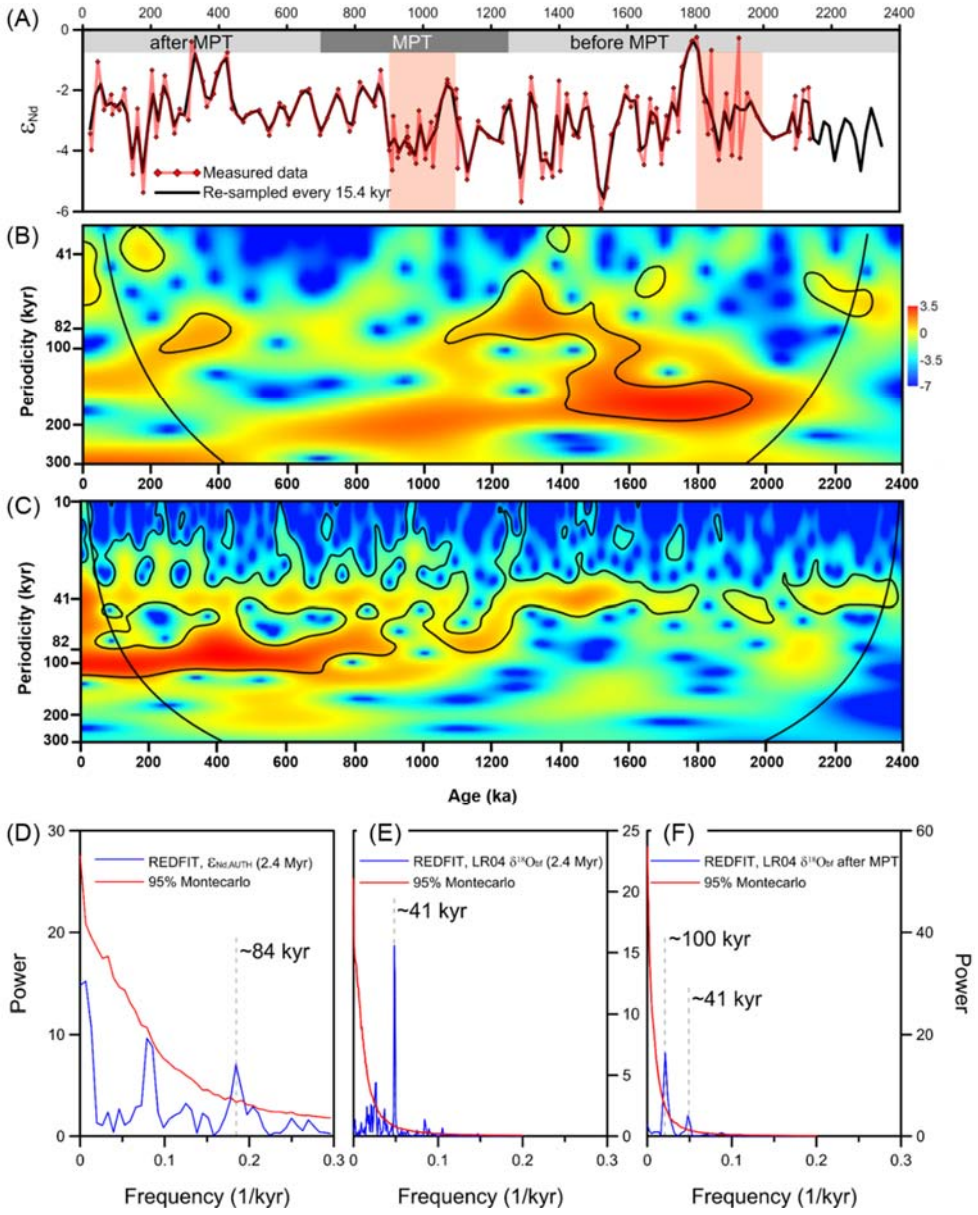

Figure 4.6. (A) Comparison between re-sampled (black) and measured $\varepsilon_{Nd,AUTH}$ (red), continuous wavelet transform of (B) re-sampled $\varepsilon_{Nd,AUTH}$ at site U1343 and (C) global LR04 $\delta^{18}O_{bf}$, and REDFIT spectra of (D) re-sampled $\varepsilon_{Nd,AUTH}$ at site U1343 over 2.4 Myr and global LR04 $\delta^{18}O_{bf}$ in different time windows such as (E) 2.4 Myr and (F) 0.75 Myr. Re-sampled $\varepsilon_{Nd,AUTH}$ are broadly correlated

with measured ones, except for age intervals for high sampling resolution (orange bars). Thick black contours in (B) and (C) and red lines in (D), (E) and (F) indicate 95% confidence level.

Chapter 5. K, Th and U concentrations derived from shipboard natural gamma radiation spectra of Bering Sea sediments and their utility as tracers of lithological sediment provenance and paleo-oceanic redox conditions

Kwangchul Jang, Youngsook Huh and David De Vleeschouwer

Abstract

Potassium, Th and U concentrations can be estimated from natural gamma radiation (NGR) spectra of marine sediments cored during the International Ocean Discovery Program (IODP) using a MATLAB algorithm. As NGR spectra for IODP cores and the MATLAB algorithm are open access, downcore variability in K, Th and U concentrations faithfully provide high-resolution paleo-environmental information without extra cost and time-consuming analysis process. Here we present K, Th and U concentrations estimated from NGR spectra of sediments at sites U1341, U1342, U1343 and U1345 in the Bering Sea and constrain the primary factors controlling K, Th and U concentration. Then, we evaluate the utility of K/Th and Th/U ratios as tracers of lithological sediment provenance and paleo-oceanic redox conditions.

We firstly constrain the main mechanism causing change in K, Th and U concentration using simple sediment mixing model based on K, Th and U

concentrations from Bering Sea sediments and two main source regions, the Aleutian Arc and Alaska. According to this model, K is relatively robust element to secondary factors, while Th tends to decrease by heavy mineral sorting. Uranium also shows decrease trend by heavy mineral sorting, but U-uptake under reducing bottom water conditions partly compensates for decreased U. Since there is no significant fractionation between Th and U during sediment transportation, the Th/U ratio can be tracers of lithological sediment provenance and paleo-oceanic redox conditions. Likewise, if heavy mineral sorting resulted in uniform end-member from each source, the change in K/Th and K/U ratios would reflect the variation in lithological sediment provenance. To examine this hypothesis, we compared the K/Th, K/U and Th/U ratios with independent proxies of lithological sediment provenance and paleo-oceanic redox conditions.

The comparison of K/Th, K/U and Th/U with detrital Nd isotopes at site U1341, U1343 and U1345 shows different correlation depending on sampling sites. At site U1341, we cannot observe any correlation between them, indicating that three ratios are inappropriate to trace lithological sediment provenance. It is presumably attributed to considerable variability of grain size by glacial meltwater and paleo-oceanic redox conditions by high opal content. At site U1343, the K/Th, K/U and Th/U ratios partially interpret the variation in lithological sediment provenance. However, heavy mineral sorting and paleo-oceanic redox conditions seem to be primary factors. At site U1345, the K/U and Th/U ratios show weak correlation with detrital Nd isotopes like site U1343, but the K/Th ratio does not show any correlation. Possible interpretation would be fractionation between Th and U sorting by re-distribution of shelf sediment and/or additional sediment input from Anadyr River. We therefore suggest that the K/Th, K/U and Th/U ratios can

provide only preliminary information about lithological sediment provenance, and that heavy mineral sorting and paleo-oceanic redox conditions should be constrained for more detail. We recommend their applications in open ocean where heavy mineral sorting is completed.

The potential use of the Th/U ratio as a tracer of paleo-oceanic redox conditions is examined by monitoring the change in Th/U at the time of oxidizing bottom water conditions at site U1345. The oxidizing periods are previously suggested by peaks of authigenic Nd isotopes, light oxygen isotopes of benthic foraminifera and low abundance of *Bulimina aff. Exilis*. Increases in Th/U ratios at site U1345 generally occur under oxidizing bottom water conditions, but some exceptions are caused by change in lithological sediment provenance. Consequently, the Th/U ratio can be more useful to trace the change in paleo-oceanic redox conditions when lithological sediment provenance is constrained in advance. Once the K/Th and K/U ratios constrain lithological sediment provenance, maybe in open ocean, the Th/U ratio would find new perspective on paleo-oceanic redox conditions.

5.1. Introduction

Natural gamma radiation (NGR) spectrometry provides continuous and fundamental information about lithological properties (Mathis et al., 1984; Serra et al., 1980), and hence NGR intensity has routinely been measured in marine sediments during scientific drilling expeditions (Blum et al., 1997; Dunlea et al., 2013). DV *JOIDES Resolution* used for International Ocean Discovery Program (IODP) has equipped with the current NGR measurement device since March 2009

(Vasiliev et al., 2011). As NGR spectra are mainly composed of one ^{40}K peak and various peaks for ^{232}Th and ^{238}U series at specific energy levels, elemental concentrations of K, Th and U can be quantified by integrating the energy spectra (Blum et al., 1997; De Vleeschouwer et al., 2017; Dunlea et al., 2013). De Vleeschouwer et al. (2017) presented a MATLAB algorithm to estimate K, Th and U contents from NGR spectra of IODP cores and showed that these estimates are comparable to measurements by inductively coupled plasma (ICP) mass and emission spectrometry and X-Ray fluorescence without significant differences. The algorithm is open access, and therefore one can easily obtain K, Th and U contents for IODP cores since March 2009.

Potassium, Th and U concentrations can provide mineralogical and geochemical insight on the geological samples. All three elements are incompatible and abundant in rock-forming minerals as well as accessory heavy minerals, but the differences in ionic radius and charge between them induce their relative abundances in minerals (White, 2013). Potassium has high ionic radius and low ionic charge and is mainly presence in orthoclase, biotite and muscovite (Verdoya et al., 2001). Thorium and U have high ionic charge and further occur in heavy minerals such as zircon, rutile and monazite (Pliler and Adams, 1962; Verdoya et al., 2001). Thorium prefers to be in monazite, quartz and clay mineral, while uranium is more abundant in zircon and rutile (Anjos et al., 2006). Although no three elements are abundant in mafic minerals, there are also elemental fractionation in mafic minerals. Potassium is relatively rich in olivine and amphibole, and U is rich in orthopyroxene based on GERM partition coefficient database (http://earthref.org/GERM/). This differential affinity of K, Th and U to minerals enables their ratios to be used as lithological provenance indicators. For

example, Th/U ratio was used to constrain the provenance of sedimentary rocks (McLennan et al., 1993) based on the distinct Th/U ratios between upper continental crust (Th/U > 3.0 (ppm/ppm); Chiozzi et al., 2002; McLennan et al., 1993; McLennan et al., 1980; Tzortzis and Tsertos, 2004) and mantle-derived volcanic rock (Th/U < 3.0 (ppm/ppm); McLennan, 1989; McLennan et al., 1993). Likewise, the variable K/Th, K/U and Th/U ratios of graywackes depending on tectonic setting indicate potential use for provenance indicators of sedimentary rocks (Bhatia and Crook, 1986).

However, these provenance signals recorded in K/Th, K/U and Th/U ratios can be variable in response to secondary factors such as redox conditions, weathering/transport process and productivity are constrained. The change in redox conditions alters uranium content as urainum is naturally present in reduced (UO_2) and oxidized (UO_3) phases. Reduced U(IV) is relatively insoluble and likely to be retained in sediments under reducing conditions (Anjos et al., 2006; Brumsack, 2006; Zheng et al., 2002). Oxidized U(VI) is relatively soluble and tends to be liberated from the sediment to seawater and/or porewater under oxidizing conditions (Cochran et al., 1986). Therefore, if sediment distribution is consistent, reducing (oxidizing) sediment results in U-uptake (loss). The importance of redox conditions for U content in sediment is emphasized by high U concentration in authigenic fraction of reducing sediment from the N. Atlantic, which is more than 2 times greater than detrital U (Thomson et al., 1990). It implies that K/U and Th/U ratios of sediments are not suitable to trace the sediment provenance when oxidation states of sediments are variable. Rather, considering the relative stability of Th under redox conditions, Th/U ratio can be a useful indicator of paleo-oceanic redox conditions (e.g. Bond and Zatoń, 2003; Klinkhammer and Palmer, 1991;

Wignall and Twitchett, 1996).

The weathering and transport process can generate alteration in the elemental ratios. Potassium is a traditional labile element as used to judge the degree of chemical weathering (e.g. Nesbitt and Young, 1982) and likely to be removed during transportation. Similarly, the concentrations of Th and U in the sediments are affected by mineral sorting during transportation because two elements are abundant in heavy minerals (Anjos et al., 2006). Both Th and U contents in coarse fractions of beach sands (63 μm < ϕ < 150 μm) were considerably higher than fine fractions (ϕ < 63 μm), while K content showed insignificant variation with grain size (Anjos et al., 2006). On the other hand, Th/U ratio varied slightly with grain size (Anjos et al., 2006), emphasizing its robustness in response to weathering and transport process. Consequently, the K, Th and U contents of silt and clay sediments tend to be lower than the parent rocks, and their relative abundances such as K/Th and K/U ratios can be variable depending on transport history and depositional conditions, while Th/U is relatively consistent.

Productivity is an important factor to determine K/Th and Th/U ratios. Thorium is a very particle-reactive element, and dissolved Th tends to be adsorbed into particles in the water column (e.g. Hoffmann et al., 2013; Yu et al., 1996). Since the adsorbed Th typically accounts for ~35–50% of total thorium (Robinson et al., 2008), Th-adsorption can give rise to substantial overall increase in Th contents of sediment. Th-enrichment relative to K and U can be intense when the productivity is higher because biological components only contain adsorbed Th, while lithological ones have terrigenous K, Th and U as well as adsorbed Th. Therefore, the higher productivity is, the lower K/Th ratio (higher Th/U) will be. This phenomenon is likely to be weak under the diatom-dominated community

such as the Bering Sea becasue Th-adsorption is not vigorous when diatom flux is higher (e.g. Chase et al., 2002; Keigwin and Boyle, 2008; Siddall et al., 2005).

The IODP Expedition 323 sites in the Bering Sea are potential locations to evaluate the role of K/Th, K/U and Th/U ratios as indicators of lithological provenance and paleo-oceanic redox conditions. The terrigenous sediment of the Bering Sea are derived from two main sources, the Aleutian Arc and Alaska (Horikawa et al., 2015). As the main lithology of the Aleutian Arc is more mafic than Alaska based on the detrital Nd isotopes (Horikawa et al., 2010 and references therein), the spatial variation in sediment distribution in the Bering Sea may be recorded in K/Th, K/U and Th/U. The comparison of these ratios between the Aleutian-dominated Bowers Ridge sites and the Alaska-dominated Bering Slope sites possibly provides insightful information about the potential of these proxies (Fig. 5.1). The paleo-oceanic redox conditions can be tested using Th/U ratio at site U1345 which is located in the center of the oxygen minimum zone (OMZ) at present (Fig. 5.1). According to Jang et al. (2017), there were episodic ventilation processes over 520 kyr, which possibly varied the depth of the OMZ. When the bottom water was oxygenated, Th/U ratio would increase, resulting from U-loss from sediment to seawater.

Here, we present K, Th and U concentration generated from the shipboard NGR spectra of IODP 323 Bering Sea sediments using the MATLAB algorithm provided by De Vleeschouwer et al. (2017). We firstly evaluate the possibility of K/Th, K/U and Th/U ratios as provenance tracers. These ratios at the Bowers Ridge sites U1341 and U1342 are compared with the Bering Slope sites U1343 and U1345. Then, Th/U ratio at site U1345 is used to trace the change in paleo-oceanic redox conditions. The main question is whether Th/U ratio varies at the age

intervals when NPIW formations occur.

5.2. Background information

5.2.1. Sampling sites

We focused mainly on sites U1341 (54˚2'N, 179˚0'E, 2,150 m water depth) and U1342 (54°5’N, 176°6’W; 818 m water depth) on the Bowers Ridge and sites U1343 (57°3’N, 175°5’W; 1,950 m water depth) and U1345 (60°9’N, 179°3’W; 1,008 m water depth) on the Bering Slope retrieved during IODP Exp. 323 in 2009 (Fig. 5.1). Those sites are well studied in terms of sediment provenance (e.g. U1341, U1343 and U1345)(Horikawa et al., 2015; Jang et al., 2017) and/or change in paleo-oceanic redox conditions (e.g. U1342 and U1345)(Jang et al., 2017; Knudson and Ravelo, 2015). Cores U1341B (621.5 m CCSF-A), U1342A (58.4 m CCSF-A), U1343E (779.2 m CCSF-A) and U1345D (167.6 m CCSF-A) were used because of their longest lengths. The age model for site U1341 was tentatively constructed using oxygen isotopes of benthic foraminifera in addition to diatom and paleomagnetic datums by Horikawa et al. (2015), and site U1341 covers at least 4.3 Myr. For site U1342, the age model was only constrained down to the core depth at 35.3 CCSF-A m, which corresponds to 1,072 ka (Knudson and Ravelo, 2015). Assuming that the sedimentation rate below 35.3 m CCSF-A is the average value of entire core at site U1342, the bottom ages for site U1342 is ~1.77 Ma. The age models for sites U1343 and U1345 were previously constructed by oxygen isotopes of benthic foraminifera, and the bottom ages extend to 2.4 Ma and 530 ka, respectively (Asahi et al., 2016; Cook et al., 2016).

The sediments in the Bering Sea are generally composed of siliciclastic and biogenic lithologies. The siliciclastic lithologies are composed of diatom-bearing to diatom-rich silty clay or clayey silt, while the biogenic lithologies are diatom ooze. The main sources of siliciclastic materials are the Aleutian Arc and Alaska (Horikawa et al., 2015; Jang et al., 2017), and their sediment distributions are primarily accomplished by rivers, seawater and sea ice. The sedimentation rates are higher at the Bering Slope sites, while relative biological components are lower at the Bowers Ridge sites. This difference is attributed to higher supply of terrigenous materials from large rivers such as the Yukon as well as sediment re-distribution from the shelf area to the Bering Slope sites (Takahashi et al., 2016). Based on the detrital Nd isotopic composition of the two source areas and coring sites U1341, U1343 and U1345 (Horikawa et al., 2010; Jang et al., 2017; VanLaningham et al., 2009), the sediments on the Bowers Ridge (Bering Slope) are mostly derived from the Aleutian Arc (Alaska), probably due to their proximity to the source area.

All sampling sites are located within or near the OMZ at present, and site U1345 is located at the center depth of the OMZ. Low oxygen of sampling sites are attributed to high diatom productivity (Cook et al., 2005) and lack of ventilation process at present (Warner and Roden, 1995). However, the depth of the OMZ has changed over time according to variable diatom productivity and the ventilation events (e.g. Jang et al., 2017; Expedition 323 Scientists, 2011b). In particular, the events of NPIW formations indicate that intermediate water was episodically oxygenated at site U1345 (e.g. ~320 ka), as suggested by authigenic Nd isotopes and benthic foraminifera oxygen isotopes (Jang et al., 2017).

5.2.2. *Quantification of K, Th and U contents from NGR spectra*

We estimated K, Th and U concentration of sediments from NGR spectra based on De Vleeschouwer et al. (2017). First, the NGR spectra of sites U1341, U1342, U1343 and U1345 were downloaded as *the expanded format* from the *LIMS Online Reports* database (http://web.iodp.tamu.edu/LORE/). After that, we carried out background calibration and edge-correction from downloaded NGR spectra using the MATLAB script, *Extract_NGR_spectra.m*, provided by De Vleeschouwer et al. (2017). The background-substracted and edge-corrected data was finally converted into the K, Th and U concentrations by integration of characteristic peaks using the MATLAB script, *Quantification_K_U_Th.m* (De Vleeschouwer et al., 2017). The precision and the accuracy for the estimation were previously evaluated by the correlation coefficient and by the slope and intercept of the linear regression between the estimated and the measured data, respectively (De Vleeschouwer et al., 2017). The precisions for K, Th and U are acceptable with high correlation coefficients (r^2) of 0.89, 0.89 and 0.84, respectively, and K, Th and U are highly accurate with the slope of 0.95, 1.12 and 0.92 and the intercept of 0.60, 0.75 and 0.49, respectively (De Vleeschouwer et al., 2017).

5.2.3. *K, Th and U concentrations of the Aleutian Arc and Alaska*

Potassium, Th and U contents of whole rocks in the Aleutian Arc (n = 902, latitude: 51°N to 60°N, longitude: 168°E to 152°W) and Alaska (n = 136, latitude: 60°N to 66°N, longitude: 167°W to 140°W) are acquired using the geochemical database, *GEOROC* (http://georoc.mpch-mainz.gwdg.de). The *GEOROC* data in the Aleutian Arc cover the entire area, but data in Alaska are mostly concentrated on the eastern part of Alaska (150°W to 140°W). In terms of

rock types, the data are dominantly derived from volcanic rocks in the both sites with minor contribution of plutonic rocks. Considering that the dominant rock types in Alaska are sedimentary and meta sedimentary rocks (VanLaningham et al., 2009), data of Alaska may be not representative. To fulfill this caveat, we further obtained K, Th and U contents of plutonic rocks from the Selawik Lake, Inland Lake and Selawik Hills in the western Yukon-Koyukuk basin (YKB) of Alaska (Arth et al., 1989; Miller, 1989). Although plutonic rocks are not dominant rocks composing the drainage basins in Alaska, K-Ar age (~105 Ma) and Nd isotopic composition (ε_{Nd} ~ -8 – -11) measured here (Arth et al., 1989) are very similar with those of the Yukon River suspended and bedload samples (118 Ma and ε_{Nd} ~ -9)(VanLaningham et al., 2009), indicating that YKB data can be representative for end-member of Alaska.

5.3. Results

5.3.1. *Bering Sea sediment cores*

The true mean values of K, Th and U contents calculated using *t*-test ($p < 0.05$) are shown in Table 5.1. The true mean values of K concentrations of sampling sites range from 0.63 to 1.96 wt. %, and the those of Th and U concentrations are much smaller with 0.98 – 4.56 ppm for Th and 0.73 – 1.66 ppm for U. Overall, K, Th and U concentrations of the sites U1343 and U1345 on the Bering Slope are relatively higher than the sites U1341 and U1342 on the Bowers Ridges probably due to higher input of terrigenous sediments.

The combined ratios of the three elements such as K/Th (10^{-6} mol/mol), K/U (mol/mol) and Th/U (10^{-6} mol/mol) are also shown in Figures 5.2 –5.5 and

Table 5.2. All elemental ratios from four sampling sites show large fluctuations, and the peaks beyond 3-sigma standard deviations are predominantly observed at site U1341 (Fig. 5.2). On the other hand, there are a few outliers at sites U1342 and U1345 (star symbols in Figs. 5.3 and 5.5). The ratios of K/Th increase by factor of 10 at the bottom part of sediment core at site U1342 (Fig. 5.3), and some of them are beyond 3-sigma standard deviations. Generally, K/Th ratios are variable in response to change in sediment lithostratigraphy (Figs 5.2 and 5.3).

The true means of K/Th, K/U and Th/U ratios vary depending on sampling sites (Table 5.2). True mean K/Th ratio at site U1341 on the Bowers Ridge is comparable to neighboring site U1342, while sites U1343 and U1345 on the Bering Slope is similar each other and considerably greater than the Bowers Ridge sites. We observed the similar situations for K/U and Th/U ratios. Site U1341 shows similar true means of K/U and Th/U ratios with U1342, but two sites on the Bowers Ridge are distinctly differ from the Bering Slope sites.

5.3.2. *The Aleutian Arc and Alaska bed rocks*

The true mean K/Th, K/U and Th/U ratios in the Aleutian Arc, Alaska and YKB (*t*-test, $p < 0.05$) are shown in Fig. 5.1 and Table 5.2. The K/Th and K/U ratios in the Aleutian Arc (n = 902 from GEOROC, 2003) are indistinguishable from those in Alaska (n = 136 from GEOROC, 2003) and YKB (n = 9 from Arth et al., 1989; Miller, 1989), while the Th/U ratio in the Aleutian Arc is distinctly lower than Alaska and YKB. The true mean Th/U ratio in Alaska is consistent with that of typical upper continental crust (Chiozzi et al., 2002; McLennan et al., 1993; McLennan et al., 1980; Tzortzis and Tsertos, 2004), and that in the Aleutian Arc is located in the range of mantle-derived volcanic rocks (McLennan, 1989;

McLennan et al., 1993). The true mean Th/U ratio in YKB is higher than upper continental crust (Chiozzi et al., 2002; McLennan et al., 1993; McLennan et al., 1980; Tzortzis and Tsertos, 2004). The K/Th and K/U ratios in the Aleutian Arc and Alaska are similar to those of gabbro/basalt, but the K/Th ratios are also comparable to or slightly higher than continental crust (Pollack, 1982).

The elemental ratios of volcanic rocks are similar to those of plutonic rocks in the individual area, but the ratios of the other rocks such as sedimentary rocks, metamorphic rocks and mantle xenolith are generally different. In the Aleutian Arc, three elemental ratios of volcanic rocks (n = 775) are comparable to those of plutonic rocks within uncertainties (n = 119), but the ratios of K/Th and K/U of sedimentary rocks in the Aleutian Arc (n = 8) are twice lower than the other rocks (Table 5.2). Similarly, the volcanic rocks in Alaska (n = 118) show slightly higher K/Th, K/U and Th/U ratios than plutonic rocks (n = 6), but the metamorphic rocks (n = 5) and mantle xenolith (n = 7) in Alaska represent significantly higher K/Th and K/U ratios and lower Th/U ratio than volcanic rocks and plutonic rocks (Table 5.2).

The true mean K/Th and K/U ratios in the Aleutian Arc, Alaska and YKB are lower than four sampling sites in the Bering Sea (Table 5.2 and Fig 5.6). On the other hand, the true mean Th/U ratios in Alaska and YKB are higher than all sites in the Bering Sea, while the true mean Th/U ratio in the Aleutian Arc is between those of the Bowers Ridge sites and Bering Slope sites. The K/Th and K/U ratios at four sampling sites cannot be explained by two end-members mixing between the Aleutian Arc and Alaska, which are main sediment source areas in the Bering Sea (Horikawa et al., 2015; Jang et al., 2017). This binary mixing model can only interpret the Th/U ratios at site U1343 and U1345, which estimates that the

sediments from the Aleutian Arc accounted for 70% and 50% of sediments at sites U1343 and U1345, respectively. If we use Th/U ratio of YKB as a representative value for Alaska, the contributions from the Aleutian Arc are much higher. This estimation is contrast to results of detrital Nd isotopes that showed that the sediments at sites U1343 and U1345 are mostly derived from Alaska (Jang et al., 2017). The secondary factors such as paleo-oceanic redox conditions, weathering/transport process and productivity possibly involved in determination of K/Th, K/U and Th/U ratios.

5.4. Discussions

5.4.1. *Simple sediment mixing model*

We tentatively examined that K, Th and U concentrations at sites U1341 and U1345 are interpreted by simple mixing model based on the following equation:

$$[\ i\ ]_{site} = F_{litho} \times (f_{YKB} \times [\ i\ ]_{YKB} + f_{AA} \times [\ i\ ]_{AA}) + \alpha \quad (5.1)$$

$$f_{YKB} + f_{AA} = 1 \quad (5.2)$$

where, $[\ i\ ]_{site}$ is elemental concentration at each location, F_{litho} is fraction of terrigenous component in sediment, f is relative contribution of terrigenous component between YKB and the Aleutian Arc (AA), and α is an unexplained component.

We consider several assumptions here. (1) YKB is the end-member of Alaskan-sourced materials (see section 5.2.3). (2) The terrigenous sediments in the

Bering Sea are governed by binary mixing between the Aleutian Arc and Alaska (YKB) (Horikawa et al., 2015). (3) The f_{YKB} for site U1345 is ~1.0, and the f_{YKB} for site U1341 is ~0.5. Both estimates are based on detrital Nd isotopes (Horikawa et al., 2015; Jang et al., 2017). (4) The F_{litho} for site U1341 and U1345 are 0.4 and 0.7, respectively. Sediment stratigraphy is considered as well as opal, TOC, calcareous nannofossil and foraminifera contents (Expedition 323 Scientists, 2011b,e).

Simple mixing model indicates that the K concentration at site U1345 is solely interpreted by mixing between K-rich terrigenous component from YKB and K-free biological component (equation 5.1). The estimated α for K at site U1345 is -0.11, indicating ~5% decrease in K at site U1345. Similarly, α for K at site U1345 is -0.09, indicating ~12% decrease in K at site U1341. These estimated α values are within the uncertainty, and therefore we ruled out K-loss by weathering and transport process (e.g. Nesbitt and Young, 1982).

On the other hand, negative α values for Th and U indicate significant decrease in Th and U. The estimated α for Th at sites U1341 and U1345 are -18.5 and -6.2, respectively. These results correspond to 86% and 80% decrease in thorium at sites U1341 and U1345, respectively, which is much beyond the uncertainty. One possible scenario for Th decrease is heavy mineral sorting during transportation. As thorium is abundant in heavy minerals such as zircon, rutile and ilmenite, mineral sorting process during sediment transportation gives rise to Th decrease in silt and clay sediments (e.g. Anjos et al., 2006). The estimated α values for U at sites U1341 and U1345 are -0.8 and -3.0, corresponding to 54% and 64% decrease in uranium, respectively. The U decrease can be also attributed to heavy mineral sorting. Considering that heavy mineral sorting causes an

insignificant Th/U variation (Anjos et al., 2006), relatively small decrease in U can results from U-uptake under reducing bottom water conditions (e.g. Bond and Zatoń, 2003; Klinkhammer and Palmer, 1991; Wignall and Twitchett, 1996). The difference of decrease rates between sites U1341 and U1345 is mainly related to uncertainty of estimation but possibly reflects sediment grain size, main lithological component and/or contents of biological component. For example, numerous sandy patches and layers at site U1345 may reduce the influence of mineral sorting (Expedition 323 Scientists, 2011e). However, there were no significant differences of true means K/Th, K/U and Th/U ratios between sand layers and entire core. We cannot constrain the effect of biological productivity on Th content with a given uncertainty (e.g. Hoffmann et al., 2013; Yu et al., 1996). Therefore, the difference of decrease rates between two sites are within the uncertainty.

5.4.2. *Lithological provenance tracer?*

We tentatively examined the potential use of K/Th, K/U and Th/U ratios as a lithological provenance tracer. As shown in section 5.4.1, potassium is refractory element to secondary factors, while Th and U are easily liberated from sediment by heavy mineral sorting during transportation. Although thorium and uranium behave together without significant fractionation by heavy mineral sorting (Anjos et al., 2006), reducing bottom water conditions in the Bering Sea causes to increase in U concentration. Therefore, it is not appropriate to compare the elemental ratios of sampling sites directly to those of parent rocks in order to trace the lithological provenance of sediments in the Bering Sea. However, if heavy mineral sorting causes to decrease in Th and U concentration at a fixed rate, K/Th

and K/U ratios of parent rocks would be constrained using simple mathematic calculation (dashed lines in Fig. 5.6), and K/Th and K/U ratios would be useful tracer for sediment provenance. Likewise, if paleo-oceanic redox were uniform, we would acquire modified Th/U ratios of parent rocks to elucidate the change in terrigenous sediment sources (dashed lines in Fig. 5.6).

To assess these hypotheses, we compared the K/Th, K/U and Th/U ratios with detrital Nd isotopes records at sites U1341, U1343 and U1345 (Fig. 5.7). Detrital Nd isotopes are generally accepted as a lithological provenance indicator (Hemming et al., 1998; Pimentel et al., 2001; Roy et al., 2007). As sampling resolutions of detrital Nd isotopes are much lower than three elemental ratios, we resampled K/Th, K/U and Th/U ratios at the time scale of detrital Nd isotopes using linear interpolation.

At site U1341, there were no linear correlations between three ratios and detrital Nd isotopes (Fig. 5.7). It can be caused by change in sediment distribution pattern in response to glacial-interglacial variability. Site U1341 is proximal to the Aleutian Arc, and hence the sediments here are transported from the Aleutian Arc by seawater current and sea ice (Expedition 323 Scientists, 2011b). On the other hand, the sediment distribution from Alaska is also accomplished by proglacial meltwater as well as southward seawater current and sea ice rafting (Horikawa et al., 2015). This proglacial meltwater flows in the Bering Sea through the glacial Alaskan Stream entry where is proximal to the Bowers Ridge (Expedition 323 Scientists, 2011a) (Fig. 5.1). Melt stream gives rise to considerable grain size variability (Fenn and Gomez, 1989; Haritashya et al., 2010), which may attribute to large fluctuation in K/Th and K/U ratios at site U1341 (Fig. 5.2). High opal contents and their high variability at site U1341 (34.8 ± 11.1%, 1σ from Kanematsu

et al., 2013) can result in variable redox conditions (Expedition 323 Scientists, 2011b), possibly obscuring the primary Th/U signal. We therefore conclude that K/Th, K/U and Th/U ratios at site U1341 are not appropriate for lithological provenance tracer.

The K/Th, K/U and Th/U ratios at sites U1343 partially interpret lithological sediment provenance (Fig. 5.7). Higher K/Th ratios are generally associated with radiogenic detrital Nd isotope ratios, while higher K/U and Th/U ratios are accompanied by unradiogenic detrital Nd isotope ratios (Fig. 5.8). The effect of heavy mineral sorting is relatively stable at site U1343 than site U1341, which is presumably attributed to the long distance from site U1343 to the entrance of glacial Alaskan Stream (Fig. 5.1). A few outliers of K/Th, K/U and Th/U ratios support this interpretation (Fig. 5.4). The discrepancy between K/Th and detrital Nd isotopes (e.g. ~1.8 Ma) may be caused by adsorbed Th increase associated with higher opal content (Fig. 5.8). The correlation between Th/U ratio and detrital Nd isotopes at site U1343 is higher than site U1341 probably due to low opal content (9.1 ± 4.0%, 1σ from Kanematsu et al., 2013), but its coefficient (r = -0.3) is still low, reflecting strong influence of U-uptake under reducing bottom water. Therefore, the variation in K/Th, K/U and Th/U ratios at site U1343 broadly indicate change in lithological sediment provenance, but they also reflect the information such as heavy mineral sorting, paleo-oceanic redox conditions and productivity.

Site U1345 show similar result with site U1343 except for K/Th ratio (Fig. 5.7). The Th/U ratios reflect lithological sediment provenance in addition to paleo-oceanic redox conditions, while the K/U ratios record lithological sediment provenance and heavy mineral sorting. The main cause for lack of correlation

between K/Th and detrital Nd isotopes is uncertain but probably relates to the involvement of additional source and/or different behavior of Th and U during heavy mineral sorting. Site U1345 is proximal to shelf area and hence easily influenced from redistribution of sediment once deposited on the shelf area (Expedition 323 Scientists, 2011a). Considering the proximity of site U1345 to the Anadyr River mouth, the Anadyr River can be minor source for sediments at site U1345 (VanLaningham et al., 2009). Distinct lithology of drainage basin for Anadyr River implies that this river unique K/Th, K/U and Th/U ratios. Another possibility comes from different Th/U ratios between quartz (~3 mol/mol) and clay minerals (~8 mol/mol)(Anjos et al., 2006), implying the elemental fractionation between Th and U. Although the single field study does not prove this speculation (Anjos et al., 2006), it is necessary to examine for re-distributed sediments.

Consequently, we recommend the K/Th, K/U and Th/U ratios to be used only as preliminary provenance indicators. Since K/Th, K/U and Th/U ratios can be also affected by mineral sorting, paleo-oceanic redox conditions and productivity, it is not appropriate to compare the chemical information of sediments directly to parent rocks. The sediment in the open ocean may be the best location to apply the K/Th, K/U and Th/U ratios for lithological provenance indicators because heavy mineral sorting can be constrained. They can help to identify paleo-source regions of dust and subsequently to trace the paleo-wind trajectories (Grousset and Biscaye, 2005). In the marginal sea, the K/Th, K/U and Th/U ratios of sediments collected at the river mouth can be an ideal end-member to reduce the uncertainty by mineral sorting.

5.4.3. *Paleo-oceanic redox tracer?*

Since the paleo-oceanic redox conditions has been variable in the Bering Sea (e.g. Jang et al., 2017; Expedition 323 Scientists, 2011b), the temporal variation in Th/U ratio can be interpreted by change in the sediment provenance and paleo-oceanic redox conditions. Overall decreases in Th/U ratios of Bering Sea sediments compared to parent rocks are responsible for U-uptake under reducing bottom water, which highlights the role of redox conditions in Th/U ratio in the Bering Sea. To assess the relationship between paleo-oceanic redox conditions and Th/U ratio, we observed the change in Th/U ratios of site U1345 at the time for oxidizing bottom water conditions as suggested by independent proxies (Jang et al., 2017; Expedition 323 Scientists, 2011e).

Site U1345 is chosen for this test because the change in lithological sediment provenance is not significant as recorded in detrital Nd isotopes (Fig. 5.9), the water depth is located in the center of modern OMZ, and the change in the paleo-oceanic redox conditions has been previously investigated (e.g. Jang et al., 2017). For example, Jang et al. (2017) suggested several periods when the formation of the North Pacific Intermediate Water (NPIW) occurred at site U1345 based on the prominent peaks of the authigenic Nd isotopic composition and associated light oxygen isotope ratios of benthic foraminifera (red stars in Fig. 5.10). Furthermore, the abundance of *Bulimina aff. Exilis* provides additional information about paleo-redox conditions (data from Expedition 323 Scientists, 2011e)(Fig. 5.9). The benthic foraminifera species *B. aff. Exilis* lives in low oxygen deep fauna habitat, so low abundance of *B. aff. Exilis* represents oxygen-rich conditions (Bubenshchikova et al., 2008; Kaiho, 1994). Based on the oxygen-rich periods reconstructed by independent proxies mentioned above, we observed the

variation in Th/U ratios.

We observed the general increase in Th/U ratio under the oxidizing conditions at site U1345. At the NPIW formation events, Th/U ratios are broadly higher (red stars in Fig. 5.10). Considering that lithological sediment provenance varied slightly at site U1345 (Fig. 5.10), increase in Th/U can be attributed to the liberation of uranium from the sediments (e.g. Cochran et al., 1986). Transition from insoluble U(IV) to soluble U(VI) under oxidizing conditions results in U-loss from sediment. If so, higher Th/U ratios indicate oxidizing conditions. The other Th/U peaks are also mostly accompanied by low abundance of *B. aff. Exilis* (Fig. 5.10), further supporting utilization of Th/U ratio as an indicator of redox conditions. However, there are some exceptions. For example, high Th/U ratio at ~480 ka is contrast to low *B. aff. Exilis*. It may be caused by low sampling resolution of *B. aff. Exilis* and/or by higher sediment contribution from Alaska whose representative ratio of Th/U is high. Unradiogenic detrital Nd isotope ratios at ~480 ka supports the latter interpretation.

Consequently, Th/U ratio partly indicates paleo-oceanic redox conditions, but the user firstly needs to constrain the influence of sediment provenance. We suggest that the Th/U ratio is not appropriate to reconstruct the paleo-oceanic redox conditions in the marginal sea where the sediments are supplied from more than two source areas. The Th/U ratio would be more effective in the open ocean if the change in lithological sediment provenance is constrained by K/Th and K/U ratios in advance.

5.5. Summary

Potassium, Th and U concentrations are estimated from the NGR spectra of Bering Sea sediment cores (U1341, U1342, U1343 and U1345) using the MATLAB algorithm of De Vleeschouwer et al. (2017). Based on simple sediment mixing model, K is refractory to weathering and transport process, while Th and U tend to decrease by heavy mineral sorting during sediment transportation. The U-uptake of sediments under reducing bottom water conditions acts as a counterpart of mineral sorting process, but consequent U decrease in sediments implies that heavy mineral sorting is the primary mechanism controlling U concentration in the Bering Sea. Assuming that the decrease proportion of Th and U is uniform by heavy mineral sorting, K/Th and K/U ratios can be used to trace the change in lithological sediment provenance. Likewise, since Th and U behave equally during transportation, Th/U ratio can be also sediment provenance tracer if paleo-oceanic redox conditions are stable. To test this hypothesis, we compared K/Th, K/U and Th/U ratios with detrital Nd isotopes.

The change in K/Th, K/U and Th/U ratios at site U1343 broadly reflect the variation in lithological sediment provenance, as inferred from weak correlation between three ratios and detrital Nd isotopes (r = 0.3). Site U1345 shows similar result except for K/Th, while no correlation is detected at site U1341. The sediment re-distribution from shelf area to site U1345 is plausible reason for lack of correlation for K/Th. On the other hand, zero-correlation at site U1341 is presumably attributed to sediment transport by glacial meltwater and higher opal productivity, inducing the high variability of grain size and paleo-oceanic redox conditions. Therefore, the K/Th, K/U and Th/U ratios only provide preliminary

information about lithological sediment provenance. Since heavy mineral sorting is primary factor controlling K/Th and K/U ratios, the open ocean where heavy mineral sorting is constrained would be a desirable location for application of K/Th and K/U ratios as a tracer of lithological sediment provenance.

The Th/U ratio can be used as an indicator of paleo-oceanic redox conditions. We generally observe higher Th/U ratios when the bottom water was oxidizing at site U1345, as inferred from the peaks of authigenic Nd isotopes, light oxygen isotopes of benthic foraminifera and the low abundance of *Bulimina aff. Exilis*. The change from insoluble U(IV) to soluble U(VI) possibly results in U-loss from sediment to water and consequent higher Th/U ratios. There are exceptions, which is probably influenced by the change in the sediment provenance. For the usage of Th/U ratio as a paleo-redox indicator, it is necessary to constrain the lithological sediment provenance. We recommended the K/Th, K/U and Th/U ratios to be used in the open ocean at the same time. The K/Th and K/U ratios constrain the lithological sediment provenance at start and then Th/U ratio traces paleo-oceanic redox conditions.

References

Anjos, R.M., Veiga, R., Macario, K., Carvalho, C., Sanches, N., Bastos, J., Gomes, P.R.S., 2006. Radiometric analysis of Quaternary deposits from the southeastern Brazilian coast. Mar. Geol. 229, 29-43.

Arth, J.G., Criss, R.E., Zmuda, C.C., Foley, N.K., Patton Jr, W., Miller, T., Box, S., 1989. Remarkable isotopic and trace element trends in potassic through sodic Cretaceous plutons of the Yukon-Koyukuk basin, Alaska, and the nature of the lithosphere beneath the Koyukuk terrane. J. Geophys. Res. 94, 15,957-915,968.

Asahi, H., Kender, S., Ikehara, M., Sakamoto, T., Takahashi, K., Ravelo, A., Alvarez Zarikian, C., Khim, B., Leng, M., 2016. Orbital-scale benthic foraminiferal oxygen isotope stratigraphy at the northern Bering Sea Slope Site U1343 (IODP Expedition 323) and its Pleistocene paleoceanographic significance. Deep-Sea Res. II 125-126, 66-83.

Bhatia, M.R., Crook, K.A.W., 1986. Trace element characteristics of graywackes and tectonic setting discrimination of sedimentary basins. Contrib. Mineral. Petr. 92, 181-193.

Blum, P., Rabaute, A., Gaudon, P., Allan, J.F., 1997. Analysis of natural gamma-ray spectra obtained from sediment cores with the shipboard scintillation detector of the Ocean Drilling Program: example from leg 156, In: Proc. ODP, Sci. Results, 156: College Station, TX (Ocean Drilling Program). Citeseer, pp. 183-195.

Bond, D., Zatoń, M., 2003. Gamma-ray spectrometry across the upper Devonian basin succession at Kowala in the Holy Cross Mountains (Poland). Acta

Geol. Pol. 53, 93-99.

Brumsack, H.-J., 2006. The trace metal content of recent organic carbon-rich sediments: implications for Cretaceous black shale formation. Palaeogeogr. Palaeoclimatol. Palaeoecol. 232, 344-361.

Bubenshchikova, N., Nürnberg, D., Lembke-Jene, L., Pavlova, G., 2008. Living benthic foraminifera of the Okhotsk Sea: Faunal composition, standing stocks and microhabitats. Mar. Micropaleontol. 69, 314-333.

Chase, Z., Anderson, R.F., Fleisher, M.Q., Kubik, P.W., 2002. The influence of particle composition and particle flux on scavenging of Th, Pa and Be in the ocean. Earth Planet. Sci. Lett. 204, 215-229.

Chiozzi, P., Pasquale, V., Verdoya, M., 2002. Naturally occurring radioactivity at the Alps–Apennines transition. Radiat. Meas. 35, 147-154.

Cochran, J.K., Carey, A.E., Sholkovitz, E.R., Surprenant, L.D., 1986. The geochemistry of uranium and thorium in coastal marine sediments and sediment pore waters. Geochim. Cosmochim. Acta 50, 663-680.

Cook, M.S., Keigwin, L.D., Sancetta, C.A., 2005. The deglacial history of surface and intermediate water of the Bering Sea. Deep-Sea Res. II 52, 2163-2173.

Cook, M.S., Ravelo, A.C., Mix, A., Nesbitt, I.M., Miller, N.V., 2016. Tracing subarctic Pacific water masses with benthic foraminiferal stable isotopes during the LGM and late Pleistocene. Deep-Sea Res. II 125, 84-95.

De Vleeschouwer, D., Dunlea, A.G., Auer, G., Anderson, C.H., Brumsack, H., de Loach, A., Gurnis, M.C., Huh, Y., Ishiwa, T., Jang, K., 2017. Quantifying K, U, and Th contents of marine sediments using shipboard natural gamma radiation spectra measured on DV JOIDES Resolution. Geochem. Geophys. Geosyst., doi:10.1002/2016GC006715.

Dunlea, A.G., Murray, R.W., Harris, R.N., Vasiliev, M.A., Evans, H., Spivack, A.J., D'Hondt, S., 2013. Assessment and use of NGR instrumentation on the JOIDES Resolution to quantify U, Th, and K concentrations in marine sediment. Sci. Drill. 15, 57-63.

Expedition 323 Scientists, Expedition 323 summary. In Takahashi, K., Ravelo, A.C., Alvarez Zarikian, C.A., and the Expedition 323 Scientists (Eds.), Proc. IODP, 323. Integrated Ocean Drilling Program Management International, Inc., Tokyo.

Expedition 323 Scientists, Site U1341. In Takahashi, K., Ravelo, A.C., Alvarez Zarikian, C.A., and the Expedition 323 Scientists (Eds.), Proc. IODP, 323. Integrated Ocean Drilling Program Management International, Inc., Tokyo.

Expedition 323 Scientists, 2011c. Site U1342. In Takahashi, K., Ravelo, A.C., Alvarez Zarikian, C.A., and the Expedition 323 Scientists (Eds.), Proc. IODP, 323. Integrated Ocean Drilling Program Management International, Inc., Tokyo.

Expedition 323 Scientists, 2011d. Site U1343. In Takahashi, K., Ravelo, A.C., Alvarez Zarikian, C.A., and the Expedition 323 Scientists (Eds.), Proc. IODP, 323. Integrated Ocean Drilling Program Management International, Inc., Tokyo.

Expedition 323 Scientists, 2011e. Site U1345. In Takahashi, K., Ravelo, A.C., Alvarez Zarikian, C.A., and the Expedition 323 Scientists (Eds.), Proc. IODP, 323. Integrated Ocean Drilling Program Management International, Inc., Tokyo.

Fenn, C., Gomez, B., 1989. Particle size analysis of the sediment suspended in a proglacial stream: Glacier de Tsidjiore Nouve, Switzerland. Hydrol.

Process. 3, 123-135.

GEOROC, 2003. Geochemistry of Rocks of the Oceans and Continents. Mainz, Germany, Max-Planck Institute fur Chemie. <http://georoc.mpch-mainz.gwdg.de/>.

Grousset, F.E., Biscaye, P.E., 2005. Tracing dust sources and transport patterns using Sr, Nd and Pb isotopes. Chem. Geol. 222, 149-167.

Haritashya, U.K., Kumar, A., Singh, P., 2010. Particle size characteristics of suspended sediment transported in meltwater from the Gangotri Glacier, central Himalaya - An indicator of subglacial sediment evacuation. Geomorphology 122, 140-152.

Hemming, S., Broecker, W., Sharp, W., Bond, G., Gwiazda, R., McManus, J., Klas, M., Hajdas, I., 1998. Provenance of Heinrich layers in core V28-82, northeastern Atlantic: $^{40}Ar/^{39}Ar$ ages of ice-rafted hornblende, Pb isotopes in feldspar grains, and Nd–Sr–Pb isotopes in the fine sediment fraction. Earth Planet. Sci. Lett. 164, 317-333.

Hoffmann, S.S., McManus, J.F., Curry, W.B., Brown-Leger, L.S., 2013. Persistent export of 231Pa from the deep central Arctic Ocean over the past 35,000 years. Nature 497, 603-606.

Horikawa, K., Asahara, Y., Yamamoto, K., Okazaki, Y., 2010. Intermediate water formation in the Bering Sea during glacial periods: Evidence from neodymium isotope ratios. Geology 38, 435-438.

Horikawa, K., Martin, E.E., Basak, C., Onodera, J., Seki, O., Sakamoto, T., Ikehara, M., Sakai, S., Kawamura, K., 2015. Pliocene cooling enhanced by flow of low-salinity Bering Sea water to the Arctic Ocean. Nat. Commun. 6, 7587.

Jang, K., Huh, Y., Han, Y., 2017. Authigenic Nd isotope record of North Pacific Intermediate Water formation and boundary exchange on the Bering Slope. Quat. Sci. Rev. 156, 150-163.

Kaiho, K., 1994. Benthic foraminiferal dissolved-oxygen index and dissolved-oxygen levels in the modern ocean. Geology 22, 719-722.

Kanematsu, Y., Takahashi, K., Kim, S., Asahi, H., Khim, B.-K., 2013. Changes in biogenic opal productivity with Milankovitch cycles during the last 1.3 Ma at IODP Expedition 323 Sites U1341, U1343, and U1345 in the Bering Sea. Quatern. Int. 310, 213-220.

Keigwin, L.D., Boyle, E.A., 2008. Did North Atlantic overturning halt 17,000 years ago? Paleoceanography 23, PA1101, doi:1110.1029/2007PA001500.

Klinkhammer, G.P., Palmer, M.R., 1991. Uranium in the oceans: Where it goes and why. Geochim. Cosmochim. Acta 55, 1799-1806.

Knudson, K.P., Ravelo, A.C., 2015. North Pacific Intermediate Water circulation enhanced by the closure of the Bering Strait. Paleoceanography 30, 1287-1304.

Mathis, G.L., Tittle, C., Rutledge, D., Mayer Jr, R., Ferguson, W., 1984. A spectral gamma ray (SGR) tool, SPWLA 21st Ann. Log. Symp.

McLennan, S., 1989. Archean sedimentary rocks and the Archean mantle, Workshop on the Archean Mantle, pp. 57-59.

McLennan, S., Hemming, S., McDaniel, D., Hanson, G., 1993. Geochemical approaches to sedimentation, provenance, and tectonics. Geol. S. Am. S. 284, 21-40.

McLennan, S.M., Nance, W.B., Taylor, S.R., 1980. Rare earth element-thorium correlations in sedimentary rocks, and the composition of the continental

crust. Geochim. Cosmochim. Acta 44, 1833-1839.

Miller, T.P., 1989. Contrasting plutonic rock suites of the Yukon-Koyukuk Basin and the Ruby geanticline, Alaska. J. Geophys. Res-Sol. Ea. 94, 15969-15987.

Nesbitt, H., Young, G., 1982. Early Proterozoic climates and plate motions inferred from major element chemistry of lutites. Nature 299, 715-717.

Pimentel, M., Dardenne, M., Fuck, R., Viana, M., Junges, S., Fischel, D., Seer, H., Dantas, E., 2001. Nd isotopes and the provenance of detrital sediments of the Neoproterozoic Brasılia Belt, central Brazil. J. S. Am. Earth Sci. 14, 571-585.

Pliler, R., Adams, J.A.S., 1962. The distribution of thorium and uranium in a Pennsylvanian weathering profile. Geochim. Cosmochim. Acta 26, 1137-1146.

Pollack, H.N., 1982. The heat flow from the continents. Annu. Rev. Earth Pl. Sc. 10, 459-481.

Robinson, L.F., Noble, T.L., McManus, J.F., 2008. Measurement of adsorbed and total $^{232}Th/^{230}Th$ ratios from marine sediments. Chem. Geol. 252, 169-179.

Roy, M., van de Flierdt, T., Hemming, S.R., Goldstein, S.L., 2007. $^{40}Ar/^{39}Ar$ ages of hornblende grains and bulk Sm/Nd isotopes of circum-Antarctic glacio-marine sediments: Implications for sediment provenance in the southern ocean. Chem. Geol. 244, 507-519.

Serra, O., Baldwin, J., Quirein, J., 1980. Theory, interpretation, and practical applicatons of natural gamma ray spectroscopy, SPWLA 21st Ann. Log. Symp., p. 30.

Siddall, M., Henderson, G.M., Edwards, N.R., Frank, M., Müller, S.A., Stocker,

T.F., Joos, F., 2005. $^{231}Pa/^{230}Th$ fractionation by ocean transport, biogenic particle flux and particle type. Earth Planet. Sci. Lett. 237, 135-155.

Takahashi, K., Ravelo, A.C., Okazaki, Y., 2016. Introduction to Pliocene–Pleistocene paleoceanography of the Bering Sea. Deep-Sea Res. II 125–126, 1-7.

Thomson, J., Wallace, H.E., Colley, S., Toole, J., 1990. Authigenic uranium in Atlantic sediments of the last glacial stage - a diagenetic phenomenon. Earth Planet. Sci. Lett. 98, 222-232.

Tzortzis, M., Tsertos, H., 2004. Determination of thorium, uranium and potassium elemental concentrations in surface soils in Cyprus. J. Environ. Radioactiv. 77, 325-338.

VanLaningham, S., Pisias, N.G., Duncan, R.A., Clift, P.D., 2009. Glacial–interglacial sediment transport to the Meiji Drift, northwest Pacific Ocean: Evidence for timing of Beringian outwashing. Earth Planet. Sci. Lett. 277, 64-72.

Vasiliev, M., Blum, P., Chubarian, G., Olsen, R., Bennight, C., Cobine, T., Fackler, D., Hastedt, M., Houpt, D., Mateo, Z., 2011. A new natural gamma radiation measurement system for marine sediment and rock analysis. J. Appl. Geophys. 75, 455-463.

Verdoya, M., Chiozzi, P., Pasquale, V., 2001. Heat-producing radionuclides in metamorphic rocks of the Brianconnais-Piedmont Zone (Maritime Alps). Eclogae Geol. Helv. 94, 213-219.

Warner, M.J., Roden, G.I., 1995. Chlorofluorocarbon evidence for recent ventilation of the deep Bering Sea. Nature 373, 409-412.

White, W.M., 2013. Geochemistry. John Wiley & Sons, pp. 660.

Wignall, P.B., Twitchett, R.J., 1996. Oceanic anoxia and the end Permian mass extinction. Science 272, 1155.

Yu, E.-F., Francois, R., Bacon, M.P., 1996. Similar rates of modern and last-glacial ocean thermohaline circulation inferred. Nature 379, 22.

Zheng, Y., Anderson, R.F., van Geen, A., Fleisher, M.Q., 2002. Remobilization of authigenic uranium in marine sediments by bioturbation. Geochim. Cosmochim. Acta 66, 1759-1772.

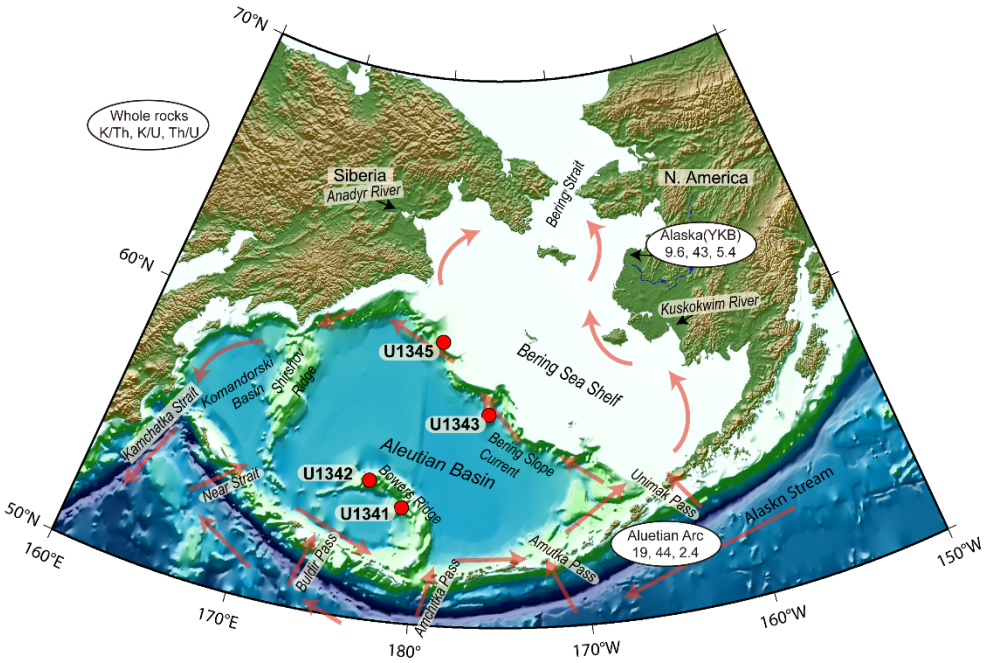

Figure 5.1. Sampling locations (red circles). The average K/Th (10^6 mol/mol), Th/U (mol/mol) and K/U ratios (10^6 mol/mol) of whole rocks from the Aleutian Arc and Alaska are shown in ellipses.

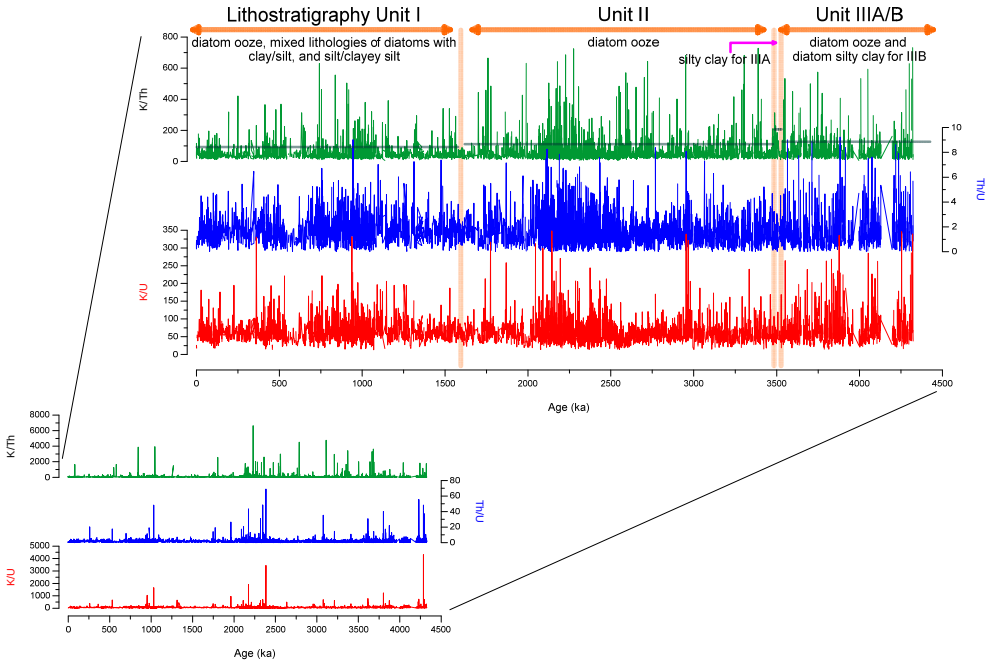

Figure 5.2. The variation in K/Th (10^6 mol/mol), Th/U (mol/mol) and K/U (10^6 mol/mol) ratios at site U1341. The sediment lithostratigraphies are divided into four groups (I, II, IIIA and IIIB from Expedition 323 Scientists, 2011b), and the true mean K/Th ratio for each group is marked with dark green lines. The lower left panel shows entire data, while the upper panel covers only data below the 3-sigma standard deviation.

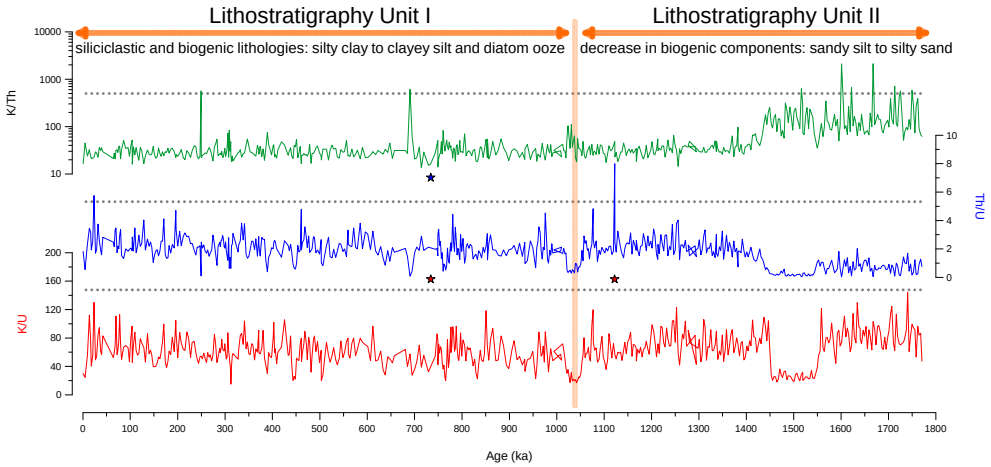

Figure 5.3. The variation in K/Th (10^6 mol/mol), Th/U (mol/mol) and K/U (10^6 mol/mol) ratios at site U1342. The sediment lithostratigraphies are divided into two groups (I and II from Expedition 323 Scientists, 2011c), and there is an increase in K/Th ratio in group II. The gray dotted lines indicate 3-sigma standard deviation, and star symbols represent data above the maximum scale of y-axis. Note that the y-axis for K/Th is log-scale.

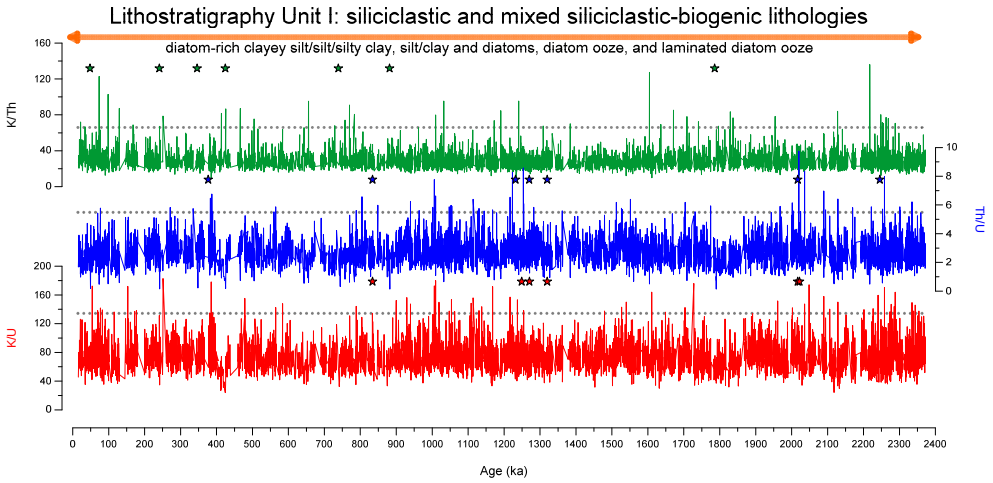

Figure 5.4. The variation in K/Th (10^6 mol/mol), Th/U (mol/mol) and K/U (10^6 mol/mol) ratios at site U1343. There is only one sediment group (Expedition 323 Scientists, 2011d). The gray dotted lines indicate 3-sigma standard deviation, and star symbols represent data above the maximum scale of y-axis.

Figure 5.5. The variation in K/Th (10^6 mol/mol), Th/U (mol/mol) and K/U (10^6 mol/mol) ratios at site U1345. There is only one sediment group (Expedition 323 Scientists, 2011e). The gray dotted lines indicate 3-sigma standard deviation, and star symbol represents datum above the maximum scale of y-axis.

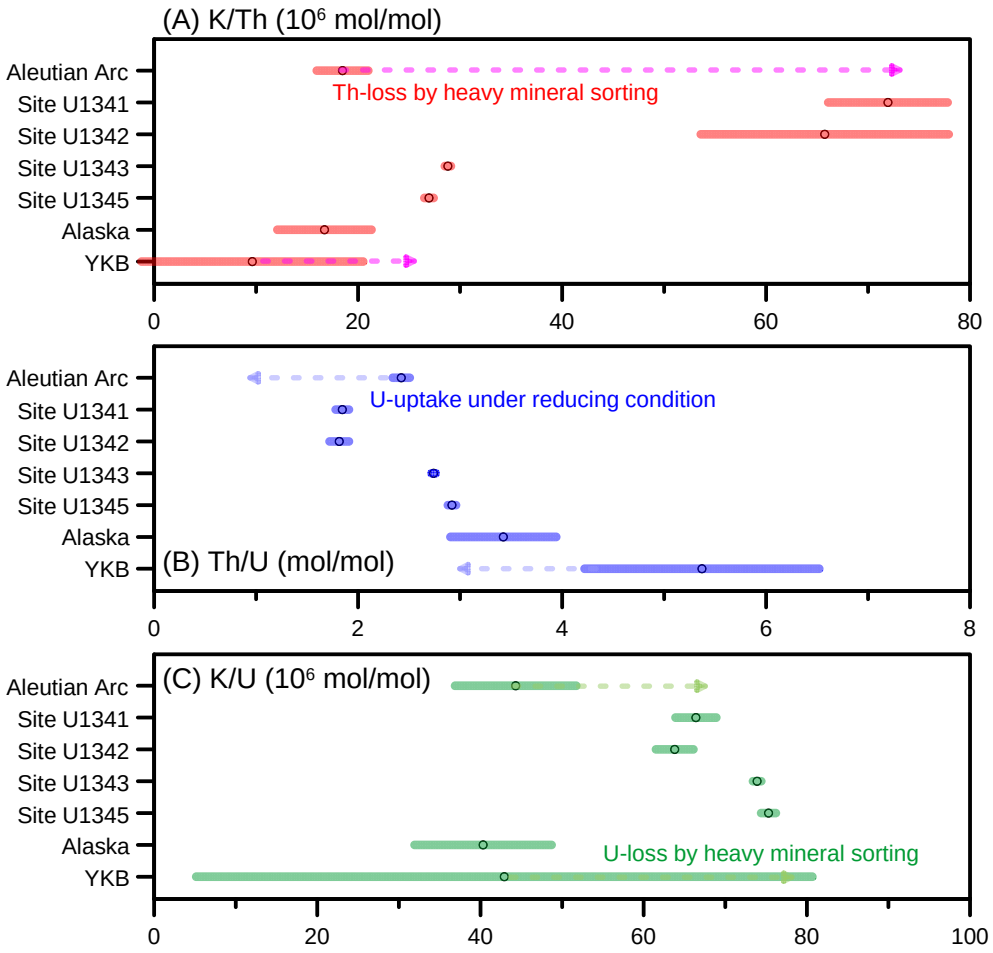

Figure 5.6. The true mean value of K/Th (10^6 mol/mol), Th/U (mol/mol) and K/U (10^6 mol/mol) ratios in the sampling sites of the Bering Sea and potential source areas. Dashed arrows indicate modified elemental ratios of parent rocks.

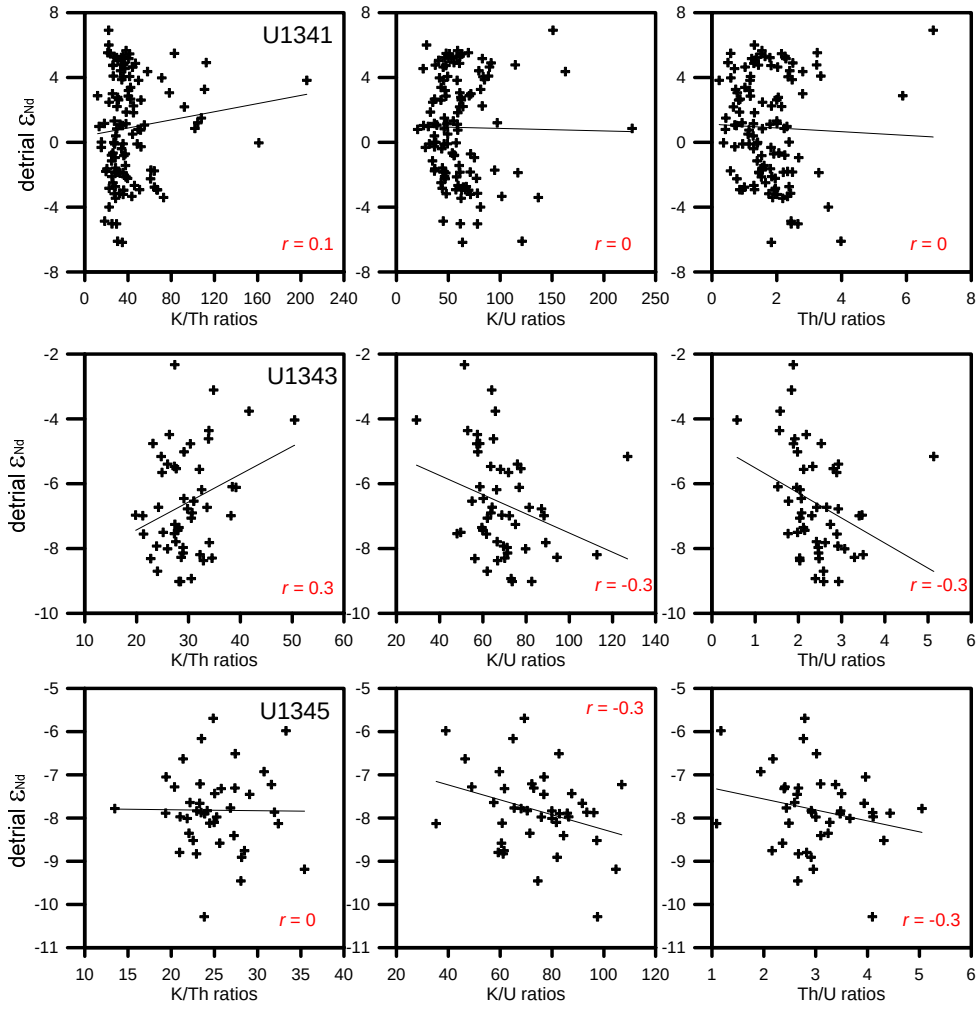

Figure 5.7. Comparison of K/Th, K/U and Th/U ratios with detrital Nd isotopes at sites U1341, U1343 and U1345. Regression lines are marked.

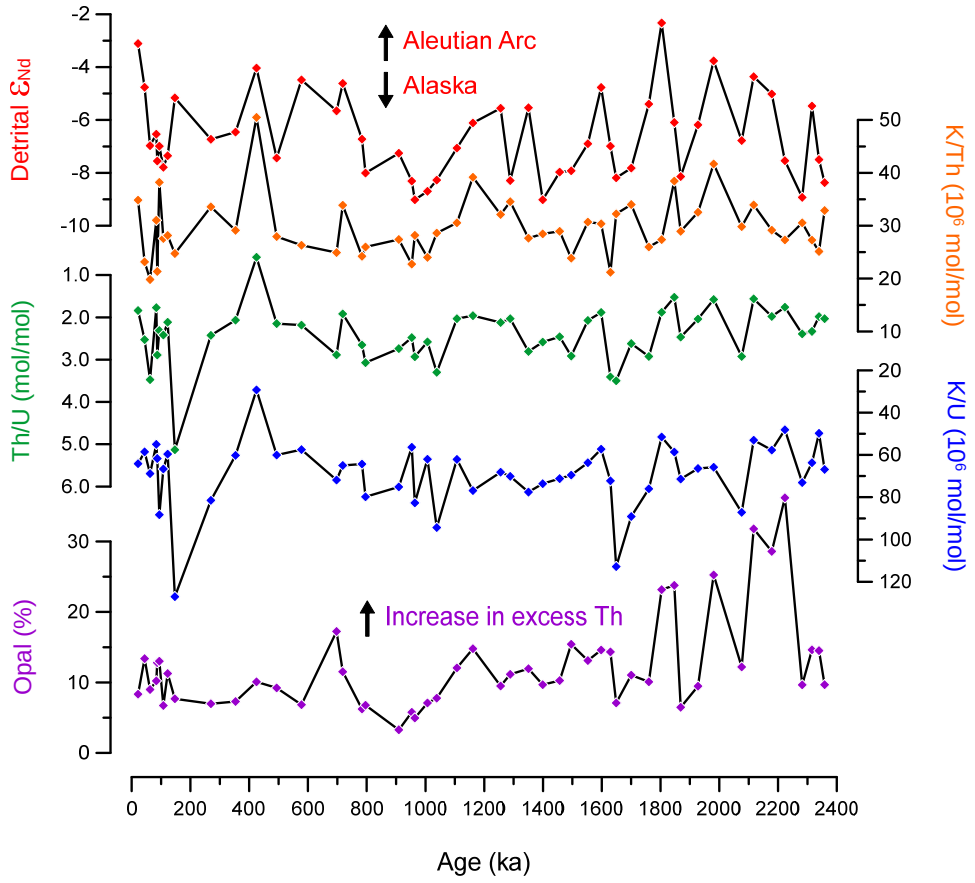

Figure 5.8. The comparison of detrital Nd isotopes (ε_{Nd}) with K/Th (10^6 mol/mol), Th/U (mol/mol) and K/U ratios (10^6 mol/mol) at site U1343. Note that y-axis of Th/U and K/U is inverse.

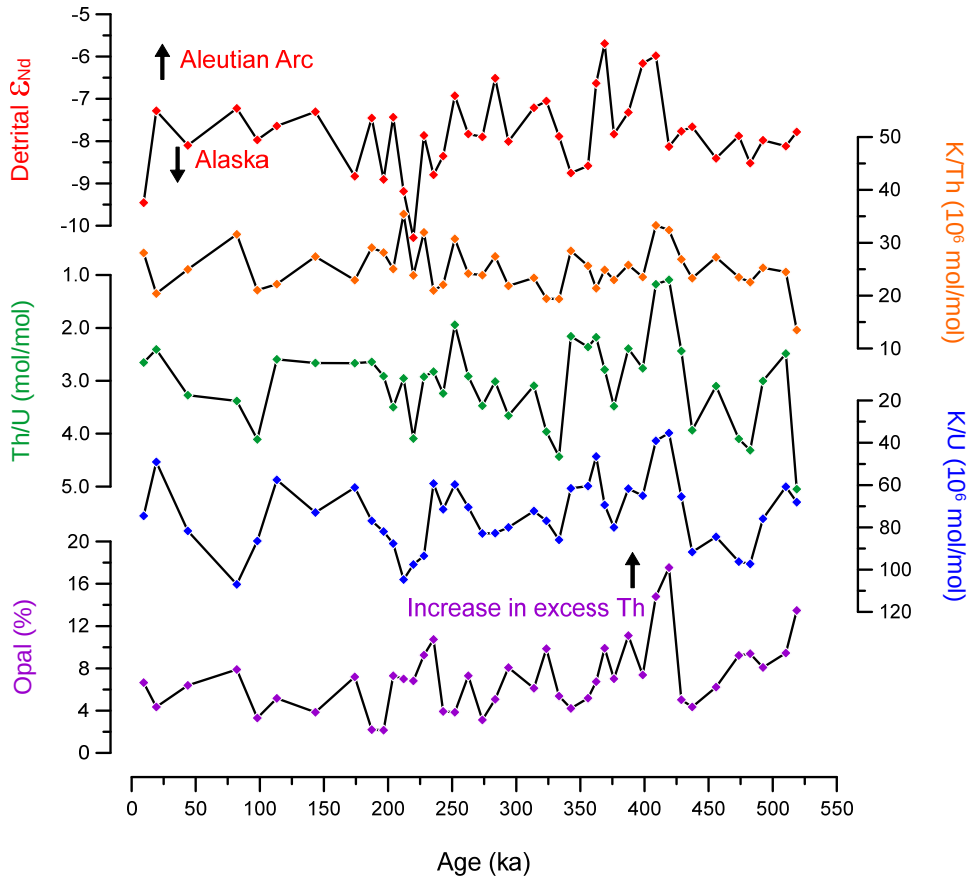

Figure 5.9. The comparison of detrital Nd isotopes (ε_{Nd}) with K/Th (10^6 mol/mol), Th/U (mol/mol) and K/U ratios (10^6 mol/mol) at site U1345. Note that y-axis of Th/U and K/U is inverse.

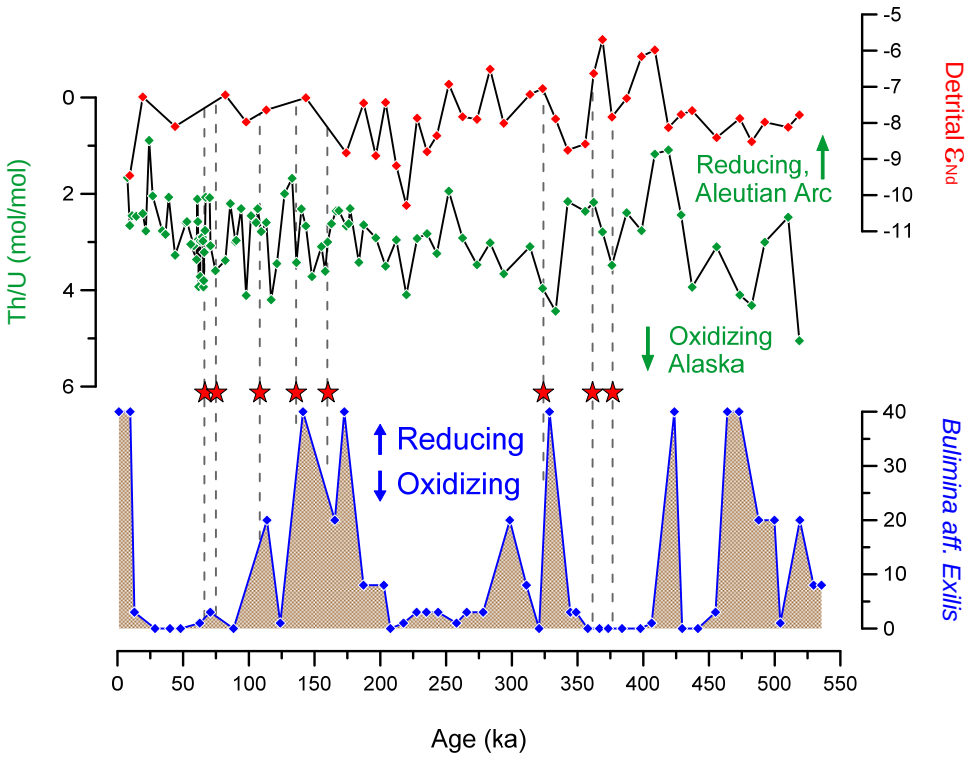

Figure 5.10. The variation in Th/U ratio at site U1345 in response to paleo-redox change indicated by benthic foraminifera species, *Buliminia aff. Exilis* (data from Expedition 323 Scientists, 2011e) and red stars that remark episodic occurrence of ventilation process recorded in peaks of authigenic Nd isotope ratios and associated light oxygen isotopes of benthic foraminifera (Jang et al., 2017). Detrital Nd isotope records indicates temporal change in lithological sediment provenance.

Table 5.1. The true mean values of K, Th and U contents at sites U1341, U1342, U1343 and U1345 in the Bering Sea. The true mean values were determined by a *t*-test ($p < 0.05$).

Locations		K (wt. %)	Th (ppm)	U (ppm)	References
Bowers Ridge	U1341 (n = 5,643)	0.63 ± 0.01	0.98 ± 0.02	0.73 ± 0.01	This study
	U1342 (n = 569)	1.39 ± 0.03	2.33 ± 0.09	1.55 ± 0.07	This study
Bering Slope	U1343 (n = 6,921)	1.71 ± 0.01	3.79 ± 0.03	1.47 ± 0.01	This study
	U1345 (n = 1,556)	1.96 ± 0.01	4.56 ± 0.05	1.66 ± 0.02	This study
Aleutian Arc	51°N – 60°N 168°E – 152°W (n = 902)	0.62 ± 0.02	2.85 ± 0.14	1.25 ± 0.06	*GEOROC*
Alaska	60°N – 66°N 167°W – 140°W (n = 136)	0.43 ± 0.08	2.81 ± 0.67	0.97 ± 0.22	*GEOROC*
Yukon-Koyuku Basin	AK728 – AK736 (n = 9)	2.96 ± 1.30	32.9 ± 15.0	6.60 ± 3.41	[1]

[1] K are from Miller (1989), and Th and U are from Arth et al. (1989)

Table 5.2. The true mean K/Th (10^{-6}), K/U (10^{-6}) and Th/U molar ratios of the sediments derived from the Bering Sea and of the whole rocks from neighboring source areas. The true mean values were determined by a *t*-test ($p < 0.05$).

Locations		K/Th	K/U	Th/U	Ref.
Bowers Ridge	U1341 (n = 5,643)	72 ± 5.9	66 ± 2.5	1.8 ± 0.1	This study
	U1342 (n = 569)	66 ± 12	64 ± 2.3	1.8 ± 0.1	This study
Bering Slope	U1343 (n = 6,921)	29 ± 0.3	74 ± 0.5	2.7 ± 0.1	This study
	U1345 (n = 1,556)	27 ± 0.5	75 ± 0.9	2.9 ± 0.1	This study
Aleutian Arc	Total (n = 902)	19 ± 2.5	44 ± 7.4	2.4 ± 0.1	*GEOROC*
	Volcanic rocks (n = 775)	18 ± 2.9	44 ± 8.5	2.4 ± 0.1	
	Plutonic rocks (n = 119)	21 ± 3.5	49 ± 10	2.7 ± 0.3	
	Sedimentary rocks (n = 8)	9.8 ± 2.9	22 ± 5.3	2.3 ± 0.3	
Alaska	Total (n = 136)	17 ± 4.6	40 ± 8.4	3.4 ± 0.5	*GEOROC*
	Volcanic rocks (n = 118)	14 ± 3.4	37 ± 8.5	3.6 ± 0.6	
	Mantle xenolith (n = 7)	24 ± 15	66 ± 56	2.4 ± 0.6	
	Plutonic rocks (n = 6)	11 ± 11	28 ± 11	3.0 ± 1.2	
	Metamorphic rocks (n = 5)	81 ± 130	96 ± 130	2.1 ± 2.3	
Yukon-Koyuku Basin	AK728–AK736 (n = 9)	9.6 ± 11	43 ± 38	5.4 ± 1.2	[1]

[1] K are from Miller (1989), and Th and U are from Arth et al. (1989)

Chapter 6. Conclusion

The variations of bottom water composition and terrigenous sediment provenance in the Bering Sea during the Pleistocene were reconstructed mainly using neodymium isotopic composition of authigenic ($\varepsilon_{Nd,AUTH}$) and detrital fractions ($\varepsilon_{Nd,DET}$) from marine sediments. $\varepsilon_{Nd,AUTH}$ is a quasi-conservative tracer of water mass, and $\varepsilon_{Nd,DET}$ is a sediment provenance indicator. To recover the authentic seawater composition within the authigenic fraction, seven different extraction methods were evaluated. The most reliable results were obtained when bulk sediment leaching is adopted without decarbonation step, and sediment-to-leaching solution is high (chapter 2).

The variation in $\varepsilon_{Nd,AUTH}$ at site U1345 over the last ~520 kyr is mainly governed by the North Pacific Intermediate Water (NPIW) formation and the boundary exchange process (chapter 3). Eight events of dense water formation including the North Pacific Deep Water were detected. The source of NPIW was mainly the Aleutian Arc and the Anadyr River, but there were also the Alaska-derived NPIW formation. Based on the constrained periods for NPIW formation, the NPIW is generally formed when the North Atlantic Deep Water formation (NADW) is reduced over the last ~200 kyr. However, several exceptions suggest an ambiguous seesaw hypothesis between NPIW and NADW.

The variation in $\varepsilon_{Nd,AUTH}$ at site U1343 over the last 2.4 Myr is primarily attributed to boundary exchange process (chapter 4). There was only North Pacific Deep Water event at ~660 ka. Boundary exchange process is defined as isotopic interaction between seawater and sediment, and hence ε_{Nd} derived from boundary

exchange ($\varepsilon_{Nd,BE}$) possibly follows ε_{Nd} of sediment, as inferred from moderate correlation coefficient between $\varepsilon_{Nd,BE}$ and $\varepsilon_{Nd,DET}$ ($r = 0.49$). However, estimated $\varepsilon_{Nd,BE}$ is generally higher than corresponding $\varepsilon_{Nd,DET}$, suggesting preferential release of radiogenic Nd during boundary exchange. Meanwhile, the repetitive occurrence of unradiogenic $\varepsilon_{Nd,DET}$ peaks can be attributed to the presence of the Alaskan glaciation during the Pleistocene. General 80-kyr periodicity of $\varepsilon_{Nd,AUTH}$ implies that obliquity-like variation drives deep-water Nd isotopic composition in the Bering Sea. Possible interpretation is that the development of the Alaskan glaciation controls the sediment supply from Alaska to the Bering Sea ($\varepsilon_{Nd,DET}$) and further deep water composition ($\varepsilon_{Nd,AUTH}$) through boundary exchange.

New proxies such as K/Th, K/U and Th/U ratios further evaluate the change in lithological sediment provenance in the Bering Sea (chapter 5). Potassium, Th and U contents are obtained from NGR spectra using a MATLAB algorithm. The temporal variations in K/Th, K/U and Th/U ratios broadly suggest change in sediment transport system at site U1343. However, the primary signal derived from parent rocks can be influenced by secondary alteration such as heavy mineral sorting and paleo-oceanic redox conditions. Consequently, K/Th, K/U and Th/U ratios provide only preliminary information about lithological sediment provenance and/or paleo-oceanic redox conditions. The collaborative cross-checking and/or strategic site-selection is necessary.

Appendix: Publication list

A1. Journal Articles

A1.1. International Journals

Jang, K., Huh, Y., Han, Y., 2017. Authigenic Nd isotope record of North Pacific Intermediate Water formation and boundary exchange on the Bering Slope. Quaternary Sci. Rev. 156, 150-163.

De Vleeschouwer, D., Dunlea, A.G., Auer, G., Anderson, C.H., Brumsack, H., de Loach, A., Gurnis, M.C., Huh, Y., Ishiwa, T., **Jang, K.**, 2017. Quantifying K, U, and Th contents of marine sediments using shipboard natural gamma radiation spectra measured on DV JOIDES Resolution. Geochem. Geophys. Geosyst.

Jang, K., Han, Y., Huh, Y., Nam, S.-I., Stein, R., Mackensen, A., Matthiessen, J., 2013. Glacial freshwater discharge events recorded by authigenic neodymium isotopes in sediments from the Mendeleev Ridge, western Arctic Ocean. Earth Planet. Sci. Lett. 369–370, 148-157.

A1.2. Domestic Journals (Korean)

Huh, Y., **Jang, K.**, 2014. Authigenic Neodymium Isotope Record of Past Ocean Circulation. J. Petrol. Soc. Korea, 23(3), 249-259.

A2. Conference Abstracts

A2.1. International Conferences

Jang, K., Han, Y., Huh, Y., 2016. Formation of the North Pacific Intermediate Water in the Bering Sea during the late Pleistocene, recorded by authigenic neodymium isotopes, *International Conference on Paleoceanography*, P-166 (poster)

Jang, K., Huh, Y., Han, Y., 2015. Change in the Nd isotopic composition of the bottom water and detrital sediments on the Bering Slope over the last 500 kyrs with implications for the formation of the North Pacific Intermediate Water, *American Geophysical Union Fall Meeting*, abstract #PP53C-2374 (poster)

Jang, K., Huh, Y., 2014. Changes in the bottom water Nd isotope composition on the BeringSlope over ~530 kyrs, *2014 Goldschmidt Conference*, pp. 1119 (poster)

Jang, K., Huh, Y., 2014. Changes in provenance of terrigenous sediments on the Bering Slope over ~530 kyrs as derived from neodymium and hafnium isotopes, *2014 Goldschmidt Conference*, pp. 1118 (poster)

Jang, K., Huh, Y., 2013. Change in Water Circulation of the Bering Sea Recorded by Authigenic Neodymium Isotopes in Sediments from the Bering Slope over 500 ka BP, *2013 Goldschmidt Conference*, pp. 1376 (poster)

Jang, K., Han, Y., Huh, Y., Nam, S-I. 2012. Authigenic Neodymium Isotopes Recording Change in Arctic Ocean Circulation, *2012 Goldschmidt Conference*, pp. 1894 (oral)

Jang, K., Han, Y., Huh, Y., Nam, S-I., Stein, R., Mackensen, A., 2012. Authigenic

Neodymium isotopes Recording Change in Arctic Deep Water Sources, *The 18th International Symposium on Polar Sciences* (oral)

A2.2. Domestic Conferences

Jang, K., Huh, Y., Han, Y., Neodymium isotopes variation in the Bering Sea across the Mid-Pleistocene Transition, *Annual Meeting of Geological Society of Korea*, pp. 56 (oral)

Jang, K., Huh, Y., 2015. 베링사면 철-망간 산화물과 쇄설퇴적물에 기록된 과거 50만년의 네오디뮴 동위원소 변화를 통한 북태평양 중층수 형성에 대한 고찰, *Annual Meeting of Geological Society of Korea*, pp. 63 (oral)

Jang, K., Huh, Y., 2014. 네오디뮴과 하프늄 동위원소 비 변화로 보는 과거 베링해 중층수/심층수 성분 및 쇄설퇴적물 기원지 변화, *Fall Meeting of Korean Society of Oceanography*, pp. 223-224 (oral)

Jang, K., Huh, Y., 2013. Ocean circulation change in the Bering Sea recorded by authigenic neodymium isotopes over ~520 ka BP, *Annual Meeting of Geological Society of Korea*, 3-10 (oral)

Jang, K., Han, Y., Huh, Y., Nam, S-I., 2011. 멘델레예프 해령 해저 퇴적물의 네오디뮴 동위원소 비 분석을 이용한 MIS 3 동안 북극 해수 순환의 추적, *Annual Meeting of Geological Society of Korea*, pp. 210 (oral)

국문초록

베링해는 해빙 및 대륙 빙상에 의한 환경적 변화가 큰 지역으로, 전 지구적 기후 시스템을 이해하기에 적합하다. 일례로, 막대한 해빙의 성장은 베링해 내에서 북태평양 중층수 혹은 심층수의 형성을 유발할 수 있고, 알라스카 대륙 빙상의 발달은 베링해로 유입되는 퇴적물에 영향을 끼칠 수 있다. 북태평양 중층수/심층수의 형성, 해저퇴적물의 기원지 그리고 기후 변화에 따른 얼음의 거동 간의 관계를 이해하기 위해, 본 학위논문에서는 국제 해저 시추 프로그램 동안 확보한 베링해 퇴적물을 대상으로 자생성 및 쇄설성 네오디뮴 동위원소, 그리고 NGR 기반의 칼륨, 토륨, 우라늄 농도를 분석 및 사용하였다. 자생성 네오디뮴 동위원소는 해수의 추적자로, 쇄설성 네오디뮴 동위원소와 NGR 기반 칼륨, 토륨, 우라늄 농도는 퇴적물 기원지의 추적자로 이용된다. 자생성분 네오디뮴 동위원소를 추출하는 과정에서 상대적으로 불안정한 화산암질의 성분에 의한 오염 요소를 배제하고자, 기존 학계에 보고된 여섯 가지의 방법을 적용하여 획득한 자생성분 네오디뮴 동위원소와 몇몇 원소들의 농도를 분석 비교하여 가장 적합한 방법을 결정하였다.

베링 사면에 위치한 U1345 사이트의 자생성분 네오디뮴 동위원소 비(이후, $\varepsilon_{Nd,AUTH}$)는 약 52 만년동안 -3.3 ± 0.9 (1σ, $n = 98$)의 평균값과 함께 큰 변동폭을 보였는데, 이는 북태평양 중층수의 형성 혹은 해수와 퇴적물 간의 바운더리 익스체인지 과정으로 설명된다. U1343 사이트에서의 $\varepsilon_{Nd,AUTH}$ 분석 결과는 240 만년동안 -3.0 ± 1.1 (1σ, $n =$

155)의 평균값을 보였으며, U1345 사이트와 마찬가지로 큰 시계열 변화를 보였다. 북태평양 심층수의 형성은 단 한차례 $\varepsilon_{Nd,AUTH}$ 변화에 관여하였고, 대부분은 해수와 퇴적물 간의 바운더리 익스체인지에 의한 변화였다. 함께 분석된 쇄설성 네오디뮴 동위원소 비(이후, $\varepsilon_{Nd,DET}$)는 -6.6 ± 1.5 (1σ, n = 70)의 평균값과 큰 변동폭을 보였는데, 이는 퇴적물의 기원지 변화를 가리킨다. 전반적으로, U1343 사이트는 알류샨 열도에 비해 알라스카 지역으로부터 퇴적물 공급을 주로 받는 것으로 여겨지며, 현저한 unradiogenic $\varepsilon_{Nd,DET}$ 피크는 알라스카로부터의 융빙수 유출로 해석된다. Unradiogenic $\varepsilon_{Nd,DET}$ 피크들이 240 만년전 이후 반복적으로 발생한다는 것을 고려해보았을 때, 적어도 240 만년 전부터 알라스카 지역에 광범위한 빙하작용이 있었음을 유추할 수 있다. 베링해 퇴적물의 시공간적인 변화는 부분적으로 NGR 기반 K/Th, K/U, Th/U 비에서도 확인할 수 있다. 바워스 해령에 위치한 U1341, U1342 퇴적물의 경우, 베링 사면에 위치한 U1343, U1345 퇴적물과 구분되는 K/Th, K/U, Th/U 비를 보였다. 하지만, 중광물의 분급 작용이나 과거 해수의 산화 환원 상태에 따라 모암으로부터 획득된 최초의 비율은 변화할 수 있으므로, K/Th, K/U, Th/U 비를 통한 베링해 퇴적물 기원지 변화 유추는 기초 데이터로서만 활용되어야 한다.

Acknowledgement